On The Frequency-Dependent Model of Grounding Systems for Power System Transient Analysis

Ghomi, Mohammad

Publication date:
2023

Document Version
Publisher's PDF, also known as Version of record

Link to publication from Aalborg University

ON THE FREQUENCY-DEPENDENT MODEL OF GROUNDING SYSTEMS FOR POWER SYSTEM TRANSIENT ANALYSIS

BY
MOHAMMAD GHOMI

DISSERTATION SUBMITTED 2023

AALBORG UNIVERSITY
DENMARK

On The Frequency-Dependent Model of Grounding Systems for Power System Transient Analysis

Mohammad Ghomi

AALBORG UNIVERSITY
DENMARK

Dissertation submitted to the Faculty of Engineering and Science at Aalborg University

For the degree of

Doctor of Philosophy in Electrical Engineering

CV

Mohammad Ghomi received his B.Sc. degree in Electrical Power System Engineering from Dezful University, Dezful, Iran, in 2002, and his M.Sc. in Power Electrical Power System Engineering from Science and Research University, Tehran, Iran, in 2007.

He is currently pursuing his study to obtain his Ph.D. degree in the Department of Energy Technology, at Aalborg University, Denmark. He has worked for several years as a senior electrical engineer in the TSO of Iran. He worked as a senior design engineer at PolyTech to develop lightning protection systems for wind turbines and blades. He is working as an Experienced Professional Engineer at Hitachi Energy on the system and grounding conceptual design for HVDC and transient overvoltage studies and insulation coordination analysis. His research interests include grounding system modeling, transient analysis of power systems, power system studies, HVDC main circuit parameters, renewable energy, and power system reliability.

English Summary

The reliable function of power systems is affected by the proper design of grounding systems (GSs). Recently, the modeling of GSs has received extended attention. Design accuracy becomes essential if power transmission lines, wind turbines, and substation components experience abnormal conditions, such as a lightning strike, to increase power system reliability and availability and decrease maintenance costs. As a result, GSs should have the ability to conduct lightning currents into the soil without harming people or damaging equipment. Generally, various time-domain platforms are used to study lightning transients, such as ATP-EMTP, EMTP-RV, and PSCAD/EMTDC. Often, these tools use lumped parameters or simple resistive models, which fail to model GSs at higher frequencies due to the high-frequency content of lightning currents. The quasi-static models are restricted to cases where the electrode length is smaller than one-tenth of the wavelength in soil. It practically restricts the model's validity to the frequency range of up to 150 ~200 kHz.

The GS has a dynamic behavior and depends on electromagnetic wave propagation through the buried electrodes in the soil. However, compared to the behavior of the GS at low frequencies, its behavior under transient conditions and high frequencies has more complexities. Despite this, there remain numerous challenges concerning the precise high-frequency modeling of GSs, such as the layered structure of the soil, soil electrical parameters frequency-dependency impact, complex arrangements of grounding of the GS, and level of accuracy in the modeling, which the literature has needed to discuss. The research starts with presenting a full-wave technique established on the method of moment (MoM) solution obtained from the full set equation of Maxwell to calculate the input harmonic impedance of vertical ground electrodes buried in homogenous (uniform) and multi-layer soil [1]. The prevailing technique can consider any number of soil layers and any GS geometry to assess their impacts on harmonic impedance and ground potential rise (GPR). Then the frequency response of the

GS is linked with the time domain simulation platforms to assess the lightning performance of a novel composite pylon tower, overvoltage on cross-arms, and GPR values at both first and return strokes, which lead to overvoltage across the insulator strings that may lead to the back flashover. It can be one of the major causes of the forced outage of the power transmission lines (PTLs) when the overvoltage transcends the withstand of the insulators due to lightning strokes.

The frequency-dependent impact of soil electrical parameters is investigated on the harmonic impedance and GPR values. Different analytical formulas are applied to model the frequency-dependent effects, and the results are discussed for different electrode geometry and soil electrical parameters. After that, an integrated model of a tower and multi-layer grounding grids based on the MoM technique is introduced. This method is employed to calculate the harmonic impedance of the HVDC full-scaled tower considering the effects of an exact model of GSs. The harmonic impedance is significantly affected by the linked GS.

To further assess the influence of the layered earth structure on the transient overvoltage, the MoM is utilized to model a medium voltage substation and its impacts on the GPR value and the generated overvoltage at power transformers to subsequent lightning currents. Different soil structures are taken into account for substation grounding soil structure, considering soil frequency-dependent impacts on the multi-terminal grounding grid harmonic impedance. The application of the proposed method to compute harmonic impedance and frequency-dependent model of the GS is investigated to study the performance of novel composite pylon towers against lightning and to optimize the insulation coordination study.

Dansk Resume

Nøgleord: frekvensafhængig model, jordingssystemmodellering, lynoverspænding, flerlags jordstruktur, transientanalyse

Den pålidelige funktion af strømsystemer påvirkes af det korrekte design af jordingssystemer. For nylig har modelleringen af jordingssystemer fået udvidet opmærksomhed.

Designnøjagtighed bliver afgørende, hvis krafttransmissionsledninger, vindmøller og transformerstationskomponenter oplever unormale forhold, såsom et lynnedslag, for at øge strømsystemets pålidelighed og tilgængelighed og reducere vedligeholdelsesomkostningerne. Som følge heraf bør jordingssystemer have evnen til at lede lynstrømme ned i jorden uden at skade mennesker eller beskadige udstyr. Generelt bruges forskellige tidsdomæneplatforme til at studere lyntransienter, såsom atp-emtp, emtp-rv og pscad/emtdc. Ofte bruger disse værktøjer sammenklumpede parametre eller simple resistive modeller, som ikke formår at modellere jordingssystemer ved højere frekvenser på grund af det højfrekvente indhold af lynstrømme. De kvasistatiske modeller er begrænset til tilfælde, hvor elektrodelængden er mindre end en tiendedel af bølgelængden i jord. Det begrænser praktisk talt modellens gyldighed til frekvensområdet på op til 150 ~ 200 khz.

Jordingssystemer har en dynamisk adfærd og afhænger af elektromagnetisk bølgeudbredelse gennem de nedgravede elektroder i jorden. Sammenlignet med opførselen af jordingssystemer ved lave frekvenser, har dens opførsel under forbigående forhold og høje frekvenser mere kompleksitet. På trods af dette er der stadig adskillige udfordringer vedrørende den præcise højfrekvensmodellering af jordingssystemer, såsom jordens lagdelte

struktur, jordbunds elektriske parametre frekvensafhængig påvirkning, komplekse arrangementer af jordforbindelse af jordingssystemer og niveauet af nøjagtighed i modelleringen, som litteraturen har haft brug for at diskutere. Forskningen starter med at præsentere en fuldbølgeteknik etableret på momentopløsningen (MoM) opnået ud fra maxwells komplette ligning for at beregne den harmoniske indgangsimpedans af vertikale jordelektroder begravet i homogen (ensartet) og flerlagsjord. Den fremherskende teknik kan overveje et hvilket som helst antal jordlag og enhver jordingssystemer-geometri for at vurdere deres indvirkning på harmonisk impedans og jordpotentialstigning (GPR).

Derefter er frekvensresponsen af jordingssystemer forbundet med tidsdomæne simulering platformene for at vurdere lynydeevnen af et nyt sammensat pylontårn, overspænding på tværarme og gpr-værdier ved både første og returslag, hvilket fører til overspænding over isolatoren strenge, der kan føre til tilbageslag. det kan være en af hovedårsagerne til det tvungne udfald af kraft transmissionsledning erne, når overspændingen overskrider isolatorernes modstandskraft på grund af lynnedslag.

Den frekvensafhængige påvirkning af jordelektriske parametre undersøges på den harmoniske impedans og gpr-værdier. Forskellige analytiske formler anvendes til at modellere de frekvensafhængige effekter, og resultaterne diskuteres for forskellige elektrodegeometri og jordbundselektriske parametre. Derefter introduceres en integreret model af et tårn og flerlags jordingsgitter baseret på mom-teknikken. denne metode bruges til at beregne den harmoniske impedans af hvdc-tårnet i fuld skala under hensyntagen til virkningerne af en nøjagtig model af jordingssystemer. den harmoniske impedans påvirkes væsentligt af den forbundne jordingssystemer.

For yderligere at vurdere indflydelsen af den lagdelte jordstruktur på den transiente overspænding, bruges mom til at modellere en mellemspændings transformatorstation og dens indvirkning på GPR-værdien og den genererede overspænding ved strømtransformatorer til efterfølgende lynstrømme. Forskellige jordstrukturer tages i betragtning for

jordstrukturen til transformerstationens jordforbindelse under hensyntagen til jordfrekvensafhængige påvirkninger på den harmoniske impedans for flerterminaljordingsnettet. Anvendelsen af den foreslåede metode til at beregne harmonisk impedans og frekvensafhængig model af jordingssystemer er undersøgt for at studere ydeevnen af nye sammensatte pylontårne mod lyn og for at optimere isolationskoordination undersøgelsen.

Table of contents

Thesis Details

Thesis Title: On the Frequency-dependent Model of Grounding System for Power System Transient Analysis

Ph.D. Student: Mohammad Ghomi

Supervisors: Prof. Claus Leth Bak

Associate Prof. Filipe Faria da Silva

The main body of this research includes the below papers:

Publications in Refereed Journals:

J1. **M. Ghomi**, H. Zhang, F. Faria da Silva, C. Leth Bak, and K. Yin, "*Integrated Model of Transmission Tower Surge Impedance and Multilayer Grounding System Based on Full-wave Approach*," Journal of Energy Power System Research, vol. 198, pp. 107355, Sept. 2021 [1].

J2. **M. Ghomi**, F. Faria da Silva, Amir abbas Shayegani Akmal, and C. Leth Bak, "*Transient Overvoltage Analysis in the Medium Voltage Substations Based on Full-Wave Modeling of Two-layer Grounding System*," Journal of Energy Power System Research, Elsevier 2022 [2].

J3. H. Zhang, **M. Ghomi**, Q. Wang, F. Faria da Silva, C. Leth Bak, K. Yin, and H. Skouboe, "*Comparison of Backflashover Performance between a Novel*

Composite Pylon and Metallic Towers," Journal of Energy Power System Research, vol.196, pp. 107263, July, 2021 [3].

J4. K. Yin, **M. Ghomi**, Q. Wang, H. Zhang, F. Faria da Silva, C. Leth Bak, Q. Wang, H. Skouboe, "*The design and optimization of the down-lead system for a novel 400 kV composite pylon*," IEEE Transactions on Power Delivery 2022 [4].

J5. K. Yin, **M. Ghomi**, H. Zhang, C. Leth Bak, F. Faria da Silva, Q. Wang, "*Lightning transient response of bifurcation structure pylon and its empirical expression with high accuracy and general application*," International Journal of Electrical Power & Energy Systems 2023, Status: accepted [5].

J6. H. Zhang, **M. Ghomi**, Q. Wang, F. Faria da Silva, C. Leth Bak, and K. Yin, "*Backflashover Performance of a Novel Composite Pylon with External Grounding Down-lead Modeled in Dynamic Surge Impedance Considering Corona Effect*," IEEE Transactions on Power Delivery, 2022 Status: Under review [6].

Publications in Refereed Conferences:

C1. M. Ghomi, C. Leth Bak and F. Faria da Silva, "*Frequency Dependence of Multilayer Soil Electrical Parameters: Effects on the Ground Potential Rise*," in 35th International Conference on Lightning Protection (ICLP) and XVI International Symposium on Lightning Protection (SIPDA), 2021 [7].

C2. M. Ghomi, C. Leth Bak and F. Faria da Silva, "*Frequency Dependence of Multilayer Soil Electrical Parameters: Effects on the Input Impedance of Grounding Systems*," 16th International Conference on AC and DC Power Transmission, IET event ACDC 2020 [8].

C3. M. Ghomi, HR. Mohammadi, HR. Karami, C. Leth Bak, F. Faria da Silva, and H. Khazraj, "*Full-wave modeling of grounding system: Evaluation the effects of multi-layer soil and length of electrode on ground potential rise*," International Conference on Power Systems Transients, IPST, pp. 1-6, 2019 [9].

C4. K. Yin, **M. Ghomi**, F. Faria da Silva, C. Leth Bak, Q. Wang, H. Zhang, H. Skouboe, "*Lightning performance and formula description of a Y-shaped composite pylon considering the effect of tower-footing impedance*," in 35th International Conference on Lightning Protection (ICLP) and XVI

16

International Symposium on Lightning Protection (SIPDA), pp. 16, 2021 [10].

C5. K. Yin, **M. Ghomi**, F. Faria da Silva, C. Leth Bak, H. Zhang, Q. Wang, "*The Effect of Frequency-Dependent Soil Electrical Parameters on the Lightning Response of a 'Y' Shaped Composite Pylon for 400 kV Transmission Lines,*" in *22nd International Symposium on High Voltage Engineering*, pp. 2046 – 2051, Nov. 2021 [11].

C6. H. Zhang, **M. Ghomi**, Q. Wang, F. Faria da Silva, C. Leth Bak, K. Yin and H. Skouboe, "*Evaluation of Lightning Backflashover Rate of a Fully Composite Pylon using Monte Carlo Method on Environmental Factors,*" proc. of IEEE Power &Energy Society General Meeting (PESGM) 2022, Denver, Colorado, 2022, Status: Accepted [12].

Collaboration papers:

P1. H. Khazraj, B. Yousefi Khanghah, P. Ghimire, F. Martin, **M. Ghomi**, F. Faria da Silva, C. Leth Bak, "*Optimal Operational Scheduling and Reconfiguration Coordination in Smart Grids for Extreme Weather Condition,*" Journal of IET Generation, Transmission & Distribution 2019 [13].

P2. R. Rezvanfar, H. Ghasemi, M. E. Mosayebian, **M. Ghomi**, F. Faria da Silva, C. Leth Bak, "*Optimal placement of phase shifting transformers based on MADM method: the considering system performance indices,*" CIGRE symposium Aalborg 2019.

This dissertation is written based on the following publications, which have been accomplished in the Ph.D. study period. The papers are accessible in the Appendix section of the dissertation. Parts of the results are used directly or indirectly in the extended summary of the thesis. The co-author statements have been made available to the assessment committee and available at the Faculty of Engineering and Science, Aalborg University.

Mohammad Ghomi
Aalborg University, Feb. 2023

Preface

This dissertation outlines the outcomes of the Ph.D. work entitled: "On the frequency-dependent model of GSs for power system transient analysis," carried out from January 2019 to December 2022 at the Department of Energy, Aalborg University, Denmark. It submitted a dissertation to the Doctoral School of Engineering and Science at Aalborg University to obtain the Danish Ph.D. degree. This thesis is provided in the collection of the paper format in six chapters.

Firstly, I would like to thank my supervisor, Professor Claus Leth Bak, for his continuous supervision, encouragement, and tolerance throughout the whole Ph.D. period. His recommendations aided me in all the study time and script of this research. I would also like to expand my most profound appreciation to my co-supervisor, Associate Professor Filipe Faria da Silva, for his recommendation and support during the whole period of the Ph.D. It has been such an honor to work under you.

I am also thankful to Prof. Amir Abbas Shayegani Akmal for allowing me to visit the high voltage research institute of Tehran University, Iran, during my study abroad and widen my understanding of transient power systems. I would like to show my greatest appreciation to my best friend, Jon Heinssen, who has always supported me. I feel profoundly thankful and fortunate that we worked together to explore more North Atlantic Inspection Service Company opportunities. I am grateful and indebted to my colleagues at the Department of Energy, Hanchi, and Kai. They have helped me use the proposed modeling in more applications to reach out for collaboration.

Finally, yet significantly, I would like to thank my wife "**Sara**" and my son "**Nikan**" for their continuous help, motivation, and goals, and for always being there for me. Sara's support and incentives have made all this possible.

Mohammad Ghomi

Aalborg, Denmark, Feb. 2023

Part I: Report

Chapter 1.   Introduction

1.1   Abstract

The introduction aims to provide an overview of the importance of the GS frequency-dependent model on transient analysis and its applications. The importance of soil structure and its electrical parameters are explored, and various techniques to achieve this feature are introduced. Different methods to model the GSs are introduced, and their feasibility for GS modeling (GSM) is discussed. To model the GS, the soil electrical parameters are a function of frequency. The constant assumptions of soil electrical parameters may lead to errors in the GS harmonic impedance at the high-frequency range. The published papers are listed in this chapter. The chapter is summarized by the project goals and outline of the dissertation.

1.2   Background and Motivations

Tall structures like wind turbines (WTs) and overhead lines (OHLs) are installed in open-air environments. Many WTs have been erected globally to a generation capacity of 743 GW in 2021 [14]. Nowadays, the wind turbine blades are becoming longer (more than 100 m) to catch more energy because winds typically increase as the length of the blade increases [15], [16]. Fig. 1 shows the increasing size of wind turbines (onshore/offshore) in recent decades.

It is more likely that blades and towers will be struck by lightning than other equipment of the power systems because they are highly exposed to lightning strikes. Therefore, transmission system operators (TSOs) and blade/turbine manufacturers are significantly interested in lightning performance and lightning protection system design of overhead lines and blades of wind turbines, respectively. Seven of the twelve reported crucial grid outages happened due to lightning strikes to power transmission lines in 2019 [17]. Utility companies have lost billions of dollars due to energy not supplied (ENS) during lightning.

An effective GS design is one of the significant factors in the power system's performance against lightning, and it reduces the outage rate [18]–[21]. The GS refers to a set of metal structures and consists of very simple (e.g., vertical or horizontal electrodes) or complex (grid shape) arrangements buried in the soil [22],

[23]. The "Grounding" means connecting the live part of the equipment (e. g., power transformer neutral terminal) or metal structures (e. g., body of towers or power transformers) to the soil.

Briefly, the main reasons for the grounding of the electrical system are [24], [25], [26]:

➢ To guarantee employee safety and avert the deterioration of installations
➢ To provide an appropriate operation of electrical equipment (for example, correct detection of fault location in grounded networks and proper operation of protective equipment)
➢ The design and modeling of the GS are crucial to calculate accurate
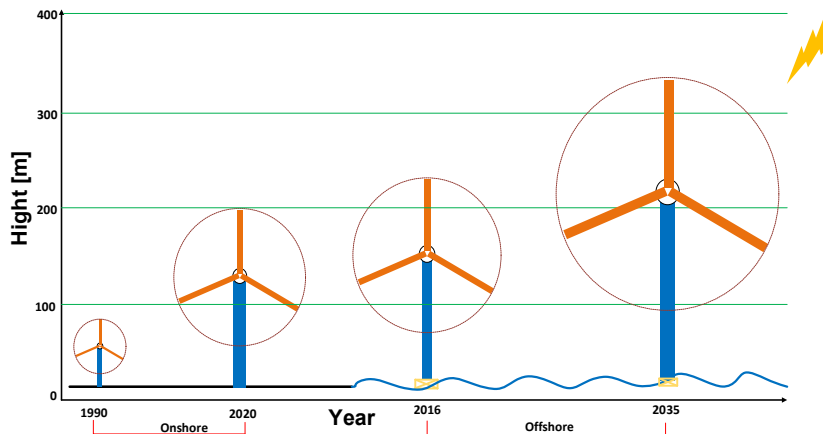
Fig. 1. Onshore/offshore wind turbines heights over time [16].

overvoltage values and voltage stress on the tower's insulator strings to increase system reliability, availability, and maintainability (RAM).
➢ To create a path with a lower impedance that could manifest on OHLs caused by abnormal conditions such as lightning-associated transients
➢ To develop acceptable safety levels in normal and abnormal operating conditions
➢ To establish voltage of common reference for power system grids and connected installations
➢ To stabilize voltage during faults and transient conditions

23

➢ To flow currents caused by lightning to the soil
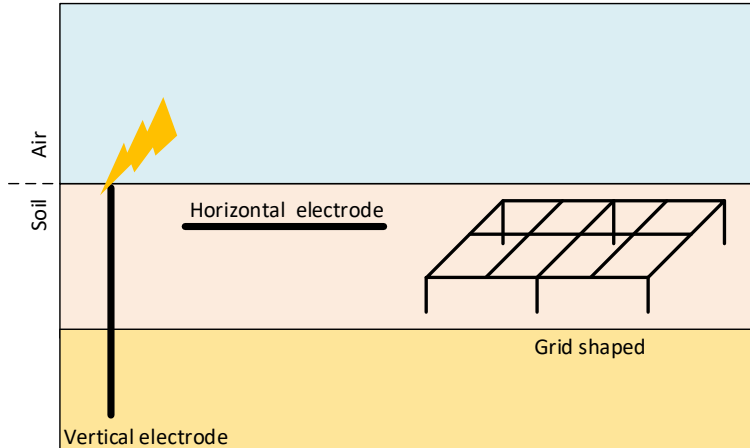
Fig. 2. Grounding system arrangement.

While injecting currents caused by lightning and short circuits into the soil, a proper GS provides a minimum potential difference among various parts of the GS. It is vital to minimize damage to electrical and electronic equipment [26]. Different arrangements of the GS are illustrated in Fig. 2.

One of the main issues concerning the behavior of the GS against lightning currents is the non-uniform potential distribution in different parts of the GS, which may lead to the creation of high-amplitude currents in other parts of the grounding grid [26]. It is essential to understand that the potential of the ground does not have a constant value during lightning strikes. Indeed, there may be considerable voltage differences between the termination of the ground that create severe safety problems for people in those areas. Additionally, such high currents may destroy the equipment in its path and cause electromagnetic fields that may affect other sensitive equipment, such as electronic equipment and microprocessors.

Generally, the GSs are investigated over a broad frequency range, from dc to a few MHz [27], [28]. It depends on the type of analysis and the source of disturbance, and whether the maximum frequency of interest is reasonable. A proper model of power system elements must be considered for precisely modeling electromagnetic transients. In power systems, transient phenomena can occur at a wide frequency range. For instance, lightning transient typically ranges from 10

kHz to about 10 MHz. The frequency range of the power system switching is about several kHz. The short circuit fault frequency is power frequency (50 or 60 Hz). The characteristics time scale of power system events is shown in Fig. 3.
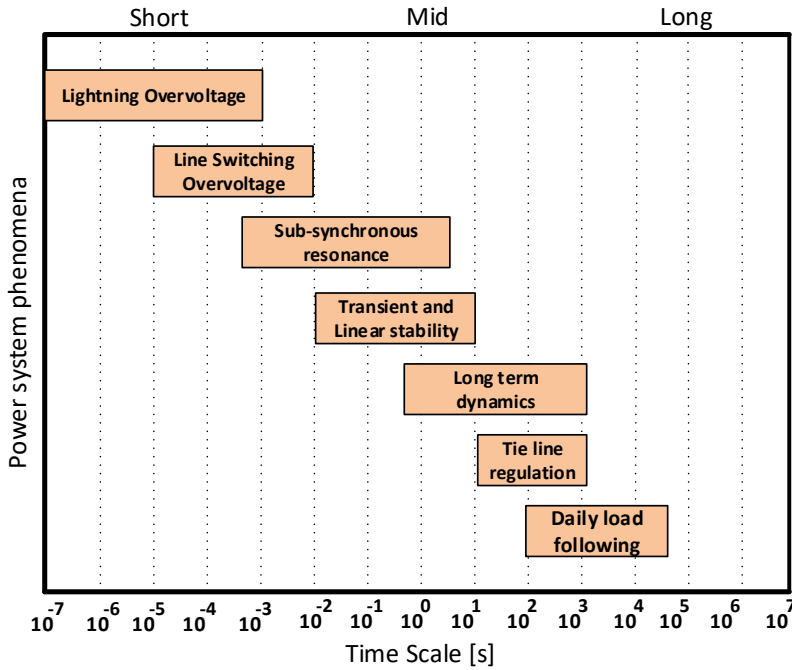
Fig. 3. Power system events classification [78].

Generally, the soil is not a uniform medium but consists of various instructed layers with different electrical characteristics. The preference to simulate the GS in layered structures can be seen in [29], [9]. The reason is that the soil is formed of different layers with various electromagnetic characteristics. Thus, the layered soil structure should be assumed in order to compute an accurate GS model. Accordingly, it is necessary to consider the soil structure when assessing the lightning transient overvoltage.

Experimental measurements have demonstrated that soil resistivity and permittivity are strongly associated with soil moisture, which changes between 4 ~ 30% of the total soil weight over a year. It means that the soil's electrical properties

can change as the seasons change significantly for the upper layers [30]. An investigation of the GS behavior is primarily based on the following characteristics:

- ➢ The geometry of the electrodes and physical specification responsible for the GSs (e. g., their shape, sizes, and material)
- ➢ Soil model assumptions
- ➢ Input current characteristics (amplitude, rise time, and shape)
- ➢ Maximum frequency limitation of the selected approach of study

The GSs can be investigated using both numerical and analytical methods. Generally speaking, to obtain the GS model, the advanced analytical methods can be classified as follows:

- Quasi-static methods
    - ➢ Circuit and image theory [31]–[33]
    - ➢ Transmission line model (TLM) [34]
- Full-wave methods
    - ➢ Method of moment (MoM) [7], [9], [13], [18], [20], [42]
    - ➢ Finite element method (FEM) [35]–[37]
    - ➢ Finite differential time-domain (FDTD) [38]–[41]

These approaches will be checked in the following sections, focusing on their drawbacks and merits.

The accurate modeling of the GSs has been a challenge to utility system designers since the full-wave approach became feasible. The most often cited reason for ignoring the full-wave methods seriously was the lack of high-performance computers in the past decades. Also, the full wave approaches are time-consuming processes and have more difficulties to model the complex grounding grids. It is also necessary to have the GS models in electromagnetic transient programs, in order to obtain the transient overvoltage. In other words, one wouldn't be able to do a full analysis with full-wave methods. To model GSs precisely, some challenging aspects must be considered. Soil layers [9], [31], [32], [42], frequency-dependent of soil electrical parameters [3], [11], [43]–[46], and ionization effects [47], [48] can deviate the accuracy or change the computational time of modeling. Another issue is selecting the study environment that should be taken into account [49]–[51]. Transient analysis of GSs can be performed in the frequency domain (FD) or direct solution of equations in the time domain [34]. Additionally, it is more difficult to predict the transient behavior of the buried electrodes of GS than the installed

metal structures or towers above the soil. In this context, there are two problems, wave propagation, and soil ionization, that should be involved in modeling GSs and, consequently, also on lightning transient analysis or lightning performance of OHLs [52].

Soil ionization happens when the lightning current has a high amplitude, influencing the low-frequency resistance value. As a result, the surface electric field of the conductors is larger than the ionization level. The propagation varies with frequency and can be investigated through the electromagnetic field theory. Based on our knowledge, there is no integrated approach in the GS modeling to incorporate propagation and soil ionization effects, and it is implemented independently [48].

Time-domain approaches to simulate GSs can easily integrate with transient analysis software packages like EMTP [53] or PSCAD/EMTDC [3], [10], [54]. Generally speaking, it is not implemented today in commercial software. However, the main drawback of time-domain simulations of GSs is that they are often unable to include soil electrical parameters with frequency variations, such as resistivity and permittivity frequency-dependent effects. Frequency-dependent of soil electrical parameters also have a major influence on GS modeling [44]. Earlier, this influence was ignored in the estimation of the GS modeling, because of the lack of appropriate expression to define it. Recently, some empirical formulations based on field and laboratory experiments have been presented to describe soil electrical parameters as a function of frequency [55].

The main disadvantage of frequency-domain techniques is that these methods perform modeling excluding the non-linear soil ionization effect in the study. The soil ionization occurs close to the electrodes when a lightning current with a large magnitude flows into the soil. The GS model can be conservative or overestimated when such effects are not considered [48]. However, some empirical expressions for influence in the GS modeling and transient analysis were proposed [48], [56]–[58]. It is important to note that this model alone cannot consider the frequency-dependent effect of electrodes [59], [60].

Several mathematical techniques like the vector fitting method (VFM) [61]–[64] and matrix pencil method (MPM) [27], [64], [65] are applied to derive an extended equivalent network for time-domain simulation. All apparatuses of the power system can be simulated in the time-domain platform above the soil. Nevertheless, these prevalent platforms have not precisely simulated GSs as an incorporated part

of electrical systems. Conventionally, transient studies of electrical systems modeled using time-domain solvers ignore the precise model of the GSs [66]. The resistive model of the GS usually uses to model the GSs. It is an independent frequency model that cannot cover fast-front overvoltage studies or high-frequency phenomena like lightning studies. With this regard, the full-wave model of the GS can link to the existing time-domain simulator to perform a transient analysis of the power system [14], [45].

When the frequency response of the GS (impedance/admittance matrix) is calculated, one can also express it mathematically as a state-space model. The state-space block (SSB) defines the correlation of voltages and currents at each point. It means that the SSB can be applied as an accurate model of GS to be applied in the time domain simulators [65]. Furthermore, the tower surge transient impedance is of considerable significance in the estimation of the generated overvoltage across the insulators string [31], [44], [67] [56]. The elements of the tower, like cross-arms, tower geometry, and guard conductors, have a notable influence on the response of the system transient. Considering such elements for lightning-related studies is likely to produce more rigorous results. The GS or tower footing GS may affect the lightning performance studies of the towers.

The full-wave approaches can be utilized to compute the surge impedance of the tower instead of the expensive measurement methods in the field. In this regard, having an accurate model of GS and tower and other apparatuses can help produce high enough accuracy [1], [49].

In this work, soil frequency dependency impacts are investigated for calculating the harmonic impedance and GPR values.

1.3   Theoretical Methods of the Grounding System Modeling

The first most extensive research on GS modeling was performed late 1970's [68]–[70]. Traditionally, GSs modeling methods are established on a simplified model or quasi-static. In contrast, the electrodes of GS are characterized by a simple resistive model [71] at the low-frequency range or lumped RLC model at the high-frequency range [72]. These are usually used to investigate impedance to remote neutral ground and ignore the soil-air interface. Nevertheless, it is not apparent how such an evaluation can be used for GS modeling when the GS dimension is larger than the maximum wavelength of the impressed current into the soil.

The GS modeling is always straightforward and well-understood at faults with power frequency content or slow-front transient events such as single phase to ground fault (L-G) (power frequency faults). The calculated voltages are equivalent to potential differences among different parts of the GS as addressed in standards [73]. In these cases, the leakage current is considered invariant along the electrode's length.

1.3.1 Circuit and Image Theory Methods

Generally, circuit and image theories can be taken into account as a particular point of the equivalence electromagnetic theory [33]. In these methods, the half-space of air is superseded with a mirror image of the positive charge and distribution of the axial current on the electrode above the interface of air and soil. The circuit method can model the GSs with an equivalent circuit, including several resistors, capacitors, and inductors. The developed circuit models have been used to address the problem of computing the GS and GPR, which are compatible with the Electromagnetic Transient Analysis platform [74].

Two sets of formulations have been widely used to predict the RLC model of the vertical ground electrode. A resistive model at low frequencies for the impedance of a vertical ground electrode (see Fig. 4(a)) buried in the soil is shown in Fig. 4(b).

There are two theoretical expressions to determine the input impedance of the vertical electrode of the GS. The first one is proposed by Rudenberg [75]. The parameters can be calculated as below:

$$R = \frac{\rho}{2\pi l}\log\left(\frac{2l}{a}\right) \qquad (\Omega) \qquad\qquad (1)$$

$$L = \frac{\mu_0 l}{2\pi}\log\left(\frac{2l}{a}\right) \qquad (H) \qquad\qquad (2)$$

$$C = 2\pi\varepsilon l \left(log\frac{2l}{a}\right)^{-1} \qquad (F) \qquad\qquad (3)$$
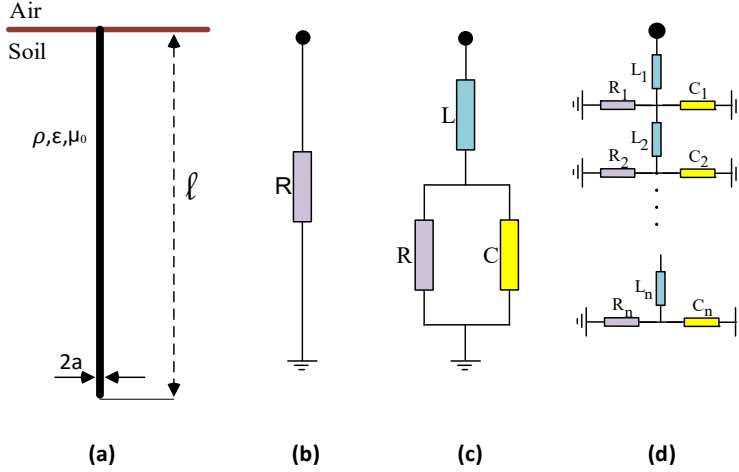
Fig. 4 Vertical ground electrode. (a) Geometry, (b) representation with the resistive model (low frequency), (c) representation with lumped RLC model (high-frequency), (d) uniform representation with RLC distributed parameter (high-frequency) for n segments.

and the second one is given below:

$$R = \frac{\rho}{2\pi l}\left(log\frac{4l}{a} - 1\right) \qquad (\Omega) \qquad\qquad (4)$$

$$L = \frac{\mu_0 l}{2\pi}\left(log\frac{2l}{a} - 1\right) \qquad (H) \qquad\qquad (5)$$

$$C = 2\pi\varepsilon l\left(log\frac{4l}{a} - 1\right) \qquad (F) \qquad\qquad (6)$$

Here, l is the length of the electrode. ρ, ε, and μ_0 are soil resistivity, relative permittivity, and air permeability, respectively [67]. In the circuit method, the grounding conductor is equivalent to a parallel capacitor and resistor connected to the series inductor. Fig. 4 shows the vertical electrode, resistive, lumped RLC, and distributed RLC models. It is assumed that $l \gg a$. The developed image techniques (see [67], [33], and [76]) have been proposed in the studies to deal with the GS modeling challenges and to find opportunities to create the RLC equivalent model in a simple way that is able to compare or check the results from the Full-wave

approaches. The exact image theory uses many RLC circuit models. Furthermore, these models can give precise results only within the quasi-static approximation. Hence, this method's time-consuming is the major restriction factor for modeling large GS [77].

The circuit method, in which finding the transient behavior of GSs is replaced by solving equivalent circuits, is easy to understand. Non-linear soil ionization behavior can also be added to this model, but the biggest drawback of this method is that it does not consider the wave propagation delay [78].

Generally speaking, the restrictions of the modified image model result in severe obstacles for investigating GS buried in layered soil structures in lightning transient studies. These defects become more articulated while considering the full-wave modeling of substation GS to be connected with electromagnetic transient platforms in the time domain simulations [77].

1.3.2 Transmission Line Method (TLM)

To evaluate transient responses of GSs, TLM is also employed [79],[80],[81]. The TLM is built on the quasi-static approximation, which presumes that the electrical system size of the GS is vastly less than the smallest of the passing current wavelength. The soil is assumed to be linear and half-space specified with constant relative permittivity and resistivity [82]. The ground electrode is modeled by its electric parameters and geometry. Presume the ground electrode is divided into n small pieces. Since $n \to \infty$, all segments are expressed by the RLC equivalent circuit. In this method, it is assumed that the electrodes are perfectly conducting wires [51]. The TLM parameters (per unit) can be computed as below:

$$G' = \frac{1}{Rl} \qquad [S/m] \qquad (7)$$

$$L' = \frac{L}{l} \qquad (H/m) \qquad (8)$$

$$C' = \frac{C}{l} \qquad (F/m) \qquad (9)$$

Here, RLC parameters can be obtained using (1) to (6).

The mutual coupling between the nearby fictitious doesn't consider in the TLM, so it could cause inaccuracy for calculating the GS model at high frequencies with

scaling up the problem dimensions like a large substation grounding grid [51], [83]. In the TLM, the ground electrode is presumed to be a transmission line component. The per unit resistance, inductance, and capacitance based on the length of the electrode can be calculated with analytical equations with maximum approximations [84]. This method ignores the mutual electromagnetic interface between the GS segments, which creates errors as presented in [85]. The assumption is that the boundary is selected so far from the electrode, which models the point that injected lightning current in the GS does not have a return path [85].

1.4   Full-Wave Methods of Grounding System Modeling

In this section, a summary of the most significant electromagnetic numerical approaches and their progress is reviewed. In the last few years, utilizing computers, the circuit, and modified image theory have been developed with more complexities to GSs modeling. Generally, the numerical methods spend more running time than quasi-static approaches [86]. Although, due to inherent quasi-static assumptions, the results obtained with this method do not agree well with the measurements at the high frequencies [76], and precision in high-frequency ranges depends on the size of electrodes and soil electrical parameters. It is necessary that the electrode size is smaller than the wavelength in the soil for this method to be valid [60], [87]. The application of the full-wave approach in GS modeling is an exciting area of study that considerable researchers have dealt with the topic. It has commencing frequently arisen in the technical literature. Finding a suitable strategy for simulation to evaluate the GS transient performance is an interesting concept from the engineering point of view, considering the full-wave field is saturated with methods, including electromagnetic field theory based on Maxwell's equations [45]–[50]. Regardless, when complex problems involve complicated equations, as is the case of complex GSs, numerical techniques effectively solve the GSs problem.

On the other hand, the development of high-speed computers is the other cause of applying numerical methods for GS modeling with more complexity and at higher frequency ranges. The ground electrode's dynamic behavior can be easily interpreted by full-wave numerical techniques [88]. Presently, a considerable improvement has been seen in the field of full-wave methods to obtain the GS model with more accuracy based on Maxwell's equations. This is mainly because

of human safety, the importance of GSs in transient overvoltage studies, and electromagnetic compatibility (EMC) concerns [22], [61], [89], [90].

Furthermore, the full-wave methods can provide a 3-D solution to calculate the current distribution along the ground electrodes and the corresponding input impedance of the system compared to quasi-static techniques. Such methods can numerically drive Maxwell's equations which are categorized in the forms of integral equations (IE) or differential equations (DF) for the specific boundary conditions [86]. On the other hand, for the modeling of GSs, frequency-domain methods have been successfully employed [86].

As we discussed earlier, in the static theory, the GS is an equipotential surface, and the voltage differences between GS terminals and their connected equipment are not taken into account. In realistic cases, the induction of electromagnetic fields creates a voltage across any two terminals, which is larger than zero. These reference voltage inequalities may be a reason for the electrical system's failure [26]. Although, full-wave methods are time-consuming depending on the size of GSs [51].

1.4.1   Method of Moment (MoM)

Harrington presented the MoM in numerical electromagnetics [91] in the frequency domain. The electromagnetic fields can be solved numerically by using integral equation (IE) techniques that have been shown as practical tools. The application of MoM for solving IEs is particularly advantageous. In this regard, different MoM forms are developed based on the use of diverse basis functions, weighting functions, and discretization strategies. The thin-wire estimation often is used for predicting current distribution along buried ground electrodes. Accordingly, the electrodes of the GS can be considered thin wires. This assumption can assist in lessening problem dimensions of integral from the surface (2-D) to the line (1-D). Also, the volume IEs can be utilized in the MoM in which the unknown parameters describe by volume currents in the 3-D coordinate system, which is more time-consuming. The use of various basis functions and the discretization process, as well as the use of modified image theory, have given a new version of MoM [92].

Implementing the Moment method process usually involves the following steps:

- ➢ Inference of an appropriate IE
- ➢ Discretization of an IE suitable for matrix equations using basis functions and test or weight functions
- ➢ Estimation of matrix elements
- ➢ To solve the matrix equation and obtain the unknown parameters

The proper surface segmentation based on the geometry of the problem is the most influential factor performed using triangular patches. It is also required to take the relation between segment size and wavelength into account. The preliminary expression of this method is an IE, utilizing Green's functions (GFs) in the free space.

The most important advantage of this method is the high accuracy and the lowest possible assumption, although working with this method is complicated. Another disadvantage, given that it is in the frequency domain is the inability to model the non-linear behavior of soil ionization.

1.4.2   Finite Element Method

The finite element method (FEM) is utilized for solving partial differential equations (PDEs) as another computational approach. This method has remarkable adaptability to define problem geometry in various media. The geometrical domain of a boundary value of the buried ground electrode is discretized utilizing finite elements [93]. This method also converts the PDEs into a matrix equation like MoM, considering the minimization of system energy based on the physical concept. The simulation can implement either in the time or frequency domain. But FEM is mainly applied to frequency domains [94]. This method is straightforward in considering the soil electrical parameters and accurate characteristics of the used material for the GSs [36].

The model used in FEM includes information about the geometry of GS, excitation, and boundary conditions (potential at the point of injection equal to 1 p.u. and at remote terminal is set to zero. The FEM analysis consists of 4 preliminary steps [95]:

- ➢ Discretization of the solution region into sub-regions or elements, usually in the form of triangles or rectangular
- ➢ To obtain field equations at the levels of each element

> ➢ To assemble all the parts in the solution area using the equation matrix
> ➢ To solve the resulting equation system

Modifications can be made to the mesh elements produced to match the dimensions below the relevant area. The electric and magnetic fields at the edges of the parts are calculated. FEM can also be applied to the Helmholtz wave vector equation, which is directly derived from the Maxwell equations.

One of the disadvantages of this method is that it requires the study of a large area (considerably larger than the ground meshes) to be able to model the remote ground (boundary conditions) as a zero voltage. As a result, the solution domain must be constrained using the domain end boundary [96], [97].

One of the most critical advantages of FEM is its high flexibility in discretizing the GS and the media. This model also can consider non-linear soil ionization behavior in simulation. [96].

The GS modeling applies the solution of Laplace's equation (10) to compute its current field using scalar potential $\emptyset$, as below [34]:

$$\nabla([\tfrac{1}{\rho}]\nabla\emptyset) = 0 \tag{10}$$

Here, $\rho = \sigma^{-1}$ is the resistivity of soil and $\emptyset$ is electric scalar potential. The problem boundary conditions can be expressed as follows:

$$\emptyset = 0, \qquad \text{(at infinity)} \tag{11}$$

$$\nabla^2\emptyset = 0, \qquad \text{(on the surface of the soil)} \tag{12}$$

By using the standard weighted residual method, the 3-D finite element equations can be computed as below:

$$\sum_e \iiint (\nabla N_i^e)\, \sigma_s^e\, (\nabla\emptyset_s^e)\, d\theta = 0 \,, \; \emptyset = \sum_{j=1}^{m} N_j \emptyset_j \tag{13}$$

Where N is the interpolation function and θ denotes 3-D finite element volume. Finally, the FEM equation can be expressed as:

$$[A]\{\emptyset\} = \{B\} \tag{14}$$

1.4.3   Finite-Difference Time-Domain (FDTD)

In the time domain simulation, one of the considerably prevalent approaches to address GS modeling is FDTD. This approach is based on the discretization of Maxwell equations, directly in time and space, and the division of the studied volume into individual cells. Usually, the mesh produced for such cells must be uniform, so the lattice density is determined by the smallest component studied. The basic idea of this algorithm is established by using the finite difference method in the differential form of Maxwell equations [93]. Then, the frequency domain response can be obtained using the Fourier transform. Ease of conversion between time and frequency domains is one of the attractions of using this method [95].

This method is numerically stable and is suitable for investigating the response of GSs with unusual geometry and the non-linear environment when exposed to high-frequency transients. FDTD mesh elements are made up of rectangular cells, each edge of which is connected to an electric field. In this method, it is possible to determine different materials for each edge of the mesh. FDTD is a time-step process in which electric and magnetic fields are calculated at each time step. These fields are propagated in the mesh and represent the propagation phenomenon.

Table 1. Numerical approach benchmark [86].

Approach	Complexity	Understanding	Accuracy	Impementation procedure	Required RAM
FDTD	Simple	Easy	Reasonably accurate	simple	small
MoM	Complex	hard	Reasonably accurate	Complex	large
FEM	Complex	Very hard	Reasonably accurate	Complex	very large
TLM	Simple	Very easy	Non-accurate	simple	large
Quasi-Static	Simple	Very easy	Non-accurate	simple	small

Due to this, FEM and FDTD require to segmentize the whole media of simulation, but the MoM will only require segmentation of the conductor based on thin wire approximation. This is a benefit of utilizing MoM for the modeling of the transient

36

behavior of GSs, which provides a practical approach. Therefore, the MoM is employed in this research for numerical modeling. Crucial benchmarks related to numerical approaches discussed previously for the GSs modeling are expressed in [86].

Generally, one of the benefits of the electromagnetic estimation techniques, over the quasi-static techniques, is that they let a stable full-wave approach for the distribution of current on electrodes and resultant electromagnetic fields in three dimensions, but they are computationally pricey. All numerical methods are accurate reasonably at high frequency as well.

1.5   Power System Transient Analysis

A power system transient occurs when there is a variation in normal operating conditions. Short circuit faults, lightning currents, and significant changes in the loads or system configuration can lead to transients in the power system. The worth of their investigation is primarily owing to the consequences of transients that influence the performance of the system or the damage they may inflict on installations. The mentioned transients can create overcurrent or overvoltage that can increase the heat in the elements or break down the insulation, respectively.

After an overcurrent fault occurs, the faulty section should be immediately disconnected from healthy parts of the grid using protection relays in order to protect the personnel/apparatus. It is possible to protect components against overvoltage by choosing an acceptable insulation level and/or installing a surge arrester to limit the transient overvoltage.

As a first step toward setting sufficient protection against transients, it is essential to understand their source, analyze the worst-case scenarios, and estimate the maximum overcurrent and/or overvoltage values they may create.

The process of transient analysis can generally be broken down into the following steps [96]:

> ➤ To determine the area of the power system that is needed to be incorporated in the simulation to be investigated.
> ➤ To select the best model for every element incorporated in the analysis area.

➤ To execute the simulation utilizing one of the methods available for evaluation of the outcomes.

1.6   Dynamic Behavior of the Grounding System

The behavior of GSs is understandable in the low-frequency range, and straightforward techniques for their implementation are broadly proposed [98]. On the other hand, the performance of GSs can be completely distinct, and occasionally, it might significantly influence the protection and safety effectiveness when subjected to lightning. Even though the amount of research in this field, there has yet to be a substantial conclusion on how to use current wisdom to design real GSs with excellent performance in the high-frequency range [99].

It is clear that after the current is discharged into the soil via a brief portion of the ground conductor close to the injection terminal, the pulse propagation at a finite speed through the ground electrode causes extreme values of voltage at the excitation point. The wave speed is not constant, and it is time-dependent and decreases with it [75].

The soil resistivity has a considerable impact on the propagation of the lightning wave. For example, in [22], different resistivity of soil (10, 100, 1000) are examined to check the impact of soil resistivity on wave propagation speed and distribution of GPR at the injected terminal. It can be seen that for the mentioned soil resistivities, at the first 0.5 μs the speed is respectively about 0.05 c, 0.15 c, and 0.33 c which c is the speed of light. The maximum GPR values are 3.5, 14.5, and 63 kV, respectively, while the pulse current, $1\ kA$, $^1/_{50}\ \mu s$, is injected to the left end of a 60 m horizontal ground electrode [22].

In the time domain simulation, two-time periods can be determined. The first period (fast transient) and the second period (slow transient) occur before and immediately after the wave has arrived at the other side of the horizontal conductor. The first period is described by non-uniform potential distribution, and the next one is denoted by an almost uniform distribution [22]. The fast-transient duration relies on both the length of the ground conductor and the speed of wave propagation which can indicate the dynamic characteristics of GS electrodes. The fast-transient duration decreases with the soil resistivity increasing (50 μs, 15 μs, and 5 μs). The second period usually has a larger section of the total duration of the lightning current than first period.

Numerous definitions of the GS impedance in the time or frequency domain have been developed over the past several years. The expressions of the low-frequency resistance (Frequency independent model), transient impedance (time-domain model), and harmonic impedance (Frequency-dependent model) are presented below. A low-frequency (R_{LF}) resistance or DC resistance is the fundamental quantity that describes GS's performance at low frequency. This value is a frequency-independent and can be determined as:

$$R_{LF} = \frac{V}{I} \tag{15}$$

Here, V is the voltage difference between the injection and remote terminal (V=0), and I is the impressed current at the ground terminal.

To analyze GSs quickly, empirical formulas for GSs with unique structures have been developed. Engineers and designers have access to these expressions through international standards. Using these expressions, grounding grid resistance and safety factors such as step and touch voltages can be obtained for the network while analyzing a grounding grid. Among the various formulas, the formula given in the IEEE 80 standard is as follows:

$$R_{LF} = \frac{\rho}{4}\sqrt{\frac{\pi}{A}} + \frac{\rho}{G} \tag{16}$$

where G is the entire length of electrodes inserted in the earth with a resistivity of ρ and A is the GS area [100]. Transient impedance, $z_g(t)$, is given in (17).

$$z_g(t) = \frac{v(t)}{i(t)} \tag{17}$$

Here, v(t) and i(t) are, respectively, the voltage difference between the injection and remote terminal (V=0) and impressed current. The transient impedance includes the behavior of the GS during the fast and slow transients in the time domain. The harmonic impedance, $Z(s)$, is defined in (18).

$$Z(s) = \frac{V(s)}{I(s)} \qquad\qquad s = j\omega \tag{18}$$

Here, in the frequency domain, $V(s)$ is the vector of steady-state harmonic voltage between the excitation and remote terminals. $I(s)$ is the vector of the impressed current. The frequency range is from zero up to several MHz.

Fig. 5 presents the harmonic impedance and transient impedance of a 3-m vertical electrode. The relative permittivity is set to 10. The electrode is placed in the earth with a resistivity of 10 Ωm. The lightning current is characterized by a peak value of about 12 kA, steepness of 40 kA/μs, and time of zero to peak of about 0.8 μs (see Fig. 5(a)). It can be seen that the value of low-frequency resistance is about 3Ω. It has appeared in the low-frequency range in Fig. 5(b) and the slow transient period of Fig. 5(c).

In the low-frequency range (0 – 120 kHz), the absolute value harmonic impedance is constant and identical to the low-frequency resistor (3 Ω). In the high-frequency range of up to 10 MHz, the vertical ground electrode behaves as an inductor. Its value is larger than low-frequency ones: It increases with increasing frequency, being frequency-dependent. The high-frequency behavior of the ground electrode can also become capacitive. It depends on soil resistivity and the length of the electrode [101], [102].

Generally speaking, the harmonic impedance of GSs can be used to determine the behavior of GS as an inductive, resistive, or capacitive behavior [103],[22]. The criteria of this definition are given in (19).

$$\begin{cases} \text{Inductive} & |Z(j\omega)| > R_{LF} > 1 \\ \text{Resistive} & |Z(j\omega)| = R_{LF} = 1 \\ \text{Capacitive} & |Z(j\omega)| < R_{LF} < 1 \end{cases} \tag{19}$$

The R_{LF} is the low-frequency resistance or DC resistance. It is the frequency-independent part of the GS frequency response.
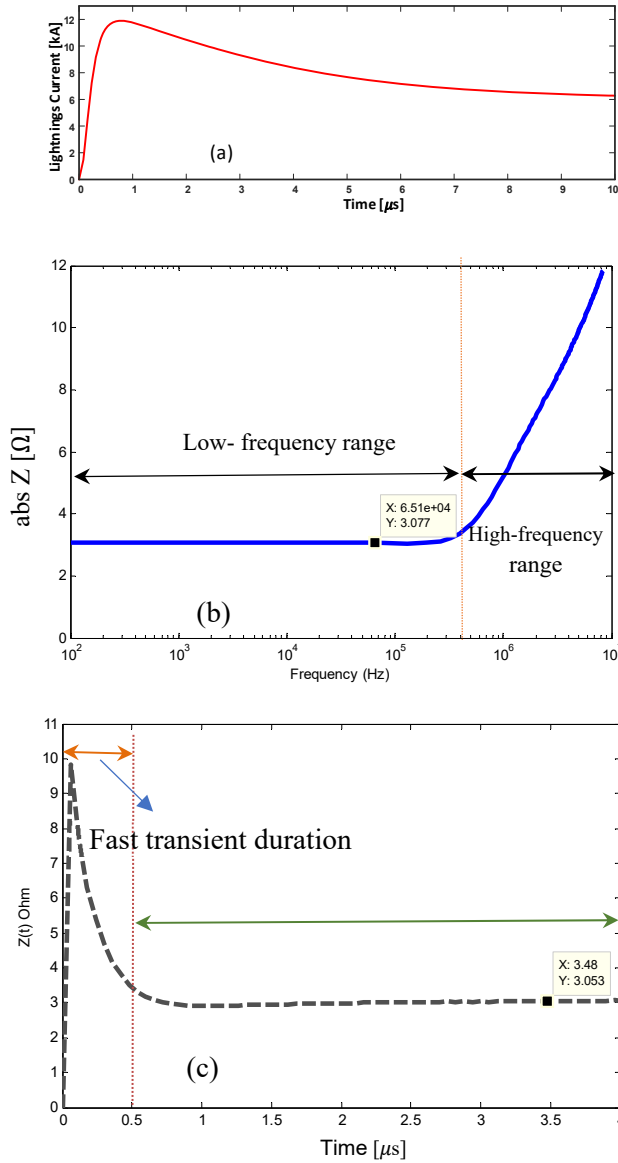
Fig. 5. Ground electrode impedance. (a) Subsequent lightning current, (b) Harmonic impedance, (c) Transient impedance.

1.7 Frequency-Dependent of Soil Electrical Parameter

In general, soils are highly complicated. Many factors like water and salt contents, dimensions, form, structure, and type affect soil behavior when exposed to lightning [104]. From 1940 to 1970, Smith-Rose [105] and Scott [106] have been demonstrated performed a comprehensive investigation on the soil electrical parameters frequency dependency in the specific range of frequency (1KHz-10

41

MHz) based on experimental measurements. The experimental data were employed to express the soil electrical parameters as a function of frequency using fit-curve models. Based on the identical practical inputs from Scott, James H., et al. [106], Smith-Longmire [30], and Messier [107] were extended to new models of soil considering this dependence.

A relatively small number of researchers assessed the frequency-dependent effect of soil electrical parameters on the harmonic impedance. Visacro and Alipio [108], [44] have verified the soil frequency-dependency using experimental field tests for various soils. Then, practical formulas were suggested by Visacro and Portela to express soil electrical parameters as a function of frequency [109]. Moreover, Portela presented another formulation to describe soil electrical parameters in function of frequency, which was mainly applicable to lightning transients using a considerable number of soil samples and structures [110].

Lately, new models have been presented by Visacro and Alipio performed on their field measurements to explain the soil electrical parameters as a function of frequency [25], [90], [93]. The model presented in [86] has the advantage of providing causal results and being based on a more significant number of measurements. In addition, this model was recently suggested in a CIGRE Brochure [112] to be considered in lightning-related studies. There has also been some other research concerning the frequency-dependent effect of soil electrical parameters. Nevertheless, their investigations are restricted to only specific soil [113].

The following three formulations and models, which have been particularly presented for the expression of soil resistivity/conductivity and permittivity as a function of frequency, are taken into account.

- ➢ Smith and Longmire's model [114]
- ➢ Visacro and Alipio model 1 [104]
- ➢ Visacro and Alipio model 2 [108]

1.8 Frequency-Domain to Time-Domain Simulation Interface

Over the past few years, intensive research has been dedicated to electromagnetic transient simulators since they are able to qualify the simulation of complicated power grids and models of installations showing dynamic behavior.

One of the significant parts impacting the performance of OHLs when exposed to lightning strikes is the GS, which has a considerable impact on induced overvoltage, insulation coordination, GPR, and decreasing the stress of voltage. Therefore, precise GS modeling is vital in the lightning protection system design.

The modified and more accurate representations of different elements of the power system, mainly above the ground, have been continuously incorporated into current time-domain programs like EMTP-RV, PSCAD, and ATP-EMTP. The improved model of power transformers, tower surge model, lightning arresters, and soil ionization phenomena at the high-frequency regime are added to these platforms. Traditionally, in the mentioned time-domain simulators, GSs are expressed as a simple or DC resistance [22]. Nevertheless, there is not a devoted model for modeling vertical, horizontal, or grid shape GSs at a broad frequency range. The adequacy level of the used models for the GSs has not been achieved as same as for other power systems elements.

Several researchers have proposed mathematical approaches to interface the built accurate models of GS to time-domain simulators transient solvers [66], [115]. To circumvent this issue, several techniques are proposed to create the link between the exact model of GSs and the existing time-domain solvers and solve the problem of lack of full-wave capability in such transient solvers [116]. Once the frequency response of the GSs is calculated, to obtain the GPR or transient overvoltage (for example, at the injected terminal or across the insulator string of the OHLs), it is required to convert the results in the frequency domain to the time domain. This way, they can be connected with electromagnetic transient (EMT) solvers.

In the frequency domain, the linear systems can be fitted with rational functions by the vector fitting method (VFM), which is widely employed. This mathematical technique utilizes to calculate the pole-residue model of the impedance/admittance matrix. It is also a powerful extension of the Sanathanan–Koerner iteration [117]. This method uses the rational basis functions and pole relocation instead of polynomials and weighting, respectively [118], [119].

One of the main benefits of using VFM is that it provides a fitting with insured stable poles. These poles can be used for systems with multiple ports, for instance, large substations. The VF algorithm involves iteratively moving an initial pole set to improved positions.

When the harmonic impedance of GS can be defined as a function of frequency Z(s), the aim is to estimate a harmonic impedance Z(s) using a rational function in the pole-residue form [119].

$$Z(s) = \sum_{m=1}^{N} \frac{r_m}{s - a_m} + \mathbf{D} + se \tag{20}$$

Here, the expressions d and e can be optional. r_m is residue matrix. The procedure of this method is discussed in [119]. In the first step, by computing the least-squares error of (21), the poles of the frequency response of $Z(s)$ which is given by (21).

$$\sigma(s)Z(s) = p(s) \tag{21}$$

$$\sigma(s) = \sum_{m=1}^{N} \frac{\widetilde{r_m}}{s - q_m} + 1 \tag{22}$$

$$p(s) = \sum_{m=1}^{N} \frac{r_m}{s - q_m} + d + se \tag{23}$$

Here, $p(s)$ and $\sigma(s)$ are vector and scalar terms, respectively. The q_m is the starting (guessed) pole. The poles can be identified as below:

$$\{a_m\} = eig\left(\mathbf{A} - \mathbf{b}, \mathbf{c}^T\right) \tag{24}$$

Here, the matrixes **A**, **b,** and $\mathbf{c}^T$ are a diagonal including the starting poles, a column vector one, and a row vector including $\{\widetilde{r_m}\}$. After pole identification using an iterative manner, the matrix of $\{r_m\}$ can be calculated by solving the least-squares problem [119].

To use the computed model in the form of a state-space model, the fitted harmonic impedance can be presented below:

$$Z(s) = \mathbf{C}(s\mathbf{I} - \mathbf{A})^{-1}\mathbf{B} + \mathbf{D} + se \tag{25}$$

Another method to implement the frequency response of GS in the time-domain solvers is to identify the equivalent of the circuit that could generate the identical response in the frequency domain. The approach suggested in [120] can be employed to use an RLC equivalent model for the modeled GSs, which is to be implemented in the EMT solvers.

1.9   Tower Surge Impedance

The surge impedance properties of a tower are vital factors in calculating the voltage stress on the tower insulator strings of OHLs and their performances when investigating the lightning response of OHLs [121], particularly in cases of such tall structures. When lightning hits a tower or respective guard wires, electromagnetic waves travel back and onward into the tower, which increases an electric potential across the insulator. This may cause a back-flashover (BF), which may lead to the failure of installations or energy not served.

Analyzing the power system transients requires a precise model of the tower. The techniques for studying towers and computing the surge impedance are categorized into three groups [122], [123]:

- ➢ Analytical method
- ➢ The full-wave method based on electromagnetic field theory
- ➢ Direct measurement method

analytical investigation of the surge impedance of towers is valuable in tower modeling. Nevertheless, the obtained results from simplified models may cause errors when compared to their results for the towers, which have more complexities [124].

The calculation of the surge impedance of towers is carried out both in the frequency and time domains. In the publications, the tower surge impedance is defined in three forms as a function of time given by (26),

$$z_{tower}(t) = \frac{v(t)}{i(t)} \tag{26}$$

Here, $i(t)$ and $v(t)$ are injected current to the tower top and instantaneous voltage values, respectively. This formula can just apply to the resistive model because the waveforms of current and voltage are identical.

The second formula of the transient surge impedance is defined when the ramp waveform of the injected current is subjected to the tower top. It is given by (27)

$$z_{tower}(t) = \frac{v(t)}{\max\{i(t)\}} \tag{27}$$

Consider the moment when the voltage peaks. The ratio of this voltage to the current is the most common explanation of surge impedance in the time domain.

$$z_{tower}(t) = \frac{\max\{v(t)\}}{I} \tag{28}$$

then I can be measured when the voltage is reached the peak value.

All noted formulas in the time domain depend on the injected current waveforms. As a solution to this problem and to determine tower surge impedance, the following frequency-domain definition is provided by (29)

$$Z_{tower}(f) = \frac{V(f)}{I(f)} \tag{29}$$

Here, the $V(f)$ is the measured voltage value and $I(f)$ is the injected current at the tower top. This value relies solely on the tower's electromagnetic characteristics and geometry. Irrespective of the method, such examination strives to either calculate an equivalent circuit model for the OHL tower with results similar to what are measured values. In the analytical methods, there is no way to include information about the tower's details, for instance, all cross arms and elements. Additionally, only the body of the tower can be modeled. There are only a few practical analyses on the existing towers because the experiments need an outage and are expensive. Nowadays, because of the limitations of the analytical and practical techniques, inventing an automated procedure to compute the surge impedance of OHL's tower is acquiring more attention [49], [1].

1.10 Modeling Methods of The Tower

Let us consider a typical double-circuit tower as illustrated in Fig. 6. The following models of the real tower (see Fig. 6(a)) are presented below:
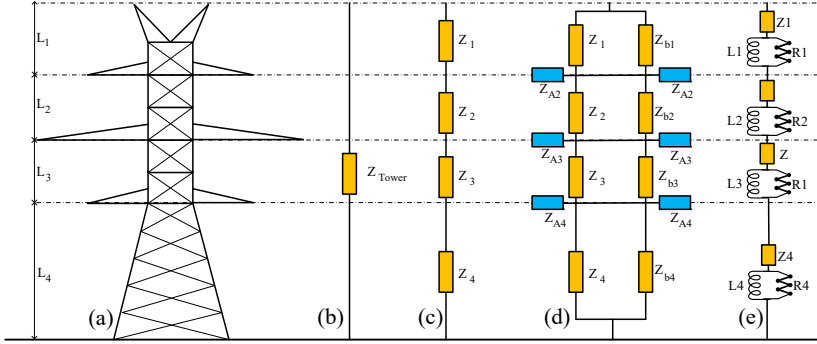
Fig. 6 (a) Tower of OHL (400kV), (b) non-frequency-dependent model with non-lossy vertical element, (c) multi-section model with a loss-free vertical element, (d) multi-section model with loss-free vertical element including bracings and cross-arms, (e) multi-story.

> ➢ Model 1: Non-frequency-dependent model with the non-lossy vertical element

In this method, the surge impedance of the tower is approximated based on the main element of the main body of the tower (the legs and cage). The tower is modeled with a cone and a vertical cylinder [125]. Therefore, by using the electromagnetic field calculations, the impedance properties of the tower are obtained as a function of height. In some papers, the current is injected into the tower top using specific waveforms (e.g., ramp, double exponential forms). These models are only applicable to specific waveforms [126]. Further, these models do not consider the impact of the cross-arms and tower bracing. Fig. 6(b) is presented the mentioned model. The estimated surge impedance of a double-circuit tower is illustrated in Table 2.

Table 2. Parameters of the tower of the 400 kV double circuit (Model 1)

Model	Formula	Z_{Tower} [Ω]
Wagner [127]	$60 \ln \left(\sqrt{2} \dfrac{2L}{a_0} \right)$	205
Jordan [128]	$60 \ln \left(\dfrac{L}{a_1} \right) - 60$	129
Sargent [128]	$60 \ln \left(\sqrt{2} \dfrac{2L}{a_3} \right) - 60$	195
Sargent [128]	$60 \ln \left(\sqrt{2} \dfrac{\sqrt{L^2 + a_0^2}}{a_0} \right) - 60$	160

47

Table 2. Parameters of the tower of the 400 kV double circuit (Model 1)

Model	Formula	Z_{Tower} [Ω]
Menemelis [126]	$35\sqrt{L} + 50$	285
Chisholm [126]	$60\ln\left(\cot\dfrac{\tan^{-1}(\frac{a_0}{L})}{2}\right) - 60$	124
Hara [126]	$60\ln\left(\sqrt{2}\dfrac{2L}{a_0}\right) - 120$	167
IEEE WG [129]	$60\ln\left(\dfrac{L}{a_0}\right)$	142

L is the tower height (L1+L2+L3+L4)
The tower diameter at the bottom, midsection, and top is $2a_0$, $2a_1$, $2a_2$, respectively.
$2a_3$ is the cylinder diameter that equals the tower.

> Model 2: Multi-section model with loss-free vertical elements

In this model, as in the previous model, only the main legs and cage (tower main body) are taken into account for the modeling. But, the separate non-lossy transmission line models (NTLM), as a function of sizes and geometry, are used for the tower surge impedance modeling. The impedance of each segment is calculated by investigating the tower elements [130] (see Fig. 6 (c)). This model is improved by adding the horizontal NTLM (the impedance model of cross-arms) and parallel surge impedance with the main body of the tower in each part (the impedance model of bracing ($Z_{bi} = 9Z_i$)) to the vertical model of the main body of tower (see Fig. 6(d)) [124]. The tower parameters value for the four-story model is presented in Table 3.

Table 3. Tower parameters of the 400 kV double circuit (Model 2)

Model	Z_1 [Ω]	Z_2 [Ω]	Z_3 [Ω]	Z_4 [Ω]
Ametani [50]	95	112	102	87
Ametani [50]	88	108	96	75
Gutierrez [131], [132]	270	253	230	167
	128	120	106	83
Hara [126]	Z_{b1} [Ω]	Z_{b2} [Ω]	Z_{b3} [Ω]	Z_{b4} [Ω]
	1152	1080	954	747

Table 3. Tower parameters of the 400 kV double circuit (Model 2)

Model	$Z_1 [\Omega]$	$Z_2 [\Omega]$	$Z_3 [\Omega]$	$Z_4 [\Omega]$
	$Z_{A1} [\Omega]$	$Z_{A2} [\Omega]$	$Z_{A3} [\Omega]$	$Z_{A4} [\Omega]$
	-	305	282	257

> Model 3: Multi-story model

In this method, the tower is divided into four sections based on the position of the phase arms. In each part, the NTLM is connected to a set of resistance-inductance parallel circuits. The damping resistor R denotes the traveling wave attenuation in the tower. The inductance L refers to the wave tail form and sets the propagation speed of electromagnetic waves in the model. Based on experimental tests performed on existing towers, these models are presented [50],[121]. However, this method is only applicable to towers of these types [133]. The presentation of the multi-story model [127], [128] is shown in Fig. 6(e). The tower parameters value for this model is presented in Table 4.

Table 4. Tower parameter (Model 3)

Model	$Z_1 [\Omega]$	$Z_2 [\Omega]$	$Z_3 [\Omega]$	$Z_4 [\Omega]$	$R_1 [\Omega]$	$R_2 [\Omega]$	$R_3 [\Omega]$	$R_4 [\Omega]$	$L_1 [\mu H]$	$L_2 [\mu H]$	$L_3 [\mu H]$	$L_4 [\mu H]$
Ishi [127]	220	220	220	150	8	20	20	33	3.5	8.5	8.5	14
Yamada [128]	120	120	120	120	9	16	17	43	2.8	5	5.1	12.9
Motoyama [128]	120	120	120	120	5.8	11.7	9.3	26	2.3	4.6	3.7	10.6
Baba [128]	200	200	180	150	20	30	25	25	6	9	15	1.5

> Model 4: Numerical method (Full-wave model)

The propagated traveling wave on high towers from tower top to the bottom cannot be studied by the TLM approach accurately because of the below causes [41]:

> Traveling-wave electric force lines cannot wholly contact the soil surface. Therefore, determining capacitance to the ground is ineffective.
> Magnetic fields produced by the traveling wave cannot wholly penetrate the soil. Therefore, the actual inductance per unit length is distinct from those calculated values based on the quasi-static ones.

Thus, the numerical techniques can be used to compute tower surge impedance with more accuracy by solving Maxwell equations. The numerical methods consist of:

- ➢ Method of Moments (MoM) [122], [134]
- ➢ Finite Element Method (FEM) [120], [135]
- ➢ Finite Different Time Domain (FDTD) [40], [41], [136]

1.11 Research Questions and Objectives

The principal objective of this thesis is to estimate an accurate model for GSs considering layers and frequency-dependent impacts of soil. The application of the exact model of the GS on the transient overvoltage analysis is evaluated for the medium voltage (MV) substation and novel composite pylon towers. The following essential questions and discussions about this study are taken into account:

- Do the quasi-static methods unable to predict the harmonic impedance of GSs at high frequencies?
- How the accurate frequency-dependent model of GSs reduces the over/underestimate of lightning overvoltage/GPR values?
- What are the benefits of using the full wave approach to calculate harmonic impedance during lightning studies?
- To determine what impact the full-wave method would have on insulation coordination design and overall GS performance.
- To assess what considerations are required for the GS modeling at high frequency

Also, the following research queries can be emanated:

Which factors have the most significant influence on the peak value of ground potential rise (GPR)?

- Considering the complexity of the soil structure and geometry of GSs, how can the effect of the grounding electrode length, the soil electrical parameters frequency-dependence, and the layers of soil influence the harmonic impedances and the lightning performance of a GS?
- Considering lightning strokes with a high-frequency content, how can the precise model of the GS of the substation buried in the layered structure

of soil be developed to estimate the transient overvoltage in the frequency domain?

- In case the dynamic behavior of the GS influences the earthing design and performs transient studies, how can the created model be added to the time domain solvers?

The following objectives can be determined for this Ph.D. study based on the questions.

➢ Development of the full-wave method to evaluate the harmonic impedance of a layered grounding grid

In the first objective, to address lightning overvoltage studies in the frequency domain with higher accuracy, a numerical approach will be developed to estimate the harmonic impedance of multi-layer GSs. The expected result of this examination is to present a widely accepted method based on electromagnetic field theory to compute the harmonic impedance. In addition, a numerical technique according to MoM solutions of Maxwell's equations, which is one of the most accepted approaches utilized for GS modeling in a wide range of frequencies, is also investigated. The simulation includes vertical grounding electrodes of various lengths, soil resistivities, and structures such as uniform or layered.

Afterward, a detailed model of a typical tower of a full-scaled HVDC power transmission line is connected to the different models of the GS (e. g., full-wave model, resistive model) to analyze the input harmonic impedance of the tower from the high terminal which the shielding wire is connected. It is evaluated for the proposed integrated model, including the tower and its accurate GS.

➢ Evaluation of soil frequency-dependent impact on the harmonic impedance

To address the influence of soil electrical parameters on harmonic impedance and multi-layer soil structure, the analytical formula-based practical tests, and measurements that define soil electrical parameters as a function of frequency will be used to evaluate these effects on the harmonic impedance and over-voltage values. The selected frequency range will be from DC to 10 MHz. This broad range contains all the frequency content of the first and subsequent lightning currents.

➢ Transient overvoltage analysis for the MV substation considering the multi-layer soil structure

The developed model is employed for calculating lightning transient overvoltage by using the state-space model to connect with the software packages in the time domain. The importance of having a GS accurate modeling is highlighted by comparing it to the quasi-static or resistive model and by calculating the ground potential rise at the injection terminal. In other words, the GS performance is evaluated by injecting lightning currents in a buried grounding electrode.

A specific case study is an influence on lightning overvoltage of full-wave modeling of substation GSs. It is assumed that the substation GS is a multi-terminal system, and different soil structures are considered when calculating harmonic impedance. All substation components are modeled in the EMTP.RV platform. To calculate the transient overvoltage, an exact model of the substation GS in the frequency domain is transferred into the time domain solvers.

> ➤ The exact model of GS application on the lightning performance of the Pylon composite tower

In this part, the application of an accurate model of the GS is used to compute and obtain the results with fewer over or underestimations. It is assumed that the tower footing GS of the pylon tower is connected to the single and multilayer soil structures. With vector fitting techniques, the voltage across the insulator strings and GPR value are calculated based on the accurate model of the GS calculated in the frequency domain using MoM and transferred to time domain platforms like PSCAD.

In summary, as explained, the lightning overvoltage analysis (transient overvoltage (TOV)) is an important aspect of insulation coordination study, system design, availability, and maintenance strategy which are dependent on the dynamic behavior of GSs. Therefore, insulation coordination studies, lightning performance, and back-flashover evaluation are not possible unless the exact behavior of the GS is correctly considered.

To have a better identification of GS behavior that the used time domain software platforms for the lightning transient overvoltage analysis cannot fulfill this requirement, the accurate model of the GS grid is developed based on the full wave numerical method in the frequency domain. In the proposed model, the impacts of the earth layer's structure, the electrical parameter of the soil, and the frequency dependency of the soil's electrical properties are taken into account to address the existing research gaps. Then the tower-integrated model including its

connected grounding grid is proposed to provide the input harmonic impedance. The surge impedance of the tower is included in the computed harmonic impedance in the frequency domain considering an accurate model of the GS.

The GS of a wind turbine (WT) is made of very long vertical electrodes, horizontal electrodes, and rings. Various WT manufacturers have various requirements for WTG ground grid layout and resistance. Most WT manufacturers require RLF≤10.0Ω [73]. It is worth noting that the WTs with tall structures and blades attract more lightning strokes. Also, the long vertical of the ground electrode may reach the second or third layer of soil with different soil resistivity. In this condition, the significance of our research contributions in the light of practical use can be more paid attention to base on the obtained results.

The other application of the proposed model of the GS is the transient overvoltage analysis of the MV substation considering an accurate model of the GS. In this model, the layered soil structure and frequency dependency of soil electrical parameters is considered. These are not taken into account simultaneously before and the substation GS was modeled via a very simple resistive model which is valid for the slow-front transient events such as single phase to ground fault (L-G) (power frequency faults).

Finally, lightning performance, design, and optimization studies on the novel composite pylon are performed concerning the frequency-dependent model of the tower footing GS including layered soil, and the frequency-dependent model of the soil GS which was modeled via a very simple resistive model previously.

1.12   Thesis Restrictions

Numerous factors influence the harmonic impedance or even the transient impedance. Concerning the harmonic impedance that will be calculated, ionization impact is not considered in this research; however, this may impact the GS's impedance. Also, to estimate the GS harmonic impedance, the vertical electrode like a simple power transmission is simulated, and the horizontal grounding electrode is not considered.

Regarding the substation transient overvoltage analysis, only subsequent lightning stroke is considered as a system input. The subsequent lightning stroke has a higher frequency content and is very useful to show the impact of modeling the ground.

However, it should be noted that the first lightning current with a higher amplitude could have also been included.

A crucial part of the study is the model verification of the multi-layer GS, which is performed using FEM. The field and practical measurement are not considered in this study.

1.13   Thesis Outline

The findings and outcomes of the Ph.D. thesis are discussed in this Ph.D. research based on a collection of papers published during the Ph.D. period. The dissertation consists of two main sections. The first part presents a report based on the published articles. The second part of the research includes papers (J1-J6) and (C1-C6) already is published or are under review. The structure of this research is shown in Fig. 7 and prepares a framework for how the scope of the *Report* is linked to the *Publications*. The results of this study are presented in six chapters.

On the Frequency Dependent Model of Grounding Systems for Power System Transient Analysis

Selected Publications

Ch. 1 Introduction

Ch. 2

Frequency dependent model of grounding system

Soil structure effect on the harmonic impedance of ground electrode

Results and outcomes

Publications: J1, J2, C3, and C6

Ch. 3

Integrated model of tower and grounding system harmonic impedance

Full-wave modeling effects on the Lightning performance of power transmission towers

Results and outcomes

Publications: J1

Ch. 4

Effect of frequency-dependent soil models

Frequency dependent effect of soil electrical parameters on the harmonic impedance

Frequency dependent effect of soil electrical parameters on the GPR

Results and outcomes

Publications: C2 and C5

Publications: C1

Ch. 5

Grounding System Frequency-Dependent Model: Applications for Power System Transient Analysis

Frequency dependent model of large grounding system

Novel Composite Pylon Tower

Results and outcomes

Publications: J2

Publications: J3, J4, J5, J6 and C4

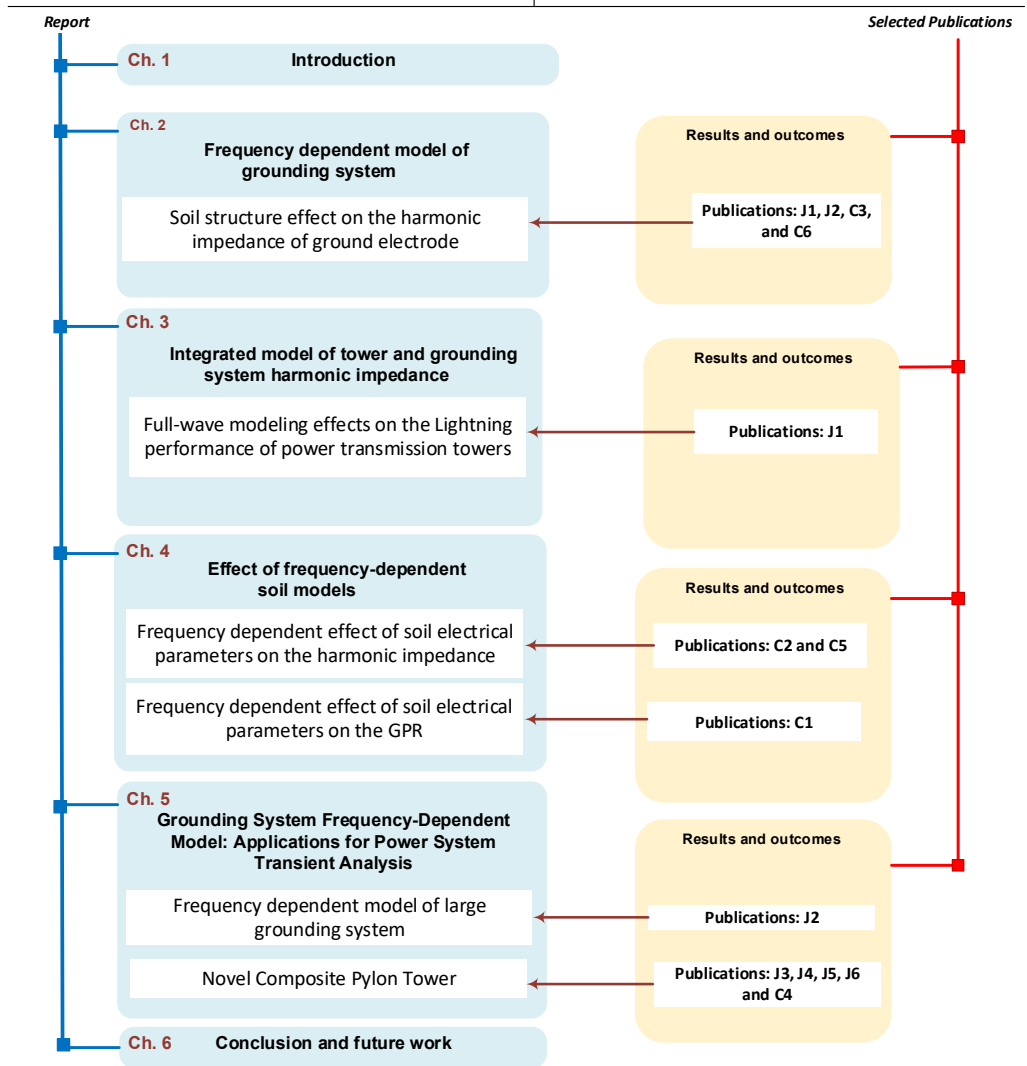**Ch. 6** Conclusion and future work

Fig. 7. Chronology of the thesis and the published papers.

An abstract of the content of each chapter in the first part of the thesis is given as follows:

Chapter 1: This chapter contains the introduction of the Ph.D. study, including the background of the dissertation subject and the study's primary purposes. It initiates with the importance of the grounding system in the transient analysis. After that, it discusses the challenges of GS modeling and the frequency-dependent impacts on harmonic impedance. The importance of soil structure and the frequency dependency of its electrical parameters are explored, and various techniques to achieve this feature are introduced. Different methods are introduced, and their feasibility for GS modeling (GSM) is discussed. The published papers are listed in this chapter. The chapter is summarized by the project goals and outline of the dissertation.

Chapter 2: In this chapter, the MoM for the investigation of GSs is briefly described. Vertical ground electrodes with different geometry buried in soil with different resistivity and layers are selected to investigate the effect of these parameters on the precision of the full-wave model. Moreover, the GPR values corresponding to the mentioned cases are calculated. The main parts of this chapter have been discussed in the papers **J1, J2, C3,** and **C6**.

Chapter 3: In this chapter, a systematic procedure based on the numerical full-wave technique is presented. The integrated model's harmonic impedance is computed directly, which includes the tower and its GS. Various level of detail for a full-scaled tower is considered in the model. The In the frequency domain, the harmonic impedance is calculated considering the accurate model of GS. The obtained results are compared to the predicted model of the towers using TLM. The main parts of this chapter have been discussed in the journal paper **J1**.

Chapter 4: This chapter presents the frequency-dependent effects of the electrical soil parameters on the harmonic impedance. Different formulations for this dependency are used. The GPR value is computed when GS is subjected to lightning current. Several soil structures (uniform and multi-layer) and different lengths of vertical electrodes are taken into account. The results are compared when the soil electrical parameters of the GS are frequency-independent. The main parts of this chapter have been discussed in papers **C1**, **C2**, and **C5**.

Chapter 5: In this chapter, the application of the grounding grid full-wave modeling is evaluated. First, the GS of a real MV substation is assumed to predict the frequency response of the GS. The MoM is developed to model the large substation GS. The transient overvoltage study is performed and the lightning and switching transient voltage are calculated. Then, a detailed analysis of the influences of substation grounding soil structure on the power system transients is discussed. The MoM solution is applied. This study is done for two soil structures: 1) single-layer and 2) two-layer structures. The effects of both soil structures on the overvoltage values are examined. The VFM is employed to develop an appropriate link between obtained multi-terminal harmonic impedance and time-domain platforms. All power system equipment above the ground is modeled in the EMTP.RV.

Second, this application is tested for the novel composite pylon to perform lightning performance analysis. The impact of a precise model of GS on the insulation coordination design is discussed. The full-wave approach is used to model the vertical grounding electrode and the vector fitting technique is employed to connect the accurate GS model to the pylon tower. The state space model is used to transfer the model from the frequency domain into the time domain simulators. The outcomes are assessed to indicate the importance of the soil layer's necessities in the substation design and lightning protection system. The main parts of this chapter have been discussed in the papers **J2**, **J3**, **J4**, **J5**, **J6,** and **C4**.

Chapter 6: The Ph.D. thesis is summarized, and the future path of this research is outlined.

1.14   Scientific Contribution

- ✓ Multi-layer GS modeling using an accurate full-wave approach is performed
- ✓ Different soil frequency models are involved in the multilayer GS, and the respective influences are investigated on the harmonic impedance and GPR values.
- ✓ The proposed integrated model of the tower and its grounding grid to compute the input harmonic impedance based on a multi-layer media concept using a full wave technique.

- ✓ Proposed full-wave modeling application for MV substation GS to predict transient overvoltage.
- ✓ The proposed model is connected to the novel composite pylon to perform detailed electrical design and insulation coordination.

1.15 List of Publications

The results of the Ph.D. study have been published in several different forms, namely articles in journals (Jx) and conference papers (Cx), as shown below. Most of them are utilized in the Ph.D. thesis.

Publications in Refereed Journals:

J1. **M. Ghomi**, H. Zhang, F. Faria da Silva, C. Leth Bak, and K. Yin, "*Integrated Model of Transmission Tower Surge Impedance and Multilayer Grounding System Based on Full-wave Approach*," Journal of Energy Power System Research, Elsevier 2021 [1].

J2. **M. Ghomi**, F. Faria da Silva, Amir abbas Shayegani Akmal, and C. Leth Bak, "*Transient Overvoltage Analysis in the Medium Voltage Substations Based on Full-Wave Modeling of Two-layer Grounding System*," Journal of Energy Power System Research, Elsevier 2022 [2].

J3. H. Zhang, **M. Ghomi**, Q. Wang, F. Faria da Silva, C. Leth Bak, K. Yin, and H. Skouboe, "*Comparison of Backflashover Performance between a Novel Composite Pylon and Metallic Towers*," Journal of Energy Power System Research, vol.196, pp. 107263, July, 2021 [3].

J4. K. Yin, **M. Ghomi**, Q. Wang, H. Zhang, F. Faria da Silva, C. Leth Bak, Q. Wang, H. Skouboe, "*The design and optimization of the down-lead system for a novel 400 kV composite pylon*," IEEE Transactions on Power Delivery 2022 [4].

J5. K. Yin, **M. Ghomi**, H. Zhang, C. Leth Bak, F. Faria da Silva, Q. Wang, "*Lightning transient response of bifurcation structure pylon and its empirical expression with high accuracy and general application*," International Journal of Electrical Power & Energy Systems, 2023 Status: accepted [5].

J6. H. Zhang, **M. Ghomi**, Q. Wang, F. Faria da Silva, C. Leth Bak, and K. Yin, "*Backflashover Performance of a Novel Composite Pylon with External Grounding Down-lead Modeled in Dynamic Surge Impedance*

Considering Corona Effect," IEEE Transactions on Power Delivery, 2023
Status: Under review [6].

Publications in Refereed Conferences:

C1. **M. Ghomi**, C. Leth Bak and F. Faria da Silva, "*Frequency Dependence of Multilayer Soil Electrical Parameters: Effects on the Ground Potential Rise*," in 35th International Conference on Lightning Protection (ICLP) and XVI International Symposium on Lightning Protection (SIPDA), 2021 [7].

C2. **M. Ghomi**, C. Leth Bak and F. Faria da Silva, "*Frequency Dependence of Multilayer Soil Electrical Parameters: Effects on the Input Impedance of Grounding Systems*," 16th International Conference on AC and DC Power Transmission, IET event ACDC 2020 [8].

C3. **M. Ghomi**, HR. Mohammadi, HR. Karami, C. Leth Bak, F. Faria da Silva, and H. Khazraj, "*Full-wave modeling of grounding system: Evaluation the effects of multi-layer soil and length of electrode on ground potential rise,*" International Conference on Power Systems Transients, IPST, pp. 1-6, 2019 [9].

C4. K. Yin, **M. Ghomi**, F. Faria da Silva, C. Leth Bak, Q. Wang, H. Zhang, H. Skouboe, "*Lightning performance and formula description of a Y-shaped composite pylon considering the effect of tower-footing impedance,*" in 35th International Conference on Lightning Protection (ICLP) and XVI International Symposium on Lightning Protection (SIPDA), pp. 16, 2021 [10].

C5. K. Yin, **M. Ghomi**, F. Faria da Silva, C. Leth Bak, H. Zhang, Q. Wang, "*The Effect of Frequency-Dependent Soil Electrical Parameters on the Lightning Response of a 'Y' Shaped Composite Pylon for 400 kV Transmission Lines*," in 22nd International Symposium on High Voltage Engineering, pp. 2046 – 2051, Nov. 2021 [11].

C6. H. Zhang, **M. Ghomi**, Q. Wang, F. Faria da Silva, C. Leth Bak, K. Yin and H. Skouboe, "*Evaluation of Lightning Backflashover Rate of a Fully Composite Pylon using Monte Carlo Method on Environmental Factors*," proc. of IEEE Power &Energy Society General Meeting (PESGM) 2022, Denver, Colorado, 2022, Status: Accepted [12].

Collaboration papers:

P1. H. Khazraj, B. Yousefi Khanghah, P. Ghimire, F. Martin, **M. Ghomi**, F. Faria da Silva, C. Leth Bak, "*Optimal Operational Scheduling and Reconfiguration Coordination in Smart Grids for Extreme Weather Condition*," Journal of IET Generation, Transmission & Distribution 2019 [13].

P2. R. Rezvanfar, H. Ghasemi, M. E. Mosayebian, **M. Ghomi**, F. Faria da Silva, C. Leth Bak, "*Optimal placement of phase shifting transformers based on MADM method: the considering system performance indices*," CIGRE symposium Aalborg 2019.

Chapter 2.   Frequency-dependent Model of Grounding System

2.1   Abstract

In this section, based on J1, J2, C3, and C6, the methodology of GS calculation in the frequency domain is discussed. The numerical method, MoM, as a full-wave technique, is used to find the frequency-dependent impedance of GS for several soil structures. The harmonic impedance of the vertical electrode with different lengths buried in the various soil structures/resistivities, including uniform and multi-layer, are analyzed. The obtained simulation results for different vertical ground electrodes are compared. Then, the impacts of the ground electrode geometry and soil resistivity are studied. Finally, using the proposed lightning model by Heidler, the GPR values are computed based on the accurate frequency-dependent model of GSs.

2.2   Method of Moment Solution

Using the GSs aims to conduct the currents caused by lightning or faults into the soil in the best possible way and dampen them in the shortest possible time. In addition, as far as possible, uniform potentials are created within the protected area so that the electrical potential difference between different points is not hazardous for personnel and installations. In practice, electromagnetic induction causes the potential difference between the two locations to be greater than zero. These point inequalities concerning the reference voltage and the resulting disturbances can cause damage to electrical and electronic systems connected to the GSs. As a result, for accurate transient analysis of the system, especially in the event of fast transients such as lightning strikes, we need to obtain the amount of voltage at each of the connection points where our electrical equipment, such as transformers and surge arresters or substations, is grounded. The electromagnetic field method [5] is used to obtain the characteristic of the GS in the frequency domain. This method is based on the antenna theory and the application of Maxwell's equations, which are solved by the moment method [6]. It is worth

noting that this method is one of the most accurate methods available, especially at high frequencies (up to several MHz), for analyzing the harmonic impedance of GSs and the lightning performance of GSs. In the continuation of this chapter, we will describe the problem and solve it. The vertical and horizontal conductors might be able to meet these requirements. Also, more complex structures or combinations of several vertical and horizontal electrodes should be used to improve the performance of GSs.

Due to the nature of the GSs, which include a conductor in a lossy media, we use the solution of the electric field integral equation in the frequency domain to obtain the current distribution of the GSs. The aim here is to compute the current distribution of the GS electrodes in the frequency domain to investigate the transient performance of GSs. In this context, the frequency analysis should perform in the desired frequency range at each frequency. The current injected into the soil (such as lightning current) is in the time domain, and the electromagnetic fields associated with it are in the time domain. The electromagnetic modeling of the GSs is based on the following assumptions:

- The layered media is assumed. Each layer consisting of resistivity and permittivity is separated by a horizontal planar boundary (parallel to the x-y plane of a rectangular coordinate system), as shown in Fig. 8.
- The air and the layered soil reside in half-spaces.
- Soil and conductors have linear, isotropic properties, and the electrical parameters of the soil are frequency-dependent.
- The ratio of the length of the conductor to its radius is ten or more based on thin wire approximation [137].
- Simulation is performed using an ideal current source with a specific frequency, one end of which is connected to the ground system, and the other end is connected to the ground at infinity.
- The current is injected at an endpoint of one of the ground electrodes to excite the GS.

Let us briefly review the procedure of harmonic impedance calculation in the frequency domain, which is proposed in [19], [21], [56], [124]. As it is mentioned earlier, the media is layered. The used simulation approach builds on the formulation of a dyadic Green's functions (DGFs) of spectral-domain for the layered soil [77] to calculate the electromagnetic field generated by a vector source. Therefore, it can be used for large GSs and different electrode

configurations (vertical and horizontal electrodes). Furthermore, the problem with layered structure cannot restrict the presented technique [33]. The thin wire assumption decreases the integral dimension from the surface-to-line integration as well as the computational time of the modeling.
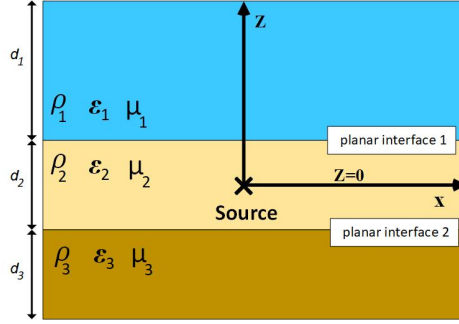

Fig. 8. Figure from J1, the multilayer media demonstration [1].

In the MoM technique, the electrodes are divided into small segments. r' and r vectors show the location of the source and observer segments along the ground electrode's surface. A mixed-potential integral equation (MPIE) as a foundation mathematical form is employed to describe Maxwell's equations for modeling the layered media. Let us consider the given boundary condition in (30) for the current density on the GS's electrodes to compute MPIE.

$$\hat{n} \times \vec{E}(\vec{r}) + \hat{n} \times \vec{E}^i(\vec{r}) = 0 \qquad r \text{ on } S \tag{30}$$

where the $\vec{E}(\vec{r})$ is the scattered electric field and $\vec{E}^i(\vec{r})$ is the incident electric field due to incident current $I(\vec{r})$. $\hat{n}$ is the vector of the normal unit. The electric field can be represented in terms of the induced current on the conductor surface. $\vec{E}(\vec{r})$ is the scattered electric field as [56], [8].

$$\vec{E}(\vec{r}) = -[\nabla \emptyset(\vec{r}) + j\omega \vec{A}(\vec{r})] \tag{31}$$

It is composed of scalar potential (SP) $\emptyset(\vec{r})$ and magnetic vector potential (MVP) $\vec{A}(\vec{r})$ as

$$\begin{cases} \vec{A}(\vec{r}) = \iint G^A(\vec{r},\vec{r'}).I(\vec{r'})ds' \\ \emptyset(\vec{r}) = \iint G^\emptyset(\vec{r},\vec{r'})\rho_s(\vec{r'})ds' \end{cases} \tag{32}$$

Where $G^\emptyset$ and G^A are Green's functions of the SP and MVP, respectively. $\vec{A}(\vec{r})$ can be the result of electric current density $I(\vec{r})$ and $\emptyset(\vec{r})$ can be computed due to the density of the electric charge, $\rho_s(r)$, on the surface S of the electrode placed in the layered media. The density of electric current, $I(\vec{r})$, can be stated as [8]

$$\nabla \cdot I(\vec{r}) = -j\omega\rho_s(r) \tag{33}$$

In the layered mediums, several expressions of Green's function have been applied because the $\emptyset(\vec{r})$ and $\emptyset(\vec{r})$ are generic. For fulfilling the boundary conditions, two parts of the MVP are needed. The Green's function can be employed in the below form [8]

$$G^A = \begin{bmatrix} G_{xx} & G_{xy} & 0 \\ G_{yx} & G_{yy} & 0 \\ 0 & 0 & G_{zz} \end{bmatrix} \tag{34}$$

To compute Green's functions of the spectral and spatial domain, the proposed approach in [8] is utilized. Substituting equations (33) and (34) into (30) for $\vec{E}(\vec{r})$ yields the integral equation given by (35)

$$-\hat{n} \times \vec{E}^i(\vec{r}) = -[\nabla(\iint G^{eq}(\vec{r}.\vec{r'})\rho_s(\vec{r'})ds')$$
$$+ (j\omega \iint G^A(\vec{r}.\vec{r'}),I(\vec{r'})ds')] \tag{35}$$

The $I(\vec{r})$ is expressed as dividing the electrodes into n small fictitious in (2-8). The triangular basis function is utilized. The SP derivatives are substituted with finite differences. Thus, the impressed-current model is implemented using another 'triangle' at the excited terminal. Fig. 9 shows the basis function model that uses to compute the harmonic impedance of GS. The current distribution is calculated based on the impressed current I^t.
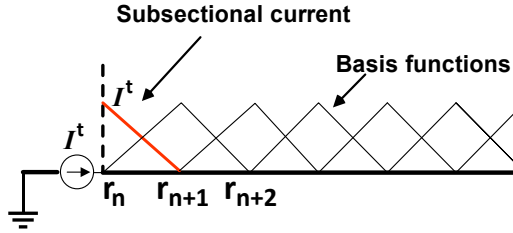
Fig. 9. Figure from **C2,** the basis function model of the injected current [127].

Here, in each segment, $I_i(\vec{r})$ and α_i are basis function and their unknown quotients, respectively. Then the IEs are converted to linear equations matrix expression given by (37)

$$I(\vec{r}) = \sum_{i=1}^{n} \alpha_i I_i(\vec{r})$$

(36)

$$[\alpha][A] = [B]$$

(37)

To calculate the unknown coefficients of the linear matrix equation of the system, α_i, the numerical solution can be employed [26]. The distribution of current (unknown current) is to be computed based on the impressed current I^t.

2.3 Harmonic Impedance Calculation

In GS modeling, the impressed current is often known. The behavior of GSs is characterized by the harmonic impedance that can be defined in a wide range of frequencies.

It means that the impedance magnitude is a function of frequency and has a different value at each frequency or content of frequency. The harmonic impedance is used only in the frequency region. As mentioned in Chapter 1, the GSs have dynamic behavior and can behave as inductance or capacitance. This behavior can identify using the harmonic impedance or frequency response of GS.

In each frequency, to calculate the harmonic impedance of the GS, the usual method is to apply a current to the ground electrode. Voltage is then estimated as the difference between the impressed terminal and the reference point with zero voltage. The harmonic impedance $Z(\omega)$ can be determined as the ratio of voltage

$V(\omega)$ and applied current $I(\omega)$ at the injected terminal. It should be noted that (37) can be rewritten below:

$$[Z][I] = [Z'I^t] \tag{38}$$

Here, [I], [Z], and $[Z'I^t]$ are unknown current, the mutual impedance between all segments, and the excitation matrix relevant to the injecting by I^t, respectively. The Z' is the column matrix which determines the mutual impedance between the source segment and other segments [32]. The expanded form of the matrix equation given in (38) can be explained as

$$
\begin{bmatrix}
Z_{1.1} & \cdots & Z_{1.n+1} \\
\vdots & \ddots & 0 \\
Z_{1+n.1} & \cdots & Z_{1+n.n+1}
\end{bmatrix}
\begin{bmatrix}
I^t \\
\vdots \\
0
\end{bmatrix}
=
\begin{bmatrix}
V_s \\
\vdots \\
0
\end{bmatrix}
\tag{39}
$$

After calculating the current distribution for all segments, the total electric field computes. The voltage between the injected terminal and the remote terminal can be computed as

$$V_s = -\iint [\vec{E}^i(r) + \vec{E}(r)], \overrightarrow{dl} = -\iint \vec{E}^{total}, \overrightarrow{dl} \tag{40}$$

Then, the harmonic impedance at the injected terminal to the remote terminal (remote ground) can be written as

$$Z(f) = \frac{V_s}{I^t} \tag{41}$$

2.4 Soil Structure Effect on the Harmonic Impedance of Ground Electrode

Let us consider the full-wave approach to compute the harmonic impedance of GSS. The GSs dynamic behavior (current distribution along ground electrodes) depends on the soil structure, properties, and electrode geometry. In this part, to further evaluate these impacts on the harmonic impedance of GSs, different vertical ground electrodes are taken into account. These electrodes are buried in single, two-layer, and multilayer soil. In the two-layer and multilayer soil structure, the depth of the first and second layers is supposed to be 1-m. The soil funeral depth is 0.6 m. The absolute value and phase angle of the harmonic impedance are

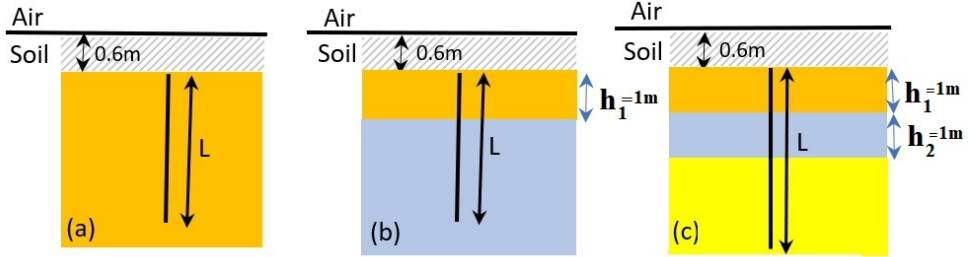computed in a broad frequency range. Several soil configurations are shown in Fig. 10.

Fig. 10. Figure from **C1**, soil structure, (a) single layer, (b) two-layer, (c) multilayer [7].

2.4.1 Uniform Soil

In the first example, the single-layer soil structure is assumed. The length of the vertical ground electrode is L =3m, and the radius of the cross-section is a=1.25 cm. The relative permittivity is set to 10. The soil is characterized by resistivities of ρ =10, 100, and 1000 Ω.m.

The harmonic impedance (absolute value (a) and phase (b)) of the GS, as a function of frequency, is presented in Fig. 11. In the low-frequency range, the absolute value of the harmonic impedance is equated to the DC resistance. From the GS dynamic behavior point of view, in the high-frequency range, the behavior of GS can be capacitive or inductive based on the soil resistance value. In this regard, this value has a significant impact on the harmonic impedance of GSs. In another case study and to analyze the effect of the electrode's length, we assume the case of a 15-m vertical electrode with the same cross-section placed in the soil with a resistivity of ρ =10, 100, and 1000 Ω.m.
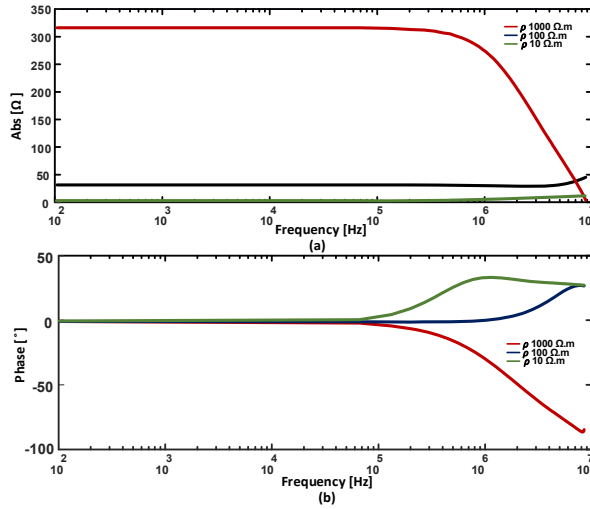
Fig. 11. Figure from **C3**, the harmonic impedance [(a) absolute (b) phase angle] of a 3-m vertical ground electrode buried in the single layer soil with resistivities of ρ=10, 100, and 1000 Ω.m and relate permittivity of 10 [9].
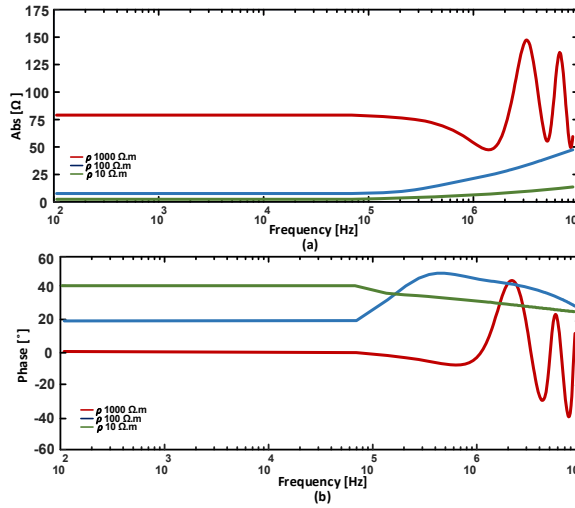

Fig. 12. Figure from **C3**, the harmonic impedance [(a) absolute (b) phase] of a 15-m vertical ground electrode buried in the single layer soil with resistivities of ρ=10, 100, and 1000 Ω.m and relate permittivity of 10 [9].

Fig. 12 is shown the frequency-dependent model (absolute value (a) and phase (b)) of this grounding electrode. It can be seen that by increasing the length of the vertical electrode, the R_{LF} value of the GS is reduced, but in the higher range of frequency, the input impedance of the GS does not improve relatively.

In the high-frequency range, the behavior of GS can be capacitive or inductive based on the soil resistivity and electrode length. To further assess the electrode's geometry effect on the GS harmonic impedance, vertical electrodes with different lengths (3, 15, and 30-m) are buried in uniform soil with the same electrical properties. The comparative results are illustrated in Fig. 13.

This evaluation is performed for the soil with a resistivity of 1000 Ω.m. As it can be shown in the computed results in Fig. 13 (left side), the 3-m vertical electrode
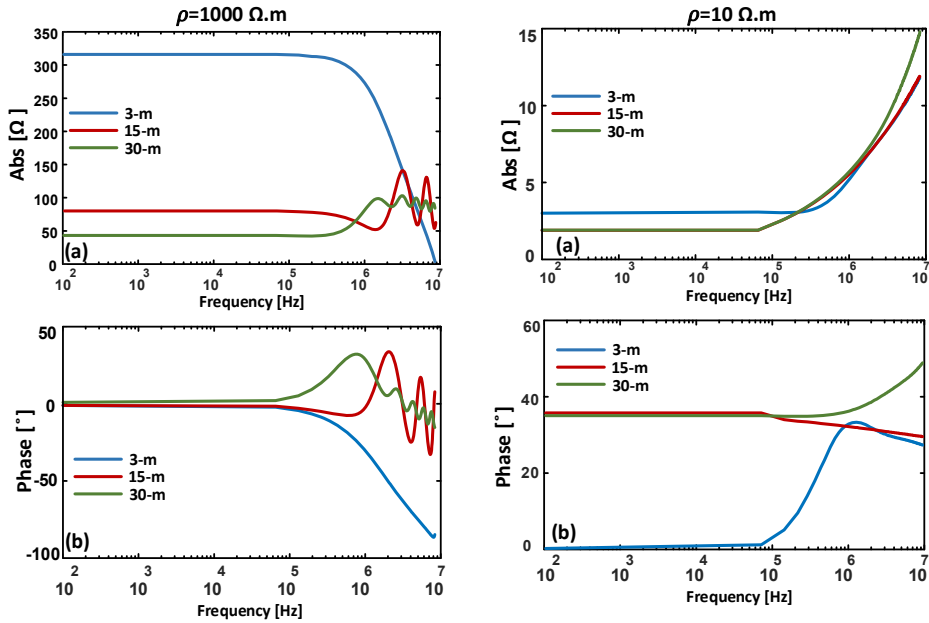

Fig. 13. Figure from **C1**, harmonic impedance [(a) absolute (b) phase] of the vertical ground electrode with different lengths (3,15, and 30-m) buried in the soil with a resistivity of [left] 1000 Ω.m and [right] 10 Ω.m [9].

behaves as a capacitance. While the length of the electrode increases, the capacitive behavior converts to inductance in poor soil conductivity. But, with the low resistivity of the soil, this behavior for different lengths is mostly inductive, as

shown in Fig. 13 (right side). Generally, it is evident from the prior results that by increasing the length of the vertical electrode, the R_{LF} value of the GS is reduced for all cases.

2.4.2 Two-layer Soil

In this part, the performance of the full-wave approach is assessed for the investigation of vertical ground electrodes buried in the two-layer soil structure. In this regard, two soil configurations are taken into account.

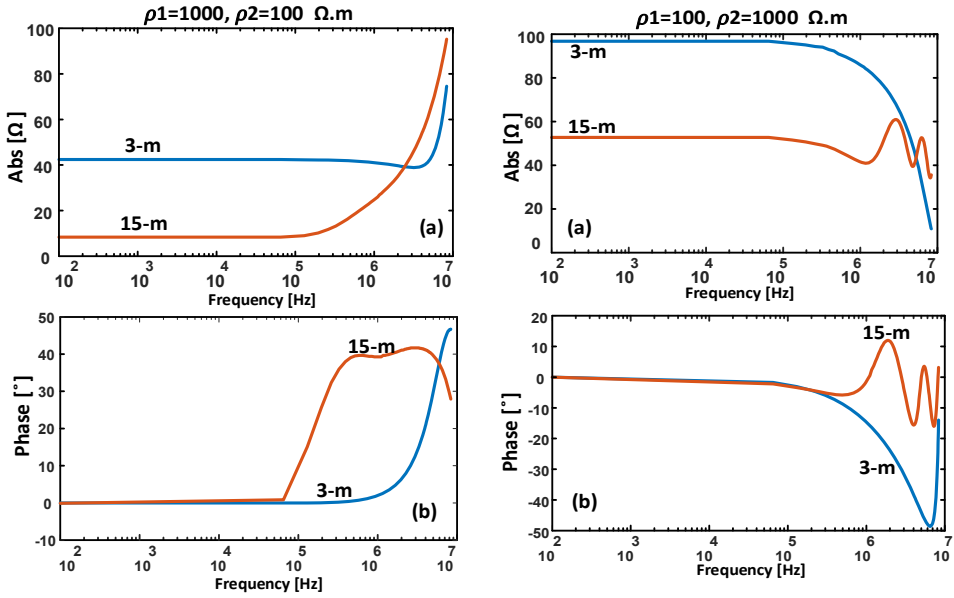First, the soil is characterized by upper-layer resistivity $\rho_1 = 1000$ Ω.m and lower

Fig. 14. Figure from **C1**, harmonic impedance [(a) absolute (b) phase] of the vertical ground electrode with different lengths (3 and15-m) buried in the two-layer soil. [left] upper layer resistivity of ρ_1=1000 Ω.m and lower layer ρ_2=100 Ω.m, [right] upper layer resistivity of ρ_1=100 Ω.m and lower layer ρ_2=1000 Ω.m [9].

layer $\rho_2 = 100$ Ω.m ($\rho_1 > \rho_2$). Then, the simulation results are performed for soil that is characterized by upper-layer resistivity of $\rho_1 = 100$ Ω.m and lower layer of $\rho_2 = 1000$ Ω.m. in the second case, the upper soil resistivity is smaller than the

lower layer ($\rho_1 < \rho_2$). The relative permittivity of both layers is set to 10. The upper layer depth is 1-m.

The simulation results for the harmonic impedance ((a) absolute value and (b) phase) of the vertical ground electrodes with several lengths (3 and 15-m) are presented in Fig. 14. Especially when the lower layer's soil resistivity is much more resistive than the upper layer, with increasing the frequency, the principal quantity of the penetrated current is conducted via a smaller section of the electrode into the soil [32].

2.5   Lightning Current Model

The consequence of lightning currents on stations or OHLs can be regarded from two different viewpoints: their stringency, namely their potential to result in insulation deterioration or operational damage, as well as the frequency with which these influences appear [140]. In the lightning overvoltage studies and to evaluate the influences of full-wave modeling of GSs on the generated overvoltage and GPR value, it is necessary to utilize the standard lightning model. Two different approaches have been applied to generate lightning models. It can be obtained from direct measurement or mathematical expression by empirical waveform quantification. It was very common for lightning studies to utilize two models of lightning currents (Heidler [141] and CIGRE [140] models). Heidler's function and CIGRE model are implemented easily and are presented in the time domain simulators. The three basic parameters need to be determined to correspond to the model of the first and subsequent lightning return strokes. These parameters are peak value, zero-to-peak time, and maximum steepness.

- **CIGRE Model**

In the CIGRE model, the peak value of the current is I_0, and the zero-to-peak time (T_f) is computed with the use of the following expression in (42)

$$T_f = \frac{I_0}{s_m} \tag{42}$$

where s_m is the maximum steepness. T_t is the wave tail time to half value. To model the CIGRE lightning current, the given parameters in Table 5 are taken into account. Fig. 15 shows the CIGRE lightning stroke curve.

Table 5. CIGRE model (first and subsequent stroke) [140].

Lightning waveform	$S_m(kA\mu s^{-1})$	I_0	$T_f(\mu s)$	$T_f(\mu s)$
First Stroke (FS)	24.3	31.1	3.83	75
Sub-sequent Stroke (SSS)	39.9	11.8	0.43	32

- **Heidler Model**

This thesis adopts the lightning parameters based on Heidler's functions. The lightning current expression can be written as below [9]:
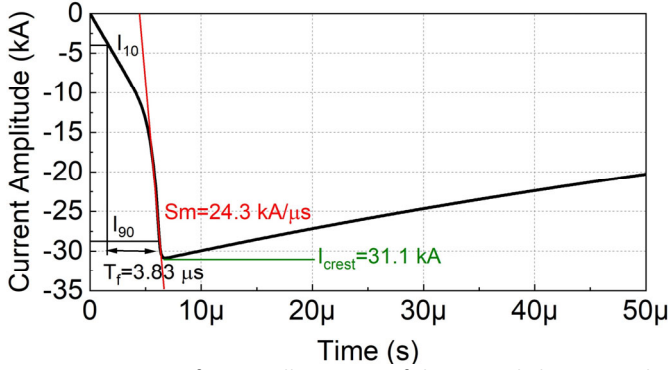

Fig. 15. Figure from **J5**, illustration of the CIGRE lightning stroke [5].

$$i(t) = (\frac{I_0}{\beta})\left[\frac{(t/\tau_1)^n}{1 + (t/\tau_1)^n}e^{(-t/\tau_2)}\right] \tag{43}$$

$$\beta = e^{-(\tau_1/\tau_2)(n(\tau_2/\tau_1))^{\frac{1}{n}}}$$

Here, I_0, τ_1, and τ_2 are peak value, front time, and tail time, respectively. The β is the peak correction factor. The value of *n* can be chosen from 2~10.

The first lightning current can be modeled by Heidler's functions in (43). The subsequent lightning current can reproduce using a sum of two given expressions in (43). To model the lightning current, the given in Table 6 parameters are taken into account [9].

72

Table 6. Heidler's parameters were applied to model waveshapes of the lightning current (first and subsequent stroke) [22].

Lightning waveform	n	I_0(kA)	$\tau_1(\mu s)$	$\tau_2(\mu s)$
First Stroke (FS)	2	28	1.8	95
Subsequent Stroke (SSS)	2	10.7	0.25	2.5
	2	6.5	2	230

The first and subsequent lightning waveforms, which are reproduced using Heidler's functions, are illustrated in Fig. 16. The first lightning current has a more considerable peak value, and the subsequent lightning current has a higher frequency content due to having larger steepness ($di/_{dt}$).
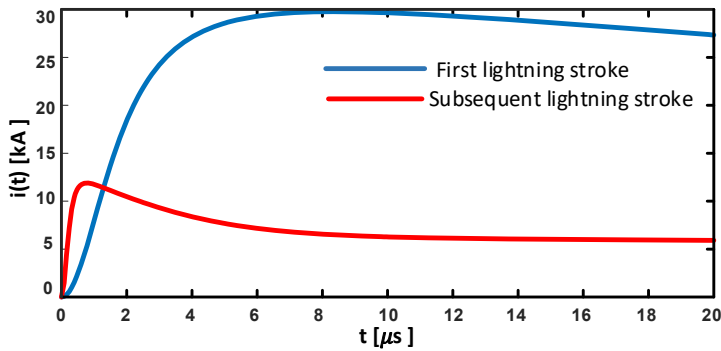

Fig. 16. Figure from **C3**, illustration of the first and subsequent lightning strokes [9].

2.6   Ground Potential Rise (GPR)

The GPR event happens if a large magnitude of current due to lightning or line-to-ground (LG) fault penetrates the ground via GSs of towers, structures, or neutral points of power transformers. The GPR, as one of the critical factors of the RAM in the power systems, can influence human safety, EMC, insulation coordination, and the protection system design of OHL/ substations [32]. In the IEEE Std. 367-2012, the GPR is explained clearly [142]. GPR's peak value depends on key factors, such as the magnitude and front time of the fault current (see Fig. 16) and GS behavior. To predict the accurate value of the GPR, it is vital to model GSs precisely.

While the harmonic impedance of GSs, $Z(f)$, has computed, and with having the Fourier transform of the injected fault current, $I(f)$, the GPR in the frequency domain can be computed as a function of frequency, $V(f)$, as below [7]:

$$I(f) = \text{L}\{i(t)\} \tag{44}$$

$$V(f) = Z(f), I(f) \tag{45}$$

$$GPR = v(t) = L^{-1}\{V(f)\} \tag{46}$$

L denotes Fourier transform and **L⁻¹** is the inverse Fourier transform operator. The GPR is calculated in the time domain.

Fig. 17 is illustrated the process of GPR calculation ((44)-(46)) in the below flowchart.
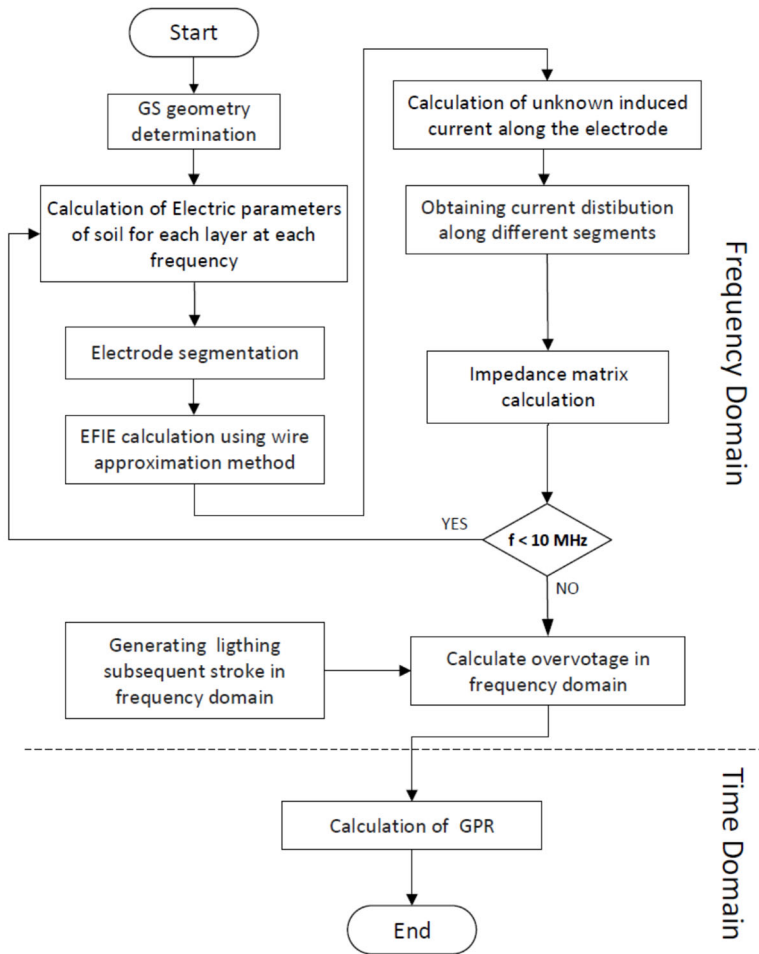
Fig. 17. Figure from **C2**, computation of GPR based on full-wave approach [7].

The GPR waveforms at the injection terminal are shown in Fig. 18 and Fig. 19 for vertical ground electrodes with different lengths (3, 15, 30-m). These ground electrodes are buried in uniform (see Fig. 18) and two-layer (see Fig. 19) soil structures. The harmonic impedances for those cases are mentioned in Chapter 2, section 02.4.
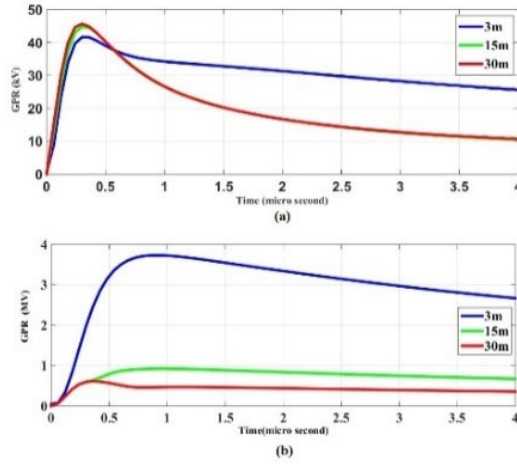
Fig. 18. Figure from **C3**, GPR waveform at the injection point against the subsequent lightning current for different vertical ground electrodes (3,15, and 30-m) buried in the uniform soil [(a) ρ=10 Ω.m, (b) ρ=1000 Ω.m] and relative permittivity of 10 [17].
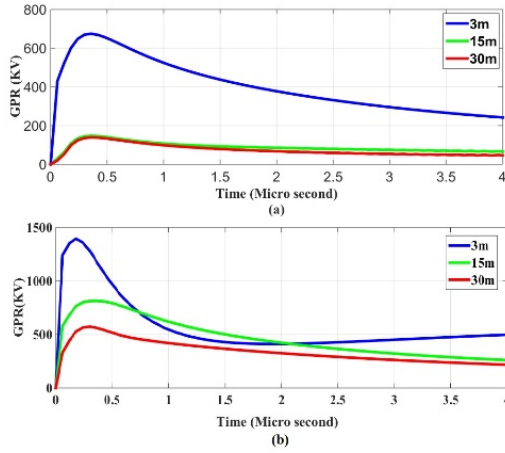

Fig. 19. Figure from **C3**, GPR waveform at the injection point against the subsequent lightning current for different vertical ground electrodes (3,15 and 30-m) buried in the two-layer soil structure [(a) ρ_1=1000, ρ_2=100Ω.m, (b) ρ_1=100, ρ_2=1000Ω.m] and relative permittivity of 10 [17].

The modeling results show that the GS structure/soil layers and ground resistivity can impact the GPR peak value.

To calculate GPR with more accuracy, the frequency-dependent effects of soil electrical parameters can involve in the harmonic impedance model. It will be discussed in Chapter 4, and its influences will be taken into account.

2.7 Summary

In this chapter, the procedure to perform a full-wave approach to the model of the GS has been introduced briefly. The main scientific contribution in this chapter is the development of the GS modeling considering different electrode geometries and layers to compute GPR. The MoM-based solution has been employed to compute the harmonic impedance of GSs. The new expression of Green's function has been employed in the model and different lengths of vertical ground electrodes have been considered in this study. Also, two different soil configurations have been considered. It has been shown by increasing the length of the vertical electrode, the R_{LF} value of the GS has been reduced, but in the higher range of frequencies, the input impedance of the ground electrode did not improve relatively.

In addition, a procedure to compute the GPR value for the vertical ground electrodes is presented, where it is illustrated that the peak of the GPR has been affected by the GS model. It has been discussed that with a rigorous full-wave model of GSs, the value of GPR can calculate with more accuracy.

Related Publications

J1. M. Ghomi, H. Zhang, F. Faria da Silva, C. Leth Bak, and K. Yin, "*Integrated Model of Transmission Tower Surge Impedance and Multilayer Grounding System Based on Full-wave Approach*," Journal of Energy Power System Research, vol. 198, pp. 107355, Sept. 2021 [1].

   Main contribution:

   A Full wave approach to calculate the input harmonic impedance (surge and grounding impedance) of the integrated model of a transmission tower and grounding system based on the electromagnetic theory in the layered medium.

J2. M. Ghomi, F. Faria da Silva, Amir abbas Shayegani Akmal, and C. Leth Bak, "*Transient Overvoltage Analysis in the Medium Voltage Substations Based on Full-Wave Modeling of Two-layer Grounding System*," Journal of Energy Power System Research, Elsevier 2022 [2].

> **Main contribution:**
>
> The procedure applied MoM to perform transient overvoltage analysis based on considering the complex grounding grid of the actual MV substation buried in the two-layer soil structure.

C3. M. Ghomi, HR. Mohammadi, HR. Karami, C. Leth Bak, F. Faria da Silva, and H. Khazraj, "*Full-wave modeling of grounding system: Evaluation the effects of multi-layer soil and length of the electrode on the ground potential rise*," International Conference on Power Systems Transients, IPST, pp. 1-6, 2019 [9].

> **Main contribution:**
>
> The introduction of the MoM solution to estimate the harmonic impedance of GS considering the layered soil structure

C6. H. Zhang, **M. Ghomi**, Q. Wang, F. Faria da Silva, C. Leth Bak, K. Yin, and H. Skouboe, "*Evaluation of Lightning Backflashover Rate of a Fully Composite Pylon using Monte Carlo Method on Environmental Factors*," proc. of IEEE Power &Energy Society General Meeting (PESGM) 2022, Denver, Colorado, 2022, Status: Accepted [12].

> **Main contribution:**
>
> To introduce the application of the frequency-dependent model of GS to evaluate the lightning performance of a fully composite pylon.

Chapter 3.   Transmission Tower Surge Impedance and Multilayer Grounding System

3.1   Abstract

*In this chapter, based on paper **J1**, the tower's GS and surge impedance are vital factors in lightning performance studies. In studying the OHL's lightning performance, it is crucial to analyze the transient behavior of towers hit by lightning. The subject has got more importance with the current application of HVDC towers with higher heights (e.g., 525 kV and 1100 kV DC power transmission lines) to more likely catch lightning stroke currents [143]. In this chapter, the full-wave technique based on MoM is applied to compute the harmonic impedance of a typical HVDC tower, including the accurate model of the GS. The same methods have been applied to calculate the surge impedance of the tower and harmonic impedance of the GSs in the frequency domain. Therefore, the integrated model of the tower and multi-layer soil structure is proposed to estimate the equivalent harmonic impedance of the system from the tower top. In order to achieve this goal, detailed geometrical data regarding the tower and electrical parameters of the multilayer structure of the GS are integrated to assess the system frequency response by the proposed method. Based on the obtained results, the amplitude of the system frequency response can be smaller at the high-frequency range than when the GS's low-frequency model (DC resistance) is used.*

3.2   Modeling Process

An electromagnetic field theory approach, like MoM, is well-fitted to the frequency-domain analysis described in Chapter 2. Supposing that the tower and its ground electrode form a linear system and considering the tower as a frequency-dependent model. The same procedure is applied to the integrated model. It consists of a tower surge impedance and GS. Moreover, it is significant to point out that electromagnetic field theory does not require voltage in the

equation. A voltage source generally determines the excitation of the tower. However, it can also be represented by a current source between two ports on the tower and the remote terminal [143], which is beneficial in lightning investigations.

For this purpose, the GS impedance/admittance matrix over the frequency range of interest is computed based on the MoM solution (numerical solution) to Maxwell's equations. Within this context, numerical solutions like full-wave approaches are mainly applied to evaluate the harmonic impedance of the metallic tower linked to the GS (integrated model).

Analytical and experimental approaches have been applied to calculate the tower surge impedance in time and frequency domains. In the time domain, the tower surge impedance depends on the excitation waveform and surge impedance definition, but it depends on the tower geometry and electromagnetic properties in the frequency domain. With this regard, a numerical solution like MoM based on the thin wire approximation can use as an effective method for the following reasons:

- reduction of problem size
- problem solution compatibility
- excitation non-dependability

The mixed potential integral equation (MPIE) is computed by satisfying the boundary condition on the electrode surface. The magnetic vector and electric scalar potentials are involved in the electromagnetic equations [1]. The Green function is not unique and can be chosen as below in (47).

$$\overline{G_A} = \begin{pmatrix} G_{xx} & G_{xy} & G_{xz} \\ G_{yx} & G_{yy} & 0 \\ G_{zx} & 0 & G_{zz} \end{pmatrix} \tag{47}$$

The metallic structure and ground electrode are inserted in the multi-planar area and are segmentized. The first segment is assumed as the excitation port. Also, the junction point between the ground electrode and the metallic tower can be chosen as the excitation terminal.

Two methods can provide the excitation source for the system harmonic impedance calculation. Delta-gap and impressed current models are the excitation waveform developed to show voltage and current sources [144]. In the impressed-current model, the current distribution in the conductors is determined when the

80

excitation current source is determined. Hence, the total electromagnetic field (the equivalent of scattered and incident electric fields) at any location and voltage as a path integral of the total electric-field vector among any two terminals along a defined path are defined.

After applying the voltage source and generating the basis function current in the tower and GS, the thin wire assumption calculates the current distribution along all case study segments. Depending on how many layers are assumed for the study, the tower is placed in the upper layer (above the ground surface), and the GS is placed in the lower layer. Therefore, the MoM approach, including multi-layer planar, is assumed to compute the input harmonic impedance of the integrated model [1]. The model setup is presented in Fig. 20(a). In the proposed model, in order to extend the density of electric current on the structure conductors, the linear basis function with the triangle form is employed (see Fig. 20(b)). The sub-sectional current, I_t, is provided by a delta-gap excitation voltage source [1].

The total harmonic impedance is computed as follows.
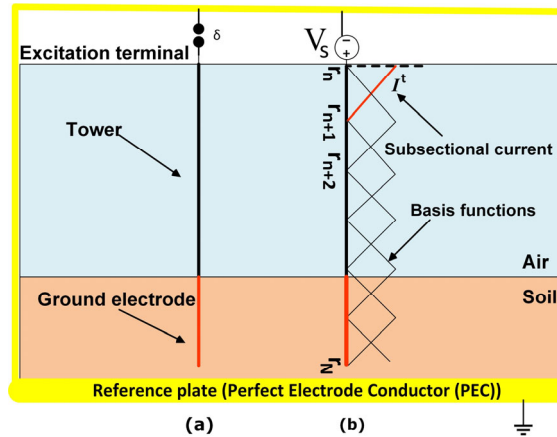
$$Z(f) = \frac{V_S}{I_t} \tag{48}$$

Fig. 20. Figure from **J1**, the harmonic impedance computation setup. a) delta-gap impression model b) linear basis function [1].

3.3 Verification of The Model

✓ Current Distribution

To check the validation of the proposed method, a two-layer medium is assumed for calculating the integrated harmonic impedance based on the full-wave method. The first layer is air, and the second layer is soil. The depth of the first layer is equal to the length of the metallic tower (0.4-m), and the depth of the soil is infinite. The length of the vertical ground electrode is 0.5-m. The electrical parameters of each layer are shown in Fig. 21. The delta-gap voltage is 1-v.
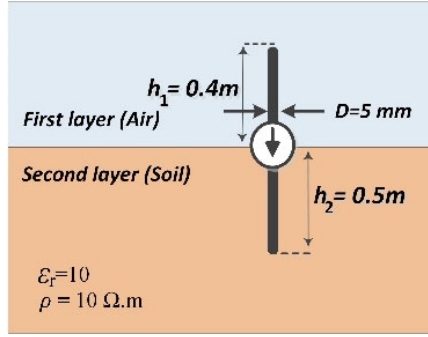

Fig. 21. Figure from **J1**, a simple tower is joined to the ground electrode to verify the proposed integrated model [1].
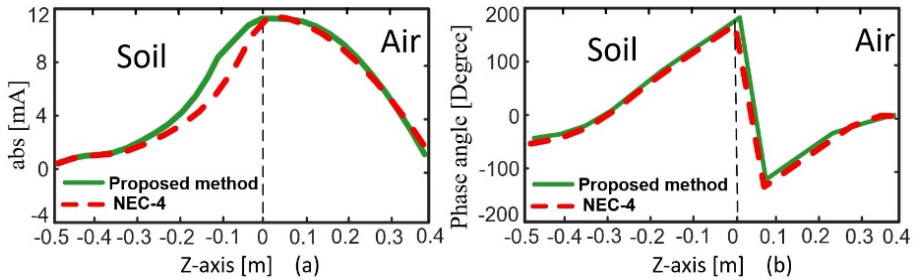

Fig. 22. Figure from **J1**, distribution of current along the ground electrode and tower at 10 kHz [1].

The absolute value of the distributed current along the system and its angle are shown in Fig. 22. The current distribution values calculated from the proposed method are in good agreement with the NEC-4 [145].

✓ **Harmonic impedance validation**

In this part, three cases (see Fig. 23) are simulated using the MoM to evaluate the GS's impact on the tower surge impedance (system harmonic impedance). In Case a, it is connected to the ideal GS. It is modeled as a medium with a resistivity of zero. In Cases b and c, the tower is linked to the vertical ground electrode buried in soil, characterized by soil resistivity of 100 and 1000 Ω.m, respectively.
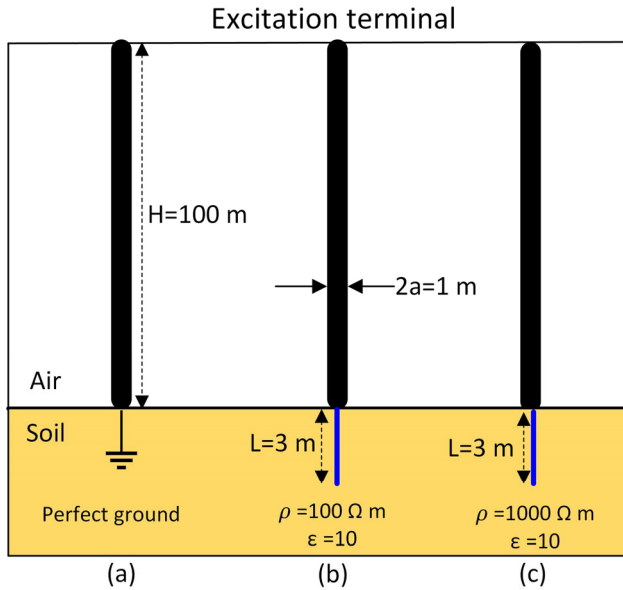

Fig. 23. Figure from **J1**, a simple case study to evaluate the proposed integrated model of the harmonic impedance of the tower [1].

The system harmonic impedance is achieved by specifying the excitation terminal at the tower top under three conditions of soil resistivity [(a) zero, (b) 100, and (c) 1000 Ω.m]. The soil relative permittivity is 10 for all cases.
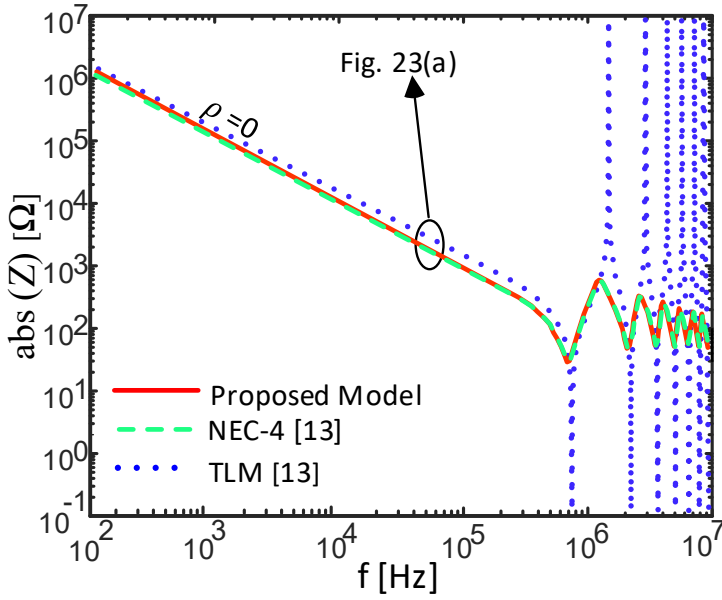
Fig. 24. Figure from **J1**, the tower harmonic impedance. Case (a) in Fig. 23. Red-solid line: Full-wave model (MoM), blue-dashed line: TLM, and green-dashed line: TLM [1].

In Case a (see Fig. 23(a)), for the assumed 100-m tower height, it is supposed that the tower is linked to the perfect GS. The harmonic impedance of the tower is computed using MoM (proposed method), TLM, and NEC-4. It can be seen that the TLM cannot predict the amplitude of the harmonic impedance at high frequencies. The MoM and NEC-4 have an excellent agreement to predict the harmonic impedance in this case. Fig. 24 demonstrates harmonic impedance behavior for TLM and electromagnetic techniques in a wide range of frequencies. Currents estimated by TLM might be considerably higher or lower than those estimated by MoM at a high-frequency range. It can be observed that deviations can grow very large when close to the resonant frequency. It might be noticed that all methods demonstrate identical behavior at the low-frequency range up to the first frequency of resonance (f=0.75 MHz). At the high-frequency range, dissimilarities are highlighted more. TLM estimates infinite or zero values of the harmonic impedance at resonance frequencies. The full wave model estimates Max. and Min. values of the amplitude of harmonic impedance at the high frequencies. The no consideration of wave radiation losses leads to these dissimilarities and errors in the Max. and Min. values of the harmonic impedance amplitude at the

resonance frequency, which the full-wave model considers. This is a representation that the utilization of TLM should be revised, particularly at the high-frequency range, while fast-front waveforms are considered with a high-frequency content like subsequent lightning currents. Dissimilarities in the system's frequency response at a higher frequency range will cause entirely different results in the transient surge impedance when usually the maximum values of the lightning appear.
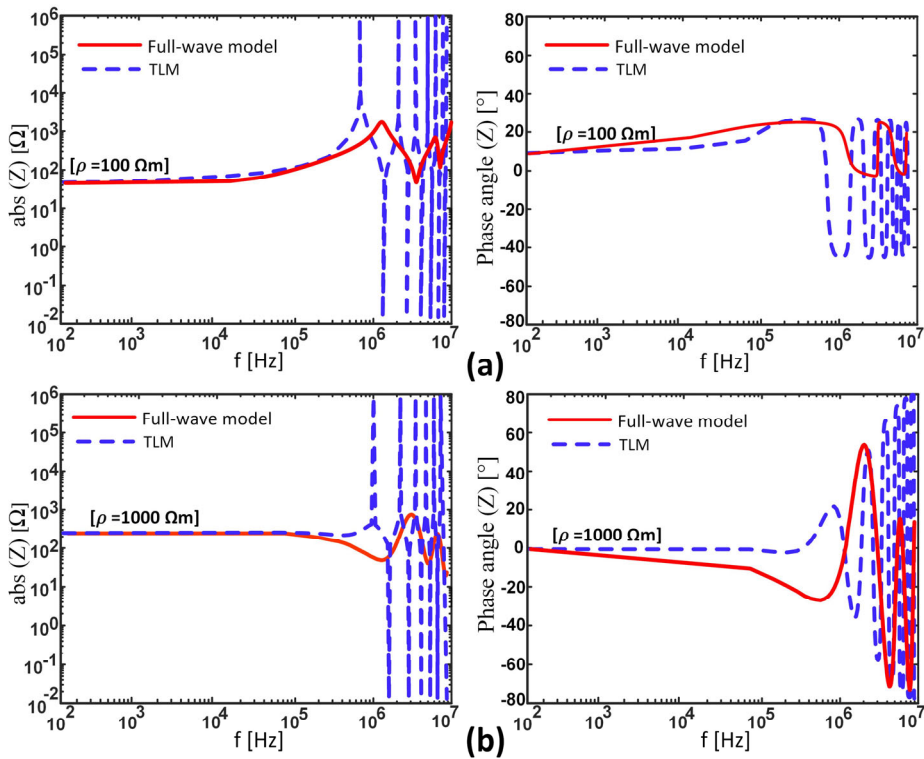

Fig. 25. Figure from **J1**, the harmonic impedance of the integrated model of the simple tower and vertical ground electrode buried in soil with a resistivity of a) 100 Ω.m b) 1000 Ω.m. Red-solid line: Full-wave model (MoM), blue-dashed line: TLM [1].

Fig. 25 (a) and (b) present the input impedances of the integrated model in the frequency domain, including vertical ground electrodes buried in the homogenous soil (Cases b and c in Fig. 23). Dissimilarities in the system's frequency response at a higher frequency range are shown. TLM cannot predict the maximum/minimum values of the harmonic impedance, and the frequency resonance is shifted due to the changing of the system's transfer function while the MoM is applied.

3.4   Metallic Tower

To evaluate the impact of the suggested methodology on the harmonic impedance of the integrated model, the results associated with the three different levels of detail for the sample of a HVDC tower are presented. The general configuration of the tower and ground electrode buried in the soil is shown in Fig. 26.

The model of the tower (a) is a very simple tower with a cross arm. Model (b) is the tower with a body and footings, and model (c) is the detailed geometry of the tower with all components, including cross arms, legs, and body. The equivalent frequency response of the tower and GS utilized for analysis and the view from the tower top for the mentioned tower are illustrated in Fig. 26 (d), (e), and (f), respectively. The complexity of the towers increases from Fig. 26(a) to (c). All towers are connected to the two-layer soil structure. The low-frequency values of the soil resistivity are presented in Table 7. The tower length (d_1) is 89.5-m and is equal to the first layer depth. The second layer (d_2) is 1-m, and the depth of the third layer is infinite.

Table 7. Low-frequency values of the resistivity of soil [1].

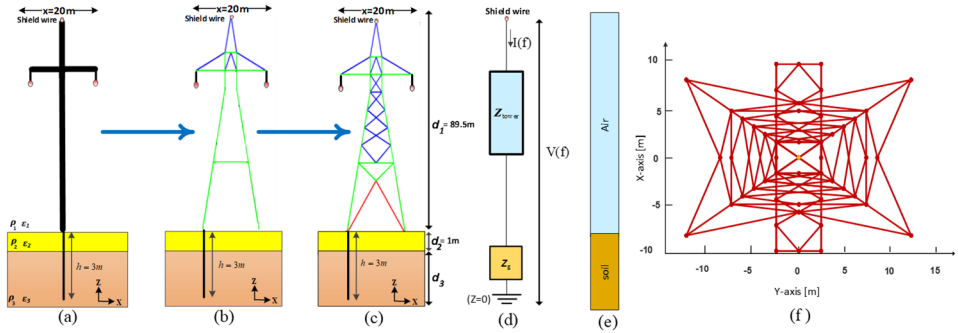| Cases	first layer	second layer
Case 1	100	100
Case 2	1000	1000
Case 3	100	1000
Case 4	1000	100

Fig. 26. Figure from **J1**, HVDC tower. (a) very simplified structure, (b) simplified structure, (c) actual model, (d) frequency-dependent representation of tower which is connected to the ground electrode, (e) medium of the integrated model, (f) 2-D top view of the actual simulated tower in the X-Y plane [1].

Fig. 27. Figure from J1, the influence of the tower model on the harmonic impedance of the integrated model. The ground electrode of the towers is buried in uniform soil (see Cases 1 and 2 in Table 7) [1].

Fig. 27 shows the obtained findings of the frequency response of the integrated model in which the tower is joined to the homogenous soil. In Cases 1 and 2, the tower models (a, b, and c) are connected to a 3-m vertical ground electrode placed in the soil with a resistivity of 100 and 1000 Ω.m. In these examples, it is apparent that the peak value of the frequency response (harmonic impedance) of the actual

model (tower (c)) differs significantly from the simplified ones (towers (a) and (b)). The peak value of the system frequency response reduces when the complexity of the tower increases. This error may increase, mainly close to the resonance frequencies. The first resonance frequency (FRF) between towers a and c varies in Case 1 from 1.4 MHz to 0.92 MHz and from 1.2 MHz to 1 MHz in Case 2 because of different attribution of the wave radiation losses, which tower model c takes it into account accurately.

To further investigate the effect of the GS on the input harmonic impedance from the tower top, the same vertical ground electrode is assumed to be used. The length of the vertical ground electrode is set to h =3-m. Cases 3 and 4 refer to a two-layer soil which is characterized by a resistivity of $\rho_1 = 100\Omega.\,m$, $\rho_2 = 1000\Omega.\,m$ and $\rho_1 = 100\Omega.\,m$, $\rho_2 = 1000\Omega.m$, respectively. The soil permittivity is set to 10. In this example, the efficiency of the proposed technique for the system frequency response analysis, including the tower and its GS buried in a two-layer soil structure.
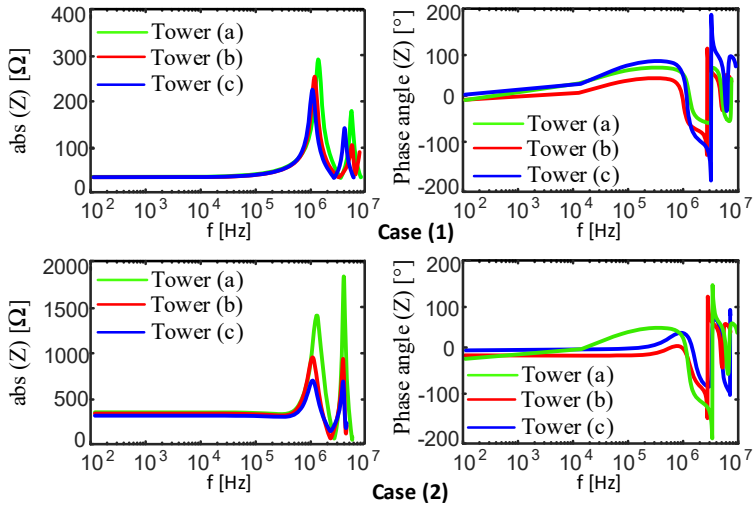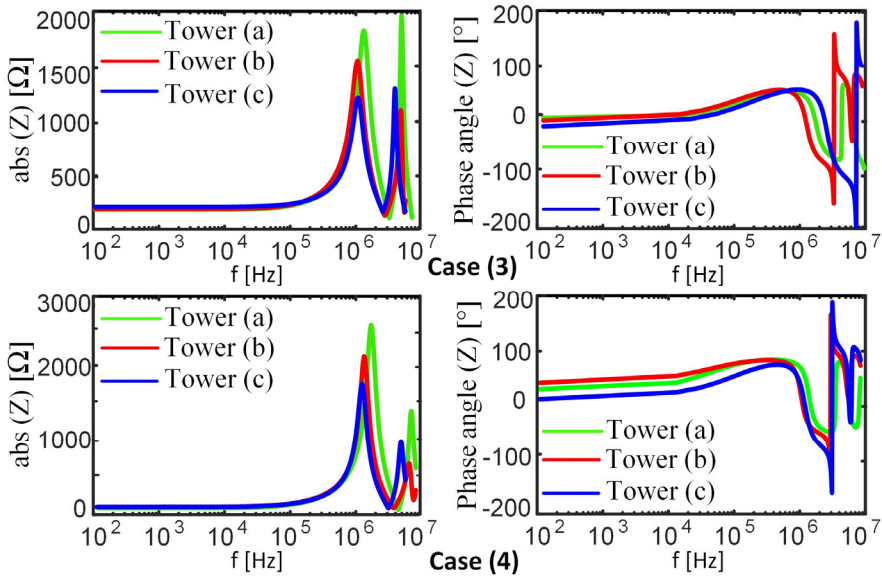

Fig. 28. Figure from **J1**, the influence of the tower model on the harmonic impedance of the integrated model. The ground electrode of the towers is buried in two-layer soil (see cases 3 and 4 in Table 7) [1].

Fig. 28 shows the results of the harmonic impedance for Cases 3 and 4 of the integrated models. It deals with a vertical ground electrode buried in a two-layer soil structure that is connected to the three models of the tower (a, b, and c). The depth of the upper layer of the soil is set to d_2 =1-m.

For Case 3, the absolute value of the frequency response of the integrated model for model (c) is smaller than the simplified model of the towers like a tower (a) and (b) near the first frequency of resonance. The peak value at the second frequency of resonance is a bit higher than the first one, but the second frequency of resonance is moved from 6 MHz for tower (a) to 4MHz for tower (c).

For Case 4, the input harmonic impedance absolute value of the integrated model for model (c) is smaller than the simplified model of the towers like a tower (a) and (b) near the first frequency of resonance. The first frequency of resonance (FRF) is reduced from 2 MHz for tower (a) to 1.1 MHz for tower (c). The peak value of the predicted input harmonic impedance of the integrated model at the second frequency of resonance is a bit higher than the first one, but the second frequency of resonance is reduced from 8 MHz for tower (a) to 5 MHz for tower (c).

As illustrated in Fig. 28, the obtained results for the tower models show that the input harmonic impedance depends on vital factors like the tower geometry, grounding grid structure, soil electrical specification, and modeling method.

Input harmonic impedance reaches its maximum values at different resonant frequencies, most likely at the FRF. Accordingly, lightning currents in lightning performance studies have high-frequency contents, and all lightning currents contain at least FRF. In the time domain, besides the tower geometry, the rise time of the injected lightning current waveform determines the order of the frequency contents, and it can be calculated using a fast Fourier transform (FFT). This algorithm converts a signal from the time domain to a representation in the frequency domain.

The following factor in (49) is defined to compare the peak values of the input harmonic impedance of the proposed method at FRF for different models of the tower.

$$diff|Z_m| = \frac{|Z_m(tower_a - tower_c|}{tower_a} \times 100 \qquad (49)$$

Table 8 summarizes the obtained results for the integrated model of the tower and its grounding grid. Generally, the estimated value of the input harmonic impedance of the system applying the full-wave approach is smaller than the computed input harmonic impedance when the simplified model of the tower has employed. The maximum difference in the harmonic impedance amplitude is for Case 2 when the resistivity of soil is 1000 Ω.m. It means that the use of a simple model of the tower may overestimate the input harmonic impedance when the resistivity of the soil increases.

Table 8. Integrated model harmonic impedance results for different models of the tower [1].

Cases	$|Z_{LF}|$ [Ω]	$|Z_{max}|$ [Ω]			$diff|Z_m|\%$	FRF [MHz]		
		a	b	c		a	b	c
Case 1	33.9	292.0	265.0	237.0	23	1.4	1.13	0.92
Case 2	313	1828	963	759	140	1.2	0.95	1
Case 3	93.5	2070	1530	1315	57	1.7	0.91	1
Case 4	42.5	2576	2275	1751	47	1.8	1	1.1

3.5   Summary

The main scientific contribution of this chapter is to propose an integrated model of the tower and its grounding grid to estimate the frequency response (input harmonic impedance) of the system equivalent based on an electromagnetic field theory. The presented approach takes improvement of the full-wave method to estimate the distribution of the current in the whole system and the harmonic impedance of the system, including the physical model of a tower and its GS. The frequency response of the tower does not relate to the excitation waveform. It is a function only of the geometry and the system's electromagnetic specification. It is better appropriate to characterize tower transient behavior. If required, constant surge impedance in the time domain may be calculated from the harmonic impedance in the frequency domain. The surge impedance of the tower can overestimate as long as the GS is assumed to be zero or it can be overestimated if the GS is perfect. As a result, the impact of the GS needs to be taken into account.

Related Publications

J1. M. Ghomi, H. Zhang, F. Faria da Silva, C. Leth Bak, and K. Yin, "Integrated Model of Transmission Tower Surge Impedance and Multilayer Grounding System Based on Full-wave Approach," Journal of Energy Power System Research, vol. 198, pp. 107355, Sept. 2021 [1].

> **Main contribution:**
>
> A Full wave approach to calculate the input harmonic impedance (surge and grounding impedance) of the integrated model of a transmission tower and grounding system based on the electromagnetic theory in the layered medium.

Chapter 4.   Effect of Frequency-Dependent Soil Model

4.1   **Abstract**

*In this chapter, based on the papers **C1, C2**, and **C5**, we consider the three most important existing frequency-dependent expressions for soil electrical properties, with particular emphasis on the suggested model's contribution to the investigation of the harmonic impedance of GSs. Then the GRP peak values are compared to the vertical ground electrode buried in different soil structures, considering soil frequency models and the constant model of soil. The GPRs based on the frequency model of soil take lower values than the constant model. The subsequent lightning current is assumed in this study due to having higher frequency content and the high-frequency behavior of GS is much more highlighted.*

4.2   **Frequency-Dependent Soli Model**

The frequency dependence model of soil electrical properties research goes back several decades. In the low-frequency regime, soil resistivity can be obtained by the well-known Wenner test method [146]. In the high range of frequencies, electromagnetic wave attenuation measurement provides a way to predict the electrical parameters of the soil.

Note that the GS response to lightning currents (as a high-frequency source) is a complicated topic. Concerning advanced available numerical techniques based on full-wave approaches, the precision of the presented modeling relates mainly to soil behavior. The soil behavior depends on several factors like type, temperature, salt content, moisture content, and particle structure. Significantly, the frequency-dependent impact of the soil's electrical parameters may influence the grounding harmonic impedance. Nonetheless, based on the field measurements, it has been proven that the soil's electrical properties are intensely frequency-dependent.

The assumption of the constant resistivity of soil can lead to conservative results. In terms of relative permittivity, its value can change from 4 to 80 based on the humidity of the soil [94]. There are presented few precise available formulations

to represent the frequency dependency impact, which has been previously mostly ignored. The highly recommended frequency-dependent models for the soil's electrical properties are reviewed in this part. The relative permittivity and resistivity of the soil can be explained as a linear function of electric fields in Maxwell's equations. It means that the total current density has two capacitive and conductive parts [108]. In the time domain, the total current density can be expressed by

$$\vec{I}(t) = \vec{I}_{Conductive} + \vec{I}_{Capacitive} \tag{50}$$

$$\vec{I}_{Conductive} + \vec{I}_{Capacitive} = \frac{\vec{E}}{\rho} + \frac{\partial(\varepsilon\vec{E})}{\partial t} \tag{51}$$

The total current density can be written by

$$\vec{I}(f) = \vec{I}_{Conductive} + j\vec{I}_{Capacitive} \tag{52}$$

$$
\begin{aligned}
\vec{I}_{Conductive} + j\vec{I}_{Capacitive} &= \frac{\vec{E}}{\rho_0} + j(2\pi f)\varepsilon\vec{E} \\
\vec{\nabla} \times \vec{H} &= \frac{\vec{E}}{\rho_0} + j(2\pi f)(\varepsilon_{real} - j\varepsilon_{image})\vec{E} \\
&= \left(\frac{1}{\rho_0} + 2\pi f\varepsilon_{image}\right)\vec{E} + j2\pi f\varepsilon_{real}\vec{E} \\
&= \sigma_{effective}\vec{E} + j2\pi f\varepsilon_{real}\vec{E}
\end{aligned}
\tag{53}
$$

The real and imaginary parts of relative permittivity are associated with the soil's pure polarizability to reserve electric energy and generated losses during material polarization. At the same time, the current is injected [108]. In general and based on the simplified macroscopic methodology given in (50-53), the effective resistivity, $\rho_{effective} = \frac{1}{\sigma_{effective}}$ and the real permittivity value, ε_{real}, decrease when the frequency is increased, respectively.

It is worth mentioning that the soil electrical parameters are expressed as a function of frequency; decreasing soil resistivity and permittivity results in the explained complex phenomena of frequency-dependency, which is in charge of the considerable decreasing peak value of harmonic impedance for soil with poor conductivities. It has been seen that the soil electrical parameters have a decreasing relationship as the frequency grows.

4.2.1 Smith and Longmire Soil (SLS) Model

Smith and Longmire developed one of the first extensive investigations in [30], which used Scott's experimental results. It was performed by a curve fitting model for the frequency range from 1Hz to several GHz. Based on the presented universal soil model by Smith and Longmire, the representation of the soil's electrical properties is explained as follows [7]:

$$\varepsilon_r(f) = \varepsilon_\infty + \sum_{n=1}^{14} \frac{a_n}{1 + (\frac{f}{F_n})^2} \tag{54}$$

$$\rho(f) = (\rho_{LF}{}^{-1} + 2\pi\varepsilon_0 \sum_{i=1}^{13} \frac{a_n F_n (\frac{f}{F_n})^2}{1 + (\frac{f}{F_n})^2})^{-1} \tag{55}$$

$$F_n = 10^{n-1} \times (\frac{M}{10})^{1.28}$$

$$\rho_{LF} = 125 \times (\frac{M}{10})^{-1.54}$$

where f is the frequency, M is the moisture content of the soil, ρ_{LF} is the low-frequency value of soil resistivity, ε_∞ is set to five as a dielectric constant at the high-frequency limit, and a_n are factors presented in Table 9.

Table 9: Factors a_n employed in the proposed soil frequency-dependent model by Smith and Longmire [30].

n	a_n	n	a_n
1	3.4×10^6	8	12.5
2	2.74×10^5	9	4.8
3	2.58×10^4	10	2.17
4	3.38×10^3	11	0.98
5	526	12	0.392
6	133	13	0.173
7	27.2	14	0

4.2.2 Grounding Harmonic Impedance Based on The SLS Model

In this part, to investigate the impact of the frequency-dependent of electrical properties of soil on the harmonic impedance based on the SLS model, it is assumed that ground electrodes are buried in uniform and two-layer soil structures. The information about the ground electrode's geometry and soil characterizations (Case 1 to 6) for each layer at the low-frequency range is given in Table 10. The simulation results are compared with and without SLS model assumptions.

Table 10: GS data

Case	L (m)	ρ_{LF1}	M_1	ρ_{LF2}	M_2	ρ_{LF3}	M_3
1 (Uniform soil)	3	100	11.5	100	11.5	100	11.5
2 (Uniform soil)	3	1000	2.5	1000	2.5	1000	2.5
3 (Two-layer soil)	3	1000	11.5	10	51	10	51
4 (Two-layer soil)	15	100	11.5	1000	2.5	1000	2.5
5 (Multi-layer soil)	3	10	51	100	11.5	1000	2.5
6 (Multi-layer soil)	15	1000	2.5	100	11.5	10	51

To compute the harmonic impedance of GSs, the full-wave method based on the MoM solution is applied. The frequency range of calculation is from zero to 10 MHz. The harmonic impedance as an impedance to remote ground at the injection terminal is the frequency response of the buried vertical ground electrode. Three different soil structures are studied. The relative permittivity and the radius cross-section are a=10 and 12.5 mm, respectively, for all six cases.

- **Uniform soil**

We first consider Cases 1 and 2 as uniform soil structures. The low-frequency soil resistivities are 100 and 1000 Ω.m, respectively, for Cases 1 and 2. As mentioned in Table 10, the ground electrode length is 3m in both cases.

Fig. 29 demonstrates the harmonic impedance [(left) absolute value and (right) phase] of the GS considering the constant (solid line) and frequency-dependent (dashed line) models for the soil calculated using the MoM technique. The low-frequency soil resistivities are 100 and 1000 Ω.m.

As the results show, in the high-frequency range for soil with high resistivity, the differences in the harmonic impedance peak values between the constant and frequency-dependent (dashed line) models are more noticeable. For instance, In Case 2, these values are 312 Ω and 148 Ω for constant and frequency-dependent models of soil electrical parameters, respectively. The phase angle of harmonic impedance is changed to about -61 degrees. It is clear that the frequency dependency of soil electrical parameters affects the performance of the ground electrode, so in the studied frequency range, the harmonic impedance shows faster changes than the soil with constant parameters.

Another conclusion to be drawn from Fig. 29(a) is that the inductive or capacitive behavior of ground electrodes is mainly determined by the electrical parameters of the soil as well as the length of the electrode. It is evident from the figure that at higher frequencies and for soils with lower resistivity, the inductive behavior is prominent.
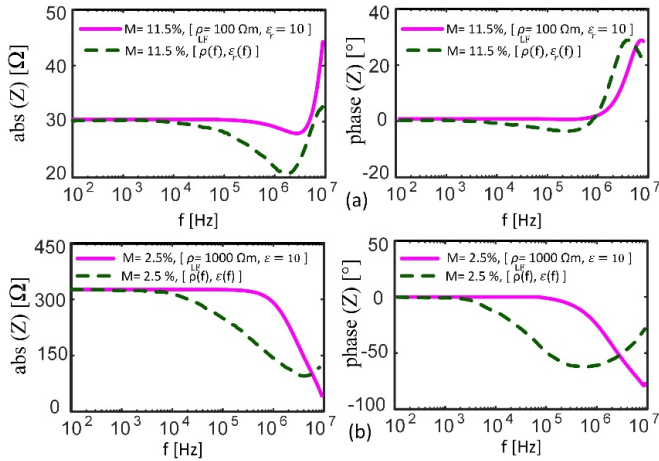

Fig. 29. Figure from **C1**, the harmonic impedance [(left) absolute value and (right) phase] of L=3m ground electrode buried in the uniform soil structure considering the constant (solid line) and frequency-dependent (dashed line) models for the soil and $\varepsilon = 10$. (a) $\rho_{LF} = 100\ \Omega.m$, (b) $\rho_{LF} = 1000\ \Omega.m$ [7].

Fig. 29(b) shows the ground electrode's capacitive behavior at the studied frequency. This behavior is in line with our expectations for the capacitive behavior of short-length ground electrodes buried in the high-resistivity of soil. At the same time, our expectation in the case of long ground electrodes is inductive behavior.

- **Multilayer soil**

Fig. 30 illustrates the simulation results for Cases 3 and 4, referred to as the two-layer soil structure. The upper layer depth is assumed to be 1m. The harmonic impedances [(left) absolute value and (right) phase] of L= 3m and 15m vertical ground electrodes are calculated. In Case 3, the vertical electrode inserted in soil characterized by resistivities $\rho_{LF1} = 1000\Omega.m$, $\rho_{LF2} = 10\Omega.m$. In Case 4, the vertical ground electrode buried in soil characterized by resistivities $\rho_{LF1} = 100\Omega.m$, $\rho_{LF2} = 1000\Omega.m$. The frequency response of the two different ground electrodes buried in the two-layer soil brings out significant variants. The frequency response of the 3m ground electrode reveals the same behavior at a higher frequency range. It is an inductive behavior dominantly with and without the frequency-dependent model assumption of the soil.
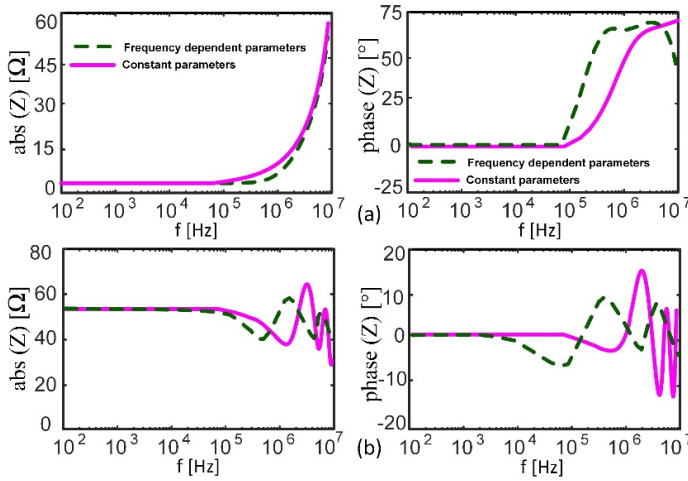

Fig. 30. Figure from C1, the harmonic impedance [(left) absolute value and (right) phase] of a 3m vertical electrode buried in the two-layer structure of soil considering the constant (solid line) and frequency-dependent (dashed line) models for the soil and $\varepsilon = 10$. (a) $\rho_{LF1} = 1000\Omega.m$, $\rho_{LF2} = 10\Omega.m$ (b) 15m, $\rho_{LF1} = 100 \ \Omega.m$, $\rho_{LF2} = 1000\Omega.m$ [7].

In addition, in Fig. 30(b), it is observed that considering the frequency-dependent effect of soil electrical parameters causes subtle changes in the harmonic impedance at high frequencies due to the oscillating behavior obtained in soil with constant electrical parameters being different.

Also, the given simulation results in Fig. 31 are the frequency response of the same grounding electrode (Case 3 and Case 4) associated with the (left) absolute values and (right) phase angle when vertical ground electrodes (L=3m and L=15m) are buried in the layered soil structure. For these cases (Case 5 and Case 6), the ground electrodes are buried in the multi-layer soil structure, considering the soil's constant and frequency-dependent models. Fig. 31(a) represents the harmonic impedance of L=3m. The resistivity of the upper layer of soil is $\rho_{LF1} = 10\Omega.m$. The middle layer soil resistivity is $\rho_{LF2} = 100\Omega.m$, and lower layer soil resistivity is $\rho_{LF3} = 1000\Omega.m$. Fig. 31(b) shows the results of vertical ground electrode with a length of 15m. The resistivities of the soil of the first, middle, and lower layers are $\rho_{LF1} = 1000\ \Omega.m, \rho_{LF2} = 100\Omega.m$, and $\rho_{LF1} = 10\Omega.m$, separately. The computed results are compared based on the constant (solid line) and frequency-dependent (dashed line) soil models for all cases. The dynamic behavior of ground electrodes buried in different soil structures is well understood and comprehensively analyzed in Chapter 2.
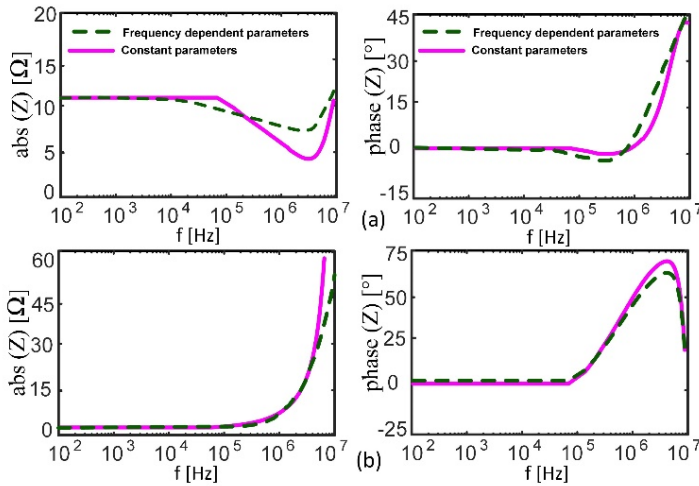

Fig. 31. Figure from **C1**, the harmonic impedance [(left) absolute value and (right) phase] of the vertical ground electrode buried in the multi-layer soil structure considering the constant (solid line) and frequency-dependent (dashed line) models for the soil and $\varepsilon = 10$. (a) 3m, $\rho_{LF1} = 10\Omega.m$, $\rho_{LF2} = 100\Omega.m$, $\rho_{LF3} = 1000\Omega.m$ (b) 15m, $\rho_{LF1} = 1000\ \Omega.m, \rho_{LF2} = 100\Omega.m, \rho_{LF1} = 10\Omega.m$ [7].

As can be observed here, there are deviations between the harmonic impedance of ground electrodes considering the constant model and frequency-dependent

models at high-frequency ranges for all mentioned cases. Obviously, the frequency-dependent model of soil can influence the GS performance. A comparison between the six examples presents different behavior in the high-frequency region. In cases 1 and 5, the GS has a capacitive behavior when the soil frequency model (SLS model) is used.

Generally, the dynamic behavior of GSs mostly depends on the electrode length and resistivity of the soil. In multilayer soil structures, the soil resistivity can be called an equivalent resistivity, which influences the capacitive or inductive behavior of GSs. The comparative analysis of the dynamic behavior of GSs with and without frequency-dependent soil models is summarized in Table 11.

Table 11: Comparison of the dynamic behavior of GSs with and without frequency-dependent models of the soil [7].

Case	L (m)	Constant model	SLS Model
1 (Uniform soil)	3	Inductive	Capacitive
2 (Uniform soil)	3	Capacitive	Capacitive
3 (Two-layer soil)	3	Inductive	Inductive
4 (Two-layer soil)	15	Capacitive- Inductive	Capacitive- Inductive
5 (Multi-layer soil)	3	Inductive	Capacitive
6 (Multi-layer soil)	15	Inductive	Inductive

Further investigation of these examples indicates that the peak values of the amplitude of the harmonic impedance based on the SLS model are smaller than their obtained results based on the constant model.

4.3   Visacro and Alipio Soil (VAS) Model 1

Another formulation of the soil electrical parameters as a function of frequency is proposed by Visacro and Alipio [108]. Using many experimental samples recorded from 30 different locations, they developed another empirical expression of the soil electrical parameters as a function of frequency. The soil pursues the empirical formulation given by (56) and (57). The valid range of frequency is from 100 Hz to 10 MHz.

$$\varepsilon_r(f) = 1,3 + 7600 \times f^{-0,4} \tag{56}$$

$$\rho(f) = \rho_0 \times \left\{1 + \left[1,2 \times 10^{-6} \times \rho_0^{0,73}\right] \times \left[(f - 100)^{0,65}\right]\right\}^{-1} \tag{57}$$
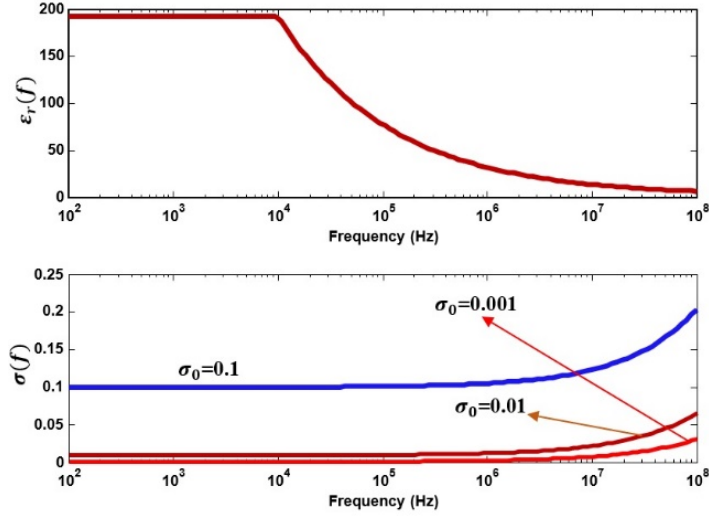
Fig. 32. Figure from **C2**, the frequency-dependent soil model based on the proposed formulas by Visacro and Alipio [108], [8].

The relationship between the soil electrical parameters and frequency for different low-frequency soil resistivities (10, 100, and 1000 Ω.m) is plotted in Fig. 32.

4.3.1   Grounding Harmonic Impedance Based on the (VAS) Model 1

Comprehensive numerical investigations have compared the simulation results based on various soil frequency models [114]. This section examines the frequency-dependent impacts of the soil frequency model on the grounding harmonic impedance based on the VAS model 1 by comparing (56) and (57) with the constant frequency model. The soil data and electrode geometry are presented in Table 12. The case studies are divided into uniform and multilayer soil structures.

- **Uniform Soil**

In order to investigate the soil frequency-dependent influences based on mentioned analytical expression, let us assume two vertical ground electrodes (3, 24m) buried in the soil with low (10 Ω.m) and high resistivity (1000 Ω.m).

100

Table 12. GS data [8].

Case No.	Electrode Length (m)	$\rho_{LF1}(\Omega.m)$	ρ_{LF2} $(\Omega.m)$
1 (Uniform soil)	3	10	10
2 (Uniform soil)	24	1000	1000
3 (Two-layer soil)	3	1000	100
4(Two-layer soil)	12	1000	100
5 (Two-layer soil)	3	100	1000

Fig. 33 and Fig. 34 present the results for a case when the harmonic impedance of the vertical ground electrode buries in uniform soil [94]. The results are also computed for the electrodes with the same lengths based on constant soil parameters. The figures show that in these cases, the soil frequency model consideration can cause a lower amplitude [45]. Furthermore, it is intriguingly apparent that since the frequency model of soil has been employed in Fig. 34 (Case 2), the frequency response of the 24m vertical ground electrode at higher frequencies behaves more smoothly compared to the constant soil electrical parameters assumption for ground electrode, which has oscillatory behavior [67]. The maximum value of harmonic impedance magnitude for both cases is lower when the soil's electrical properties are constant.
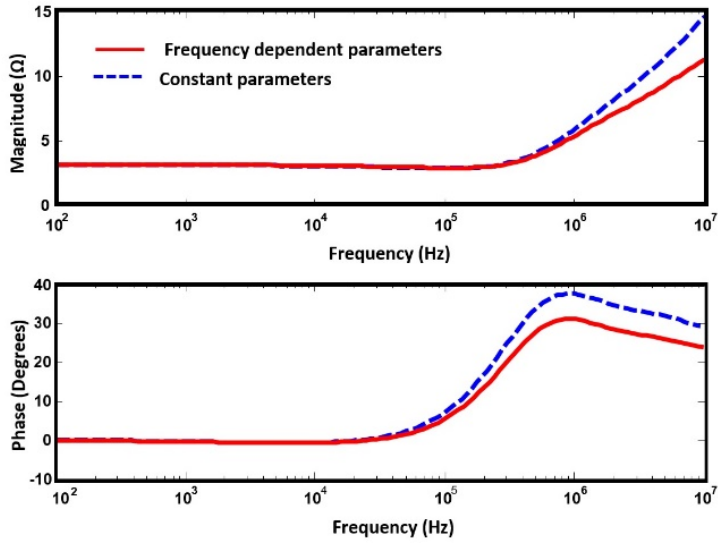
Fig. 33. Figure from **C2**, the harmonic impedance [(up) magnitude value and (down) phase] of a 3m vertical ground electrode buried in the uniform soil structure considering the constant (dashed line) and frequency-dependent (solid line) models for the soil resistivity of $10\Omega.m$ and $\varepsilon = 10$ [8].
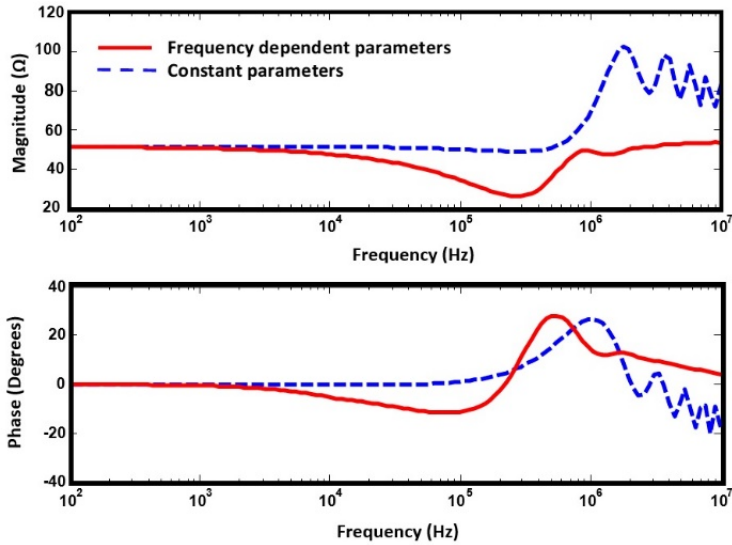

Fig. 34. Figure from **C2**, the harmonic impedance [(up) magnitude value and (down) phase] of a 24m vertical ground electrode buried in the uniform soil structure considering the constant (dashed line) and frequency-dependent (solid line) models for the soil resistivity of 1000 Ωm [8].

- **Multilayer Soil**

This section presents the simulation results for the cases when the vertical ground electrodes (L= 3 and 12m) are buried in the two-layer soil with the same soil electrical properties ($\rho_{LF1} = 1000\Omega.m$, $\rho_{LF2} = 100\Omega.m$). The impedance characteristics are computed for a specific soil resistivity ($\rho_{LF1} > \rho_{LF2}$). According to the curves shown in Fig. 35 and Fig. 36, the soil frequency response of the vertical electrode is taken into account compared to the constant model of soil electrical parameters. The amplitude values of the harmonic impedance are lower than those when the soil is assumed to be constant. The geometry of the vertical ground electrode can significantly influence the maximum value of the harmonic impedance at higher frequencies (10MHz).
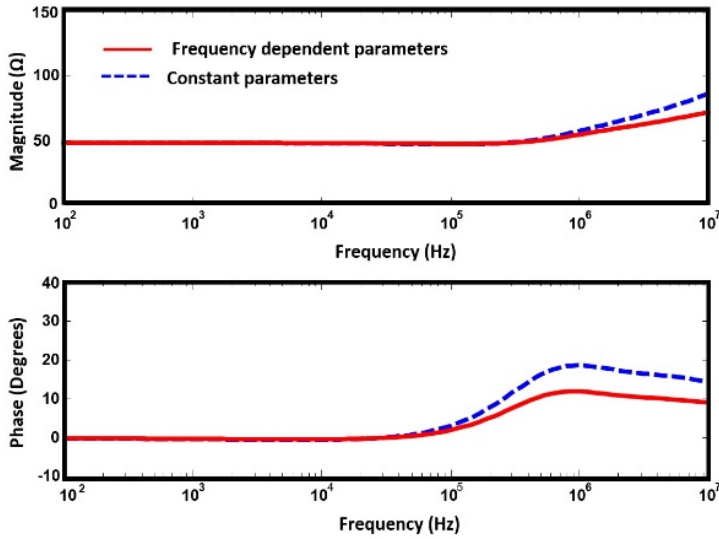

Fig. 35. Figure from **C2**, the harmonic impedance [(up) magnitude value and (down) phase] of the vertical ground electrode buried in the two-layer soil structure considering the constant (dashed line) and frequency-dependent (solid line) models for the soil and $\varepsilon = 10$. L=3m, $\rho_{LF1} = 1000\Omega.m$, $\rho_{LF2} = 100\Omega.m$ [8].
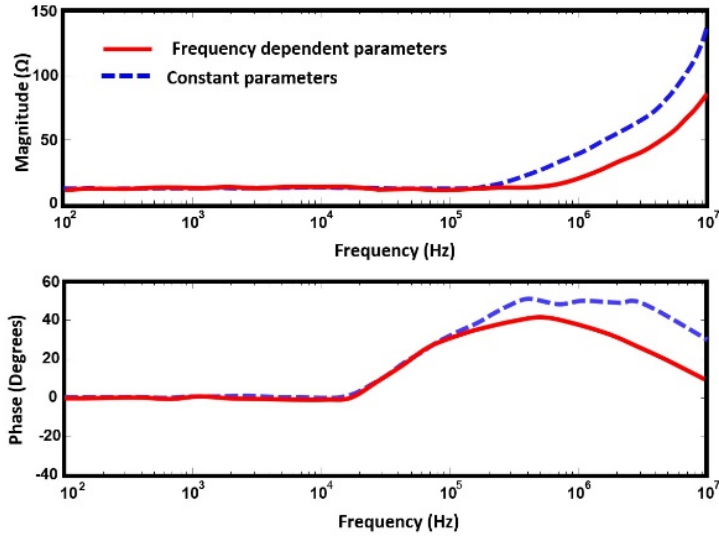
Fig. 36. Figure from **C2**, the harmonic impedance [(up) magnitude value and (down) phase] of the vertical ground electrode buried in the two-layer soil structure considering the constant (dashed line) and frequency-dependent (solid line) models for the soil and $\varepsilon = 10$. L=12m, $\rho_{LF1} = 1000\Omega.m$, $\rho_{LF2} = 100\Omega.m$ [8].

In Case 5 and in order to appraise the impact of the soil frequency model based on the VAS model 1, it is assumed that the vertical electrode buried in the two-layer soil ($\rho_{LF1} = 100\Omega.m$, $\rho_{LF2} = 1000\Omega.m$). In this case, the resistivity of the soil of the upper layer is lesser than the lower layer ($\rho_{LF1} < \rho_{LF2}$).

Fig. 37 exhibits simulation results correlated with the GS harmonic impedance [magnitude and the phase angle]. Here, we clearly see the advantages of using soil frequency models. The maximum predicted value for the magnitude of the harmonic impedance is lower when the soil frequency-dependent model of soil is used.
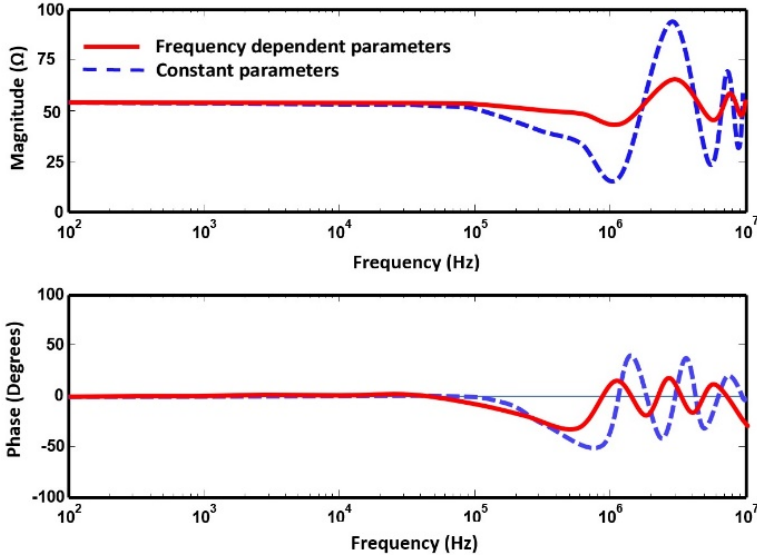
Fig. 37. Figure from **C2**, the harmonic impedance [(up) magnitude value and (down) phase] of the vertical ground electrode buried in the two-layer soil structure considering the constant (dashed line) and frequency-dependent (solid line) models for the soil and ε=10. L=3m, $\rho_{LF1} = 100\Omega.m$, $\rho_{LF2} = 1000\Omega.m$ [8].

4.3.2 Visacro and Alipio Soil (VAS) Model 2

Based on the causal results obtained from a reliable and larger dataset, Visacro and Alipio proposed other empirical models to express the frequency dependence of soil electrical resistivity and permittivity [104]. In addition, this model was recently suggested in the CIGRE Brochure [147] to be considered in lightning-related studies. The following formulas present the soil electrical parameters as a function of frequency (f).

$$\varepsilon_r(f) = 12 + (9{,}5 \times 10^4 \times \rho_0^{-0{,}27} \times f^{-0{,}46}) \tag{58}$$

$$\rho(f) = \rho_0 \times \left\{1 + 4{,}7 \times 10^{-6} \times \rho_0^{0{,}73} \times f^{0{,}54}\right\}^{-1} \tag{59}$$

Although these expressions lead to results similar to those obtained using the model proposed in [108]. In order to further evaluation of the soil frequency-

dependent model, VAS model 2 is used in the harmonic impedance modeling of the large substation GS in Chapter 5.

4.4 Frequency-Dependent Effect of Soil Electrical Parameters on Ground Potential Rise (GPR)

The study considers six examples of soil properties: two uniform and four multilayer soil structures. The GPR is calculated for uniform and multilayer soil structures to analyze the GS performance considering an accurate GS model, including frequency-dependent soil. To compute the GPR at each ground terminal in the frequency domain, the harmonic impedance of the GS is multiplied by the lightning current in the frequency domain. Then, using the inverse Laplace transform, the GPR calculates in the time domain. The effect of the frequency-dependent model of soil electrical parameters is more pronounced for ground electrodes buried in the high-resistivity soil when exposed to subsequent lightning impulses. This is due to 1) the higher frequency content of the subsequent lightning currents and 2) the higher frequency dependence of the soil conductivity for soil with high soil resistivity.

The information about the ground electrode's geometry and soil characterizations (Case 1 to 6) has been given in Table 10 in 4.2.2. The harmonic impedance figures are also shown in Fig. 29 - Fig. 31. The used frequency model of the soil electrical parameters is the SLS in these simulation results. The soil frequency model influences the harmonic impedances.

Fig. 38(a) [($\rho_=$100 Ω.m)] and Fig. 38(b) [($\rho_=$1000 Ω.m)] illustrate a comparison between the calculated GPRs for the vertical ground electrode of 3m, which corresponds to the subsequent lightning current. As observed in these results, the GPR peak with and without the frequency-dependent model of soil electrical parameters assumption took different values.

Fig. 39 presents the GPR curves considering the constant and the frequency dependence of soil electrical parameters based on the adopted GS model from Table 10 in Section 4.2.2. As mentioned, the soil has a two-layer structure. It is assumed that the 3 and 15m vertical electrodes buried in the two-layer soil ($\rho_{LF1} = 1000\Omega.m$, $\rho_{LF2} = 10\Omega.m$) and ($\rho_{LF1} = 100\Omega.m$, $\rho_{LF2} = 1000\Omega.m$) respectively. It is noticeable that the peak values of the GPR for both (left and right figures) when

the soil frequency-dependent model is used are smaller than the obtained result under the assumptions of constant soil electrical parameters.
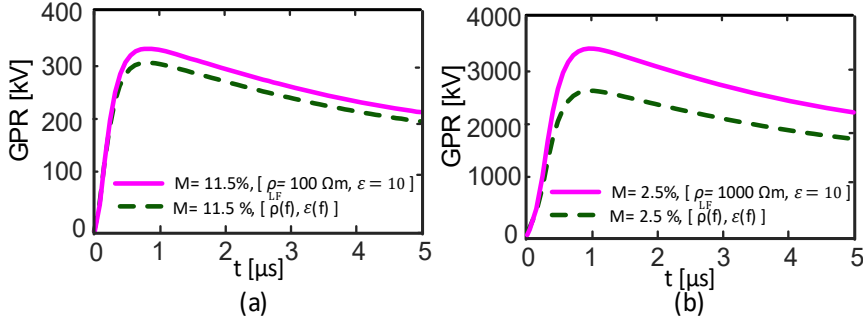

Fig. 38. Figure from **C1**, GPR value for the vertical electrode (L=3m) inserted in the homogenous soil structure; (a) ($\rho_{LF=}100$ Ω.m), (b) ($\rho_{LF=}1000$ Ω.m). It is subjected to subsequent lightning currents adopted from Heidler's functions (see Table 10). Constant (solid line) and frequency-dependent (dashed line) models [7].

Fig. 39. Figure from **C1**, GPR value for vertical ground electrode buried in the two-layer soil structure; (a) (L=3m, $\rho_{LF1=}1000$ Ω.m and $\rho_{LF2=}10$ Ω.m), (b) (L=15m, $\rho_{LF1=}100$ Ω.m and $\rho_{LF2=}1000$ Ω.m). It is subjected to subsequent lightning current adopted from Heidler's functions (see Table 10). Constant (solid line) and frequency-dependent (dashed line) models [7].
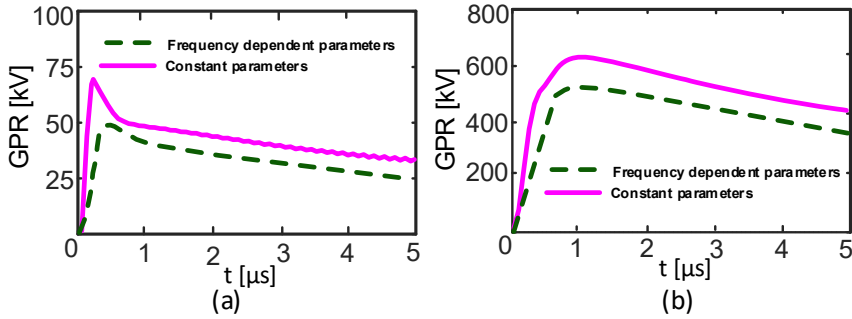
Three-layer soil configurations are considered to examine further the frequency-dependent impact of the soil electrical parameters on the GPR. As it was mentioned before, in Case 5, it is assumed that the vertical ground electrode

(L=3m) buried in the resistivity of the soil of the higher layer is $\rho_{LF1} = 10\Omega.m$, and middle layer soil resistivity is $\rho_{LF2} = 100\Omega.m$, and lower-layer soil resistivity is $\rho_{LF3} = 1000\Omega.m$. In Case 6, the vertical ground electrode (L=15m) buried in the soil with a resistivity of the upper layer is $\rho_{LF1} = 1000\Omega.m$, and middle layer soil resistivity is $\rho_{LF2} = 100\Omega.m$, and lower-layer soil resistivity is $\rho_{LF3} = 10\Omega.m$. The GPRs are compared with the corresponding vertical electrode placed in the soil with constant electrical parameters. Note that when the soil frequency-dependent model is taken into account, the peak value of the GPR is smaller than the obtained results under the assumptions of constant soil electrical parameters (see Fig. 40).
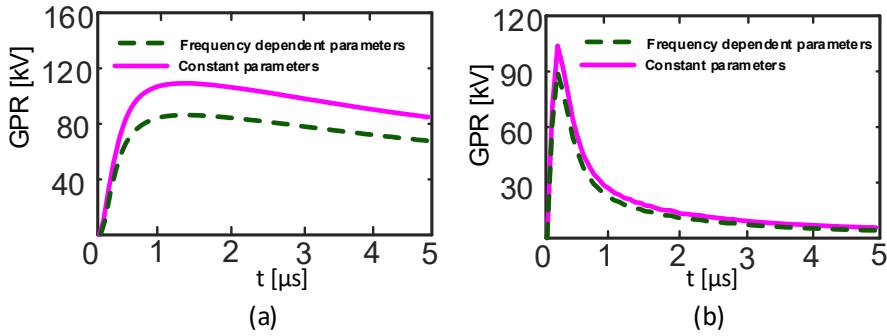

Fig. 40. Figure from **C1**, GPR value for vertical ground electrode buried in the three-layer soil structure; (a) (L=3m, $\rho_{LF1=}$10 Ω.m, $\rho_{LF2=}$100 Ω.m, and $\rho_{LF3=}$1000), (b) (L=15m, $\rho_{LF1=}$1000 Ω.m, $\rho_{LF2=}$100 Ω.m, and ρ_{LF3}= 10 Ω.m). It is subjected to subsequent lightning currents adopted from Heidler's functions (see Table 10). Constant (solid line) and frequency-dependent (dashed line) models [7].

According to the studied methodology and several empirical formulations for the soil frequency models and to further investigation of the soil electrical parameter's impacts on the GPR peak value, the reduction factor (RF) is defined as below [7];

$$RF = \frac{GPR_{SAV\ model\ 2}}{GPR_{Constant\ Parameter}} \tag{60}$$

It can be seen that the layer of the soil can contribute to the harmonic impedance. The RF is computed for all six case studies, including single-layer, two-layer, and multilayer soil structures. Table 13 shows the RF for different soil structures and lengths.

Table 13. RF for different soil structures based on the subsequent lightning current [7].

Case	Soil structure	L (m)	RF
1	(Uniform soil)	3	0.951
2	(Uniform soil)	3	0.775
3	(Two-layer soil)	3	0.714
4	(Two-layer soil)	15	0.769
5	(Multi-layer soil)	3	0.818
6	(Multi-layer soil)	15	0.902

4.5   Summary

In summary, it is worth explaining that the obtained results convey a significant frequency-dependency for the soil with higher resistivity on the harmonic impedance. The main specific scientific contribution of this chapter is to analyze the frequency-dependent impact of the soil electrical parameters on the harmonic impedance of multilayer soil structures. Then this impact is examined to compute the GPR value for different case studies. It is also observed that the GS geometry, the electrical properties of the soil, the structure of the soil, and the conditions imposed by the lightning current are the main parameters that can be affected the GPR values. It is clear that GPR curves, which ignore the frequency dependence of soil electrical parameters, overestimate the overvoltage of ground systems. In general, it can be said that GPR decreases when considering the frequency-dependent behavior of soil parameters.

Related Publications

C1. M. Ghomi, C. Leth Bak and F. Faria da Silva, "*Frequency Dependence of Multilayer Soil Electrical Parameters: Effects on the Ground Potential Rise*," in 35th International Conference on Lightning Protection (ICLP) and XVI International Symposium on Lightning Protection (SIPDA), 2021 [7].

Main contribution:

GPR calculation based on the soil frequency-dependent model considering layered soil structure.

C2. M. Ghomi, C. Leth Bak and F. Faria da Silva, "*Frequency Dependence of Multilayer Soil Electrical Parameters: Effects on the Input Impedance of Grounding*

Systems," 16th International Conference on AC and DC Power Transmission, IET event ACDC 2020 [8].

Main contribution:

Harmonic impedance evaluation of GS buried in layered soil structure based on the soil frequency-dependent model.

C5. K. Yin, **M. Ghomi**, F. Faria da Silva, C. Leth Bak, H. Zhang, Q. Wang, "*The Effect of Frequency-Dependent Soil Electrical Parameters on the Lightning Response of a 'Y' Shaped Composite Pylon for 400 kV Transmission Lines*," in *22nd International Symposium on High Voltage Engineering*, pp. 2046 – 2051, Nov. 2021 [11].

Main contribution:

Full-wave modeling application considering soil frequency-dependent model of GS for the lightning performance of the 400kV composite pylon tower.

Chapter 5. Grounding System Frequency-Dependent Model: Applications for Power System Transient Analysis

5.1 Abstract

In this section, based on the papers J2, J3, J4, J5, J6, and C4, the application of the frequency-dependent model (full-wave method) of the grounding system is checked to investigate transient overvoltages for two different cases: 1) a 63kV MV substation and 2) a novel composite Pylon tower. Significant factors influencing the overvoltage peak are the grounding structure and the electrode configuration of the GSs, the rise time and peak value of lightning, and the soil electrical parameters. First, the MoM technique is employed to implement the frequency model of the GS by using electromagnetic Maxwell's equations. Then, using the vector fitting technique, the rational approximation of the harmonic impedance/admittance matrix is computed. The fitted harmonic matrix is then utilized to make a single-terminal/multi-terminal model of the GS. It is formulated via state-space models in time domain platforms. The power system apparatus (above the soil), like towers, power transformers, etc., are also modeled in the time domain solvers. The conceptual design of the novel composite Pylon tower and transient overvoltage analysis of the MV substation is performed by considering the accurate frequency model of the grounding grid assumption.

5.2 The Applications of GS Frequency Response Model for Transient Overvoltage Analysis

The power system grids are inherently nonlinear, dynamic, and complex. The main circuit apparatus of the power system should model and take into account details of the equipment to optimize system design and operation, as well as minimization of maintenance costs. The time-domain solvers (like EMPT.RV and PSCAD) have been used to analyze the power system transients for many years. In order to investigate transient overvoltage and the time-domain simulator's abilities in the

transient analysis, these platforms are commonly handled and being developed to improve accuracy, efficiency, and capabilities to deal with new challenges of the grids.

All power system apparatus (above the soil) is well-modeled in the time-domain software. Nevertheless, the GS is a passive part placed in the soil and linked to the power system equipment via ground terminals. The used models for the GSs are elementary in time domain platforms. It has been generally considered a very simple RLC or resistive model. These models are not accurate in terms of high-frequency analysis like lightning transients.

It is worth mentioning that when lightning hits OHLs, blades of wind turbines, or apparatus of the substations, a considerable part of the lightning impulse injects into the soil via GSs. Therefore, the GS model is vital in determining the resultant inflicted stresses of the voltage on the system elements in terms of safety, insulation coordination, and protection. For instance, the injected lightning current can increase the GPR at the neutral terminal of power and earthing transformers. The GPR can also increase the body voltage of the tower of the wind turbine or OHLs. These overvoltages may create failure in the insulator string of power transmission lines by increasing the voltage across the insulator more than its withstand voltage levels (BIL) or may damage transformers if the lightning performance of the GS is not well-designed.

In order to assess the full wave technique influences of the GS modeling on transient analysis of power systems, two different case studies are considered. The generated overvoltages considering the full wave model of the GS based on MoM are obtained.

The first case study is the MV substation. In this case, all power system apparatuses above the soil are modeled in the EMTP.RV software. The GS model is added to this time domain simulator using the state-space block as an interface between frequency and time domains.

In the second example, the harmonic impedance of the GS in the frequency domain is linked via the FDNE block to the PSDCAD platform. The PSCAD platform uses the resistive model of the GS, and it may create errors in the lightning performance studies while the simple model of the GS uses. To solve this issue, the GS includes all soil details (like soil layer, geometry, and frequency model of soil) is modeled using the full wave approach, and is connected to the PSCAD. The feasibility study

for the analytical expression for different types of towers is performed to check lightning performance. The lightning transient overvoltage is compared for the Pylon, Donau, and back flashover performance of the metallic and new composite pylon towers are investigated based on an accurate model of the GS.

5.2.1 Substation Grounding System Modeling for the Power System Transient Analysis

The station GS is a vital element of the entire power system grid. It is a soil-buried metallic structure consisting of horizontal and vertical electrodes. It is developed not only to create a pathway to conduct fault currents of substation into the soil without going over the functioning specifications of the apparatus but also to prepare a secure working environment for personnel in the surroundings during normal and faulty situations.
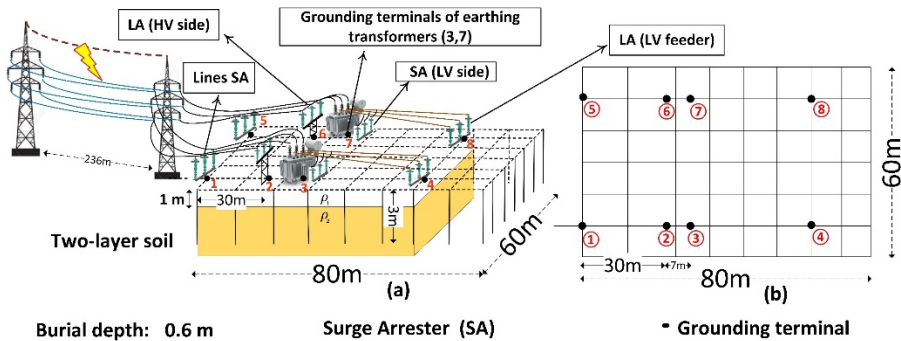

Fig. 41. Figure from **J2**, substation layout overview, a) power system apparatus b) grounding grid terminals [2].

The ionization and inductive behavior of soil are two crucial phenomena in the dynamic behaviors of the substation GS modeling. The first one is likely to enhance the performance, and the second one may decline the performance of the GSs. Nevertheless, in current publications, it has been proposed that the soil ionization influences are most likely to be slight and can thus be neglected for the large GSs installed in the HV/MV substations [148].

This study investigates how ground soil structures affect lightning/switching overvoltage transients at MV substations. The results of transient overvoltage

analysis for the 63/20 kV substation are presented. The well-known rigorous frequency domain electromagnetic method (MoM) based on the numerical solution of Maxwell integral expressions is employed to estimate the admittance/impedance matrix of the substation GS within the desired range of frequency from low frequency (power frequency) to high frequency (10 MHz). As mentioned before, the noteworthy benefit of this solver is its capability to cope with the modeling of GSs at high-frequency transients like lightning. In order to evaluate the full-wave method influences of the substation GS on transient analysis, two different soil structures (homogenous and two-layer) are studied. Table 14 presents the low-frequency values for soil with different structures. In Cases #2 and #3, the depth of the first soil layer is assumed to be 1m. The substation GS is assumed to be multi-terminal (eight ground terminals); consequently, the harmonic impedance dimension is 8×8 in this example. The soil is assumed to be frequency-dependent. The developed model by Visacro and Alipio (VAS) Model 2 is used to consider the frequency dependency of soil [104].

Table 14: Low-frequency value of the resistivity of soil for the substation grounding system [2].

Cases	Soil structure	ρ_1 [Ω.m]	ρ_2 [Ω.m]
Case 1	(Uniform soil)	100	100
Case 2	(Two-layer soil)	100	10
Case 3	(Two-layer soil)	100	1000

The technical specifications of the substation and assumptions are explained in this part. The substation layout with detailed information is shown in Fig. 41(a). GS is buried at a depth of 0.6 meters, and the cross-section of the ground electrodes, including vertical and horizontal electrodes, is 150 mm^2. The dimension of the substation GS is 80m×60m. Two power transformers are supplied via a 50 km double circuit OHL. The HV side of power transformers is solidly grounded. The GS is connected to the electrical apparatus via eight terminals (see Fig. 41(b)). Due to the large substation size, the assumption of having an equipotential surface (used in the IEEE method [98]) will not be valid for this GS. Therefore, the static analysis will not provide reliable results in this case.

5.2.1.1   Grounding System Modeling of The Large Substation

Here, the GS modeling workflow for the multilayer soil structure is discussed shortly. Further information about the implemented method for this example,

considering the frequency model of the soil, is presented in [2]. The same procedure presented in [115], [1], [66], [149] is used to compute the harmonic impedance matrix. In this example, to improve the method accuracy in the transient overvoltage calculation, the layer with the frequency-dependent electrical parameters of soil, and the high-frequency model of the main apparatus above the soil are considered in the integrated model.

To model the GS, the assumption of the thin wire theory is implemented. This assumption can assist in lessening problem dimensions of integral from an integral over the 3-D domain to the surface or the line. Using the thin-wire assumption, the distribution of the current along the segments can be expressed as a charge and current distribution at the ground electrode axes.

In this code, the model preconditioning and input data are done by identification of the geometry of the GS and its node/junction locations based on the cartesian coordinate system (x,y,z), identification of the geometry for soil structure, including the dimension and number of layers, and soil electrical properties like resistivity and permittivity values at low frequency. The simulation carries out at each defined frequency. Based on the frequency model of the soil, the soil's electrical parameters will be modified at each frequency. The next step is to divide the GS's electrode into small sections. The triangle basis function is employed to excite each of the ground terminals. The mathematical equation is developed by satisfying the boundary conditions at the surface of the substation grounding electrodes [2].

$$\hat{n} \times E^S + \hat{n} \times E^i = 0 \tag{61}$$

$$E^S = -\nabla V - j\omega A \tag{62}$$

where E^S, E^i, V and A are scattered field, incident field, electric scalar potential, and magnetic vector potential, respectively. The ∇ and ω are the angular frequency and gradient operators. The Green function [1] is not a unique matrix and can be given by (63). The electric scalar and magnetic vector potential are presented in (64) and (65).

$$\overline{G_A} = \begin{pmatrix} G_{xx} & G_{xy} & G_{xz} \\ G_{yx} & G_{yy} & 0 \\ G_{zx} & 0 & G_{zz} \end{pmatrix} \tag{63}$$

$$V = \int \boldsymbol{G}_v \rho_s \, dS' \tag{64}$$

$$A = \int \boldsymbol{G}_A \cdot J_s \, dS' \tag{65}$$

where ρ_s is the charge density on the ground conductor surface and J_s is the density of the electric current. The known mixed-potential integral equation (MPIE) is used to create the simulation model. Hence, during the computation of Green's function for the substation GS, Sommerfeld's integrals are utilized to estimate the influence of the soil structure [2].
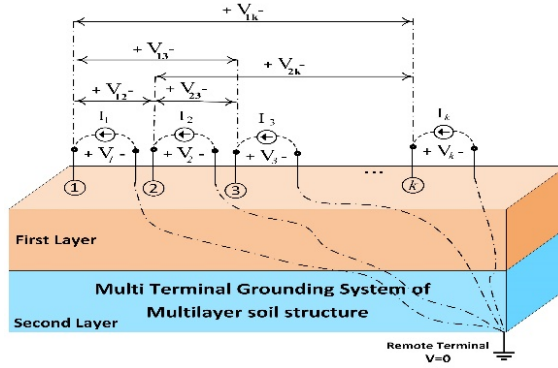

Fig. 42. Figure from **J2**, multi-terminal GS considering layered soil structure [2].

Fig. 42 shows the procedure of the current injection and the calculation of the remote voltage separately. The current distribution along the ground conductor is estimated by governing MPIE and obtained with the MoM's help. Then, the fields of electromagnetic are computed. In this stage, the current is applied to the shown input terminals (k=1, 2, …, 8), and the induced voltage between the injected and remote terminals shall be computed. At a high-frequency regime, the integral of the electric fields depends on the path between the start and endpoints. However, to compute the unique voltage along the path at each frequency, the scalar potential gradient is computed along an alone straight path and resumes to the remote terminal point (V=0). Each ground port is impressed by the excitation current, and the other seven ports remain open circuit. The self and mutual

116

elements of the harmonic impedance matrix are computed over the desired frequency range [2]. The close form of this matrix is given by

$$\boldsymbol{Z}(s) = \begin{pmatrix} z_{11}(s) & \cdots & z_{18}(s) \\ \vdots & \ddots & \vdots \\ z_{81}(s) & \cdots & z_{88}(s) \end{pmatrix} \tag{66}$$

where $Z_{ii}(s)$, $Z_{ij}(s)$, and s=jω are self-impedance, mutual impedance, and Laplace variables for (i=j= 1, 2, …k=8).
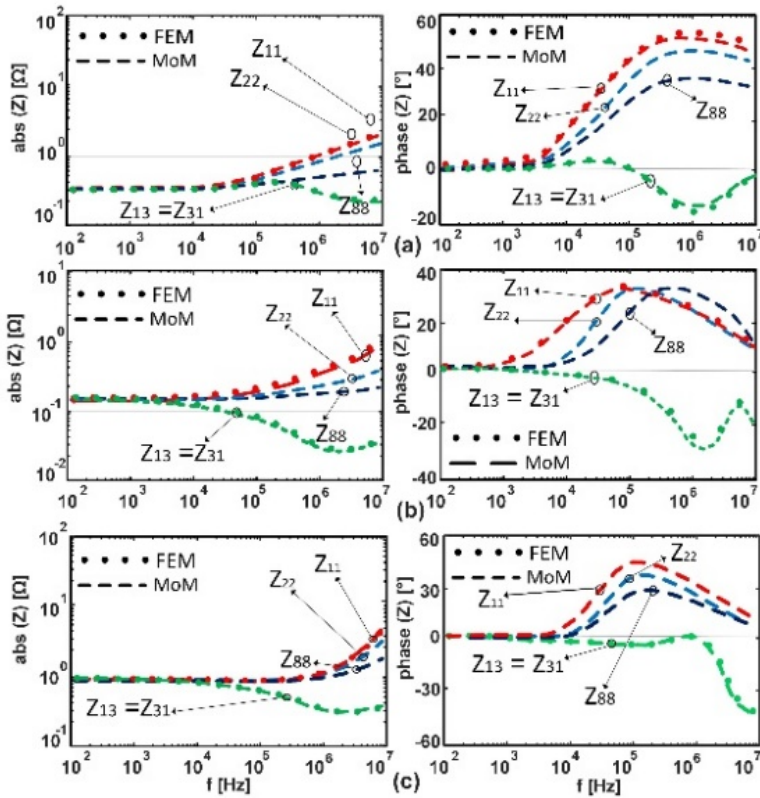

Fig. 43. Figure from **J2**, self and mutual harmonic impedances of the substation grounding system(SGS): (a) Case#1, (b) Case#2, and (c) Case#3 [2].

Fig. 43 demonstrates the computed harmonic impedance [amplitude (left) and phase angle (right)] for the mentioned cases in Table 14. The curves denote how

the harmonic impedances change with changing the frequency. In the low-frequency range for all cases, the self-harmonic impedance amplitude is constant and does not change with increasing frequency, and it takes the same value of the DC resistance to ground. In the high-frequency region, the self-impedance magnitude is a function of frequency, and the GS has frequency-dependent behavior [2].

The dynamic behavior of GSs and their frequency responses are different from each other's and depend on the geometry of the GS, soil structure, and electrical parameters of the soil.

It is worth noting that the modeling is done by the FEM to compute a few elements of the harmonic impedance matrix (Z_{11} and Z_{13}). As noticed in Fig. 43 from the initial results, an excellent agreement presents between the MoM (dashed lines) and FEM (dotted lines) methods to confirm the used method. For example, to compute the self-impedance (Z_{11}), 129 frequency samples are used in the defined frequency range (zero to 10 MHz). In the MoM, after doing the segmentation of Case #2, the number of cells is about 21,793. MoM does the modeling for each frequency within 13 min, and it is taken about 54 min for the FEM. The same hardware and RAM are used to compare the simulation time-consuming (Intel-Xeon E2286 G Processor (12M Cache, 4.00 GHz) desktop computer) [2]. Finally, the simulation times to estimate the harmonic impedance (Z_{11}) are 1677 and 3996 min for MoM and FEM, respectively [2].

5.2.1.2 Main Circuit Apparatus Modeling in the EMTP.RV

Fig. 44 shows the single-line diagram of the substation apparatus, which is placed above the soil and is connected via eight ports to the ground as it is shown before in Fig. 41(b), the ground terminals of the substation, which neutral points of the HV main circuit equipment like power transformers and arresters, are connected to the ground. A very simple model (capacitor) for other devices, such as circuit breakers, disconnector switches, busbars, and capacitance-voltage transformers, is assumed based on the test data sheet of suppliers and technical reports. The main apparatus models include two power transformers (63/20 kV) and earthing transformers, eight arresters for both low and high voltage sides, and a 63kV incoming tower and 50 km OHL to the next substation. All detailed information is presented in [2]. To perform the transient analysis of the substation, the detailed model of the GS should link with the time domain solver, which already the apparatus is modeled. To this aim, the interface tool needs to be used to make an

interface between these two parts. The mathematical model's overview will be briefly discussed in the next section.
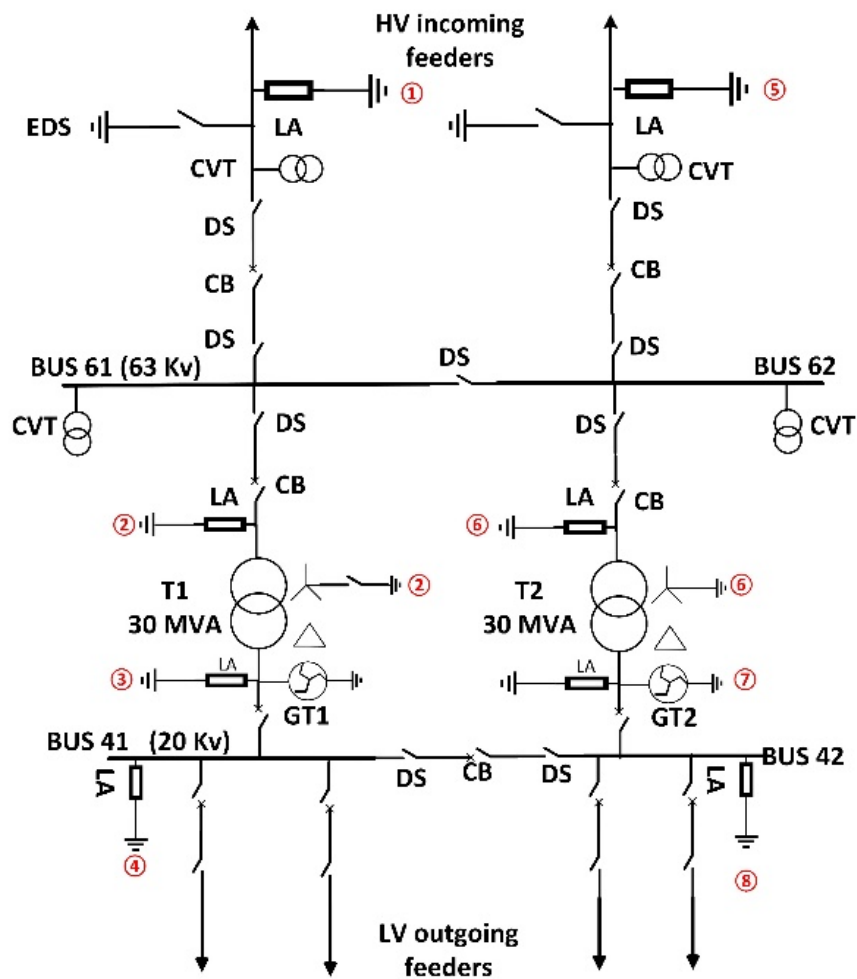

Fig. 44. Figure from **J2**, main circuit apparatus of substation [2].

5.2.1.3 Interface For Adding the Detailed Frequency Model of The Grounding System to The Time-domain Platforms

Several time domain simulators perform are able to the transient analysis of power systems like PSCAD/EMTDC, ATP-EMTP, and EMTP.RV. In addition, these solvers are very useful in terms of low and high-frequency regimes for the installed equipment above the soil. The ground models in these softwares are generally straightforward and can be considered the resistor model. The resistive model value is the same as the GS's low-frequency value of ground frequency response or harmonic impedance. In the high-frequency regime, as we mentioned before, the behavior of the GS depends on the frequency and changes with the frequency change.

To add the precise model of the GS to these platforms and to compensate for the lack of a detailed model of the GS, including a frequency model of the soil electrical parameters and soil structure at the high frequencies, vector fitting techniques can be used for making the GS state-space model in the time domain from its frequency model. For this purpose, rational fitting values of all components of the harmonic impedance matrix are derived to reproduce its pole-residue values [66]. These methods are the vector fitting method [63] and the matrix pencil method [150].

To this aim, the frequency response of the GS or each element of the harmonic impedance/admittance matrix can be described based on the pole-residue model [2] given by (67),

$$\mathbf{Y}(s)^{-1} = \mathbf{Z}(s) = \sum_{m=1}^{M} \frac{\mathbf{R_m}}{(s - a_m)} + s\mathbf{E} + \mathbf{D} \tag{67}$$

Where a_m and $\mathbf{R_m}$ are values of the passive poles and the matrix of residue values, respectively. The total number of the GS state variables (N) can be computed by multiplying the number of poles (M) and terminals (T). The passivity enforcement is done to predict all eigenvalues correctly and to take their positive values [151]–[154]. The components of the harmonic impedance matrix in the form of a state space model can be obtained below.

$$\mathbf{Y}(s)^{-1} = \mathbf{Z}(s) = \mathbf{D} + \mathbf{C}(s\mathbf{I} - \mathbf{A})^{-1}\mathbf{B} + s\mathbf{E} \tag{68}$$

However, matrices **A**, **B**, **C**, and **D** are generated from the harmonic impedance/admittance matrix in the frequency domain. With this regard, the state space block can be played the role of an accurate model of the GS in the EMTP.RV platform [2]. In the PSCAD/EMTDC platform, FDNE has the same role, and this block is developed to connect the frequency model of the GS to the apparatus above the soil [10], [11].

5.2.1.4   Model Validation in The Time Domain

To additionally evaluate the accuracy of the proposed method, Case 2 is prepared. The equivalent soil resistivity of the two-layer soil structure ($\rho_1 = 100\Omega.m$, $\rho_2 = 10\,\Omega.m$) is about 41.5 Ω.m. The equivalent DC resistance is established on the mentioned earth resistivity (LF$_{Resistance}$) GS dimensions and length of electrodes, with a cross-section of about 0.17 Ω. This simple resistive model is added to the implemented model in the EMTP.RV. The GS model at one single frequency sample (f=50 Hz) is also estimated using the proposed method in the frequency domain. The state space model (A, B, C, and D) from the impedance matrix, using the vector fitting technique, is computed to create the interface between the frequency response of the substation GS and the time domain solver. To verify the results, the short circuit test (L-G) is applied in the EMTP.RV platform. The validation procedure of the full wave GS modeling at the power frequency (50 Hz) is presented in Fig. 45.
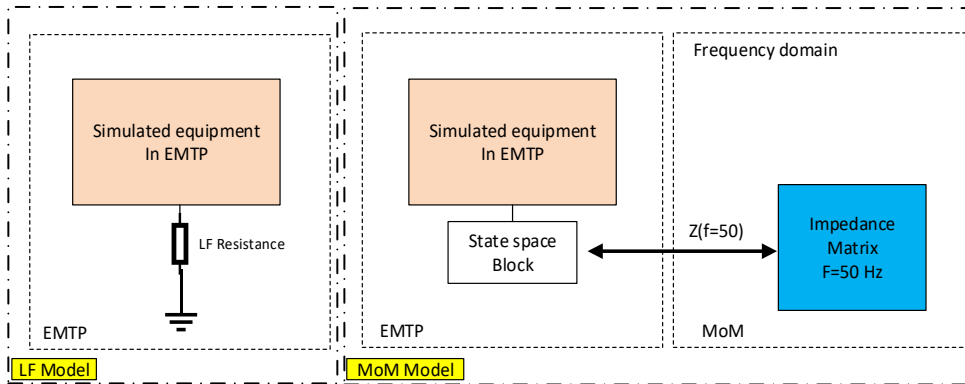

Fig. 45. Figure from **J2**, time domain validation workflow.

The voltage waveforms at the LV bushing (left side) /HV bushing (right side) of the power transformer T1 are shown when a fault happens at the distribution feeders (phase a) (see Fig. 46). The waveforms of the phase voltages are compared. At the same time, the MoM (solid line) and resistive (dotted line) techniques have been employed. As presented, the outcomes indicate that the MoM model of the substation GS is in reasonable consensus with a straightforward resistive model in the EMTP.RV. It seems that both methods in the GS modeling illustrate the same results, which is a good indication of the exactness of the proposed method at low frequency due to the low-frequency content of the short circuit current. The results also demonstrate that the proposed technique is valid for the low-frequency range (f=50 Hz).
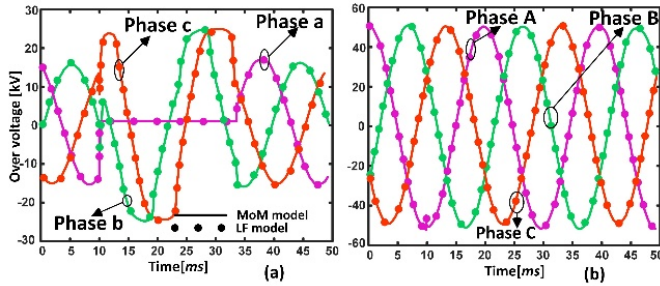

Fig. 46. Figure from **J2**, LF, and MoM models compare the overvoltage generated at the power transformer bushings while the L-G fault happens at the LV distribution feeder (Phase a). [(a): LV side and (b): HV side (right)] [2].

5.2.1.5   Ground Potential Rise Calculation for the MV substation

In this section, to calculate the GPR value and the generated overvoltage caused by lightning, the Heidler model is used to reproduce the subsequent lightning current waveform. It has high-frequency content because of having a fast front time. The first lightning stroke has a high current density. It can make a large enough electric field around the ground electrode, which is greater than the soil critical field strength value. It can consequently discharge sparks into the soil. The breakdown of the soil will occur. It is so-called soil ionization and generally cannot consider the worst case in the high-frequency regime. In this situation, the ionization due to the high lightning current magnitude can improve the dynamic performance of the substation GS and when neglected the results will be conservative. However, the subsequent lightning current with the fast front time

can generate the worst case and is suitable for engineering design. In the worst case, the inductive behavior of the GS at the high frequencies may lead to generating a large GPR. The subsequent lightning current based on the Heidler model is characterized by a front time of 0.8- µs, a steepness value of 40 kA/µs, and a peak value of 12 kA.
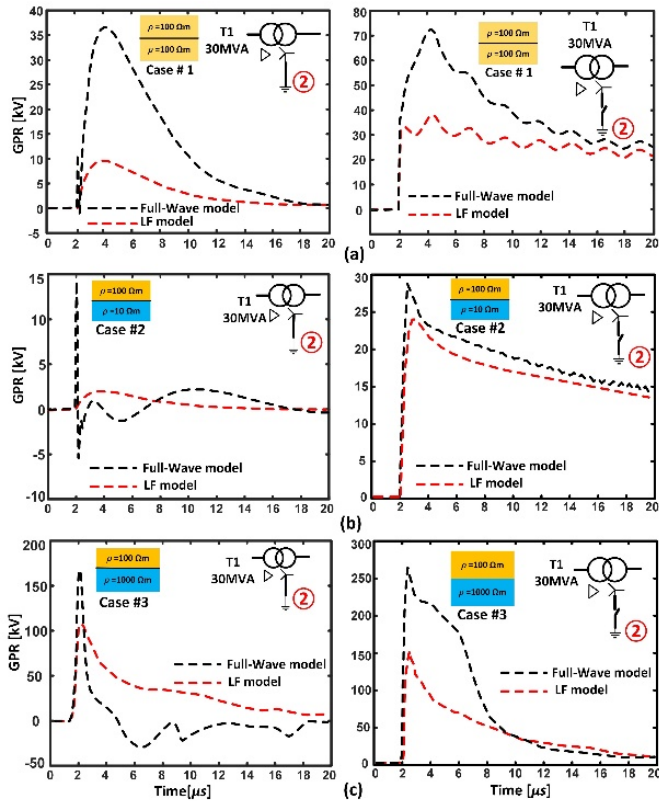

Fig. 47. Figure from **J2**, the simulated GPR (a) uniform soil structure (Case#1), (b) two-layer soil structure (Case#2), (c) two-layer soil structure (Case#3) subjected to a representative current of subsequent lightning current. [left] the neutral of T1 is solidly earthed, and [right] the neutral terminal of T1 is opened [2].

Fig. 47. illustrates the calculated GPR developed under the presumption of the low frequency (LF) model and full-wave model of the MV substation grounding grid subjected to noted subsequent lightning current for three different cases. It can be seen that in case 1, the difference between full wave and low-frequency model

assumption is about 30 kV when the neutral terminal of T1 is solidly earthed or not grounded. In this case, the soil structure is uniform, and the value of soil resistivity is 100 Ω.m (see Fig. 47(a)). In case 2, there is about a 10 kV difference between the obtained peak values of GPR for the LF and full wave models (see Fig. 47(a)). In case 3, these values change to 70 kV and 120 kV, respectively, when the neutral terminal of T1 is solidly earthed and kept open circuit (see Fig. 47(a)). The big difference for case 3 between LF and the full-wave model comes from the idea that the inductive behavior of the GS at high-frequency region considering a full-wave model of the GS is more highlighted in terms of the high resistivity of the soil. However, with the low-frequency model technique, the GPR peak values take underestimation values. In some scientific research, to reduce the computation time, the impact of the layered soil structure on the GPR in the substations ignores. This parameter also may need to be considered for estimating the GPR with minimum error.

5.2.1.6 Impact of The Frequency-Dependent Model of The Soil Electrical Parameters on the GPR

This part illustrates results concerning the influences of the soil frequency-dependent model (VAS model 2) on the GPR for the subsequent lightning current. Here, the importance of the soil frequency-dependent (FD) model in the case of high DC soil resistivity is denoted. Therefore, two different cases are taken into account with different equivalent DC resistances ([a] Case 1 and [b] Case 3). The GPR curves are shown for these cases (see Fig. 48). The equivalent DC resistance of Case 3 is greater than Case 1 due to the lower layer soil resistivity of 1000 Ω.m. The GPR peak value in Case 3 is roughly two times larger than the GPR peak observed at power transformer T1 (terminal 2) in Case 1. The constant electrical parameters of soil have been used in the simulation.

In other words, when soil resistivity is low ($\rho < 100\ \Omega.m$), the frequency-dependent model of soil electrical parameters may be neglected. The simulations almost obtained the same results when the neutral point of power transformer T1 was earthed or kept as an open circuit.
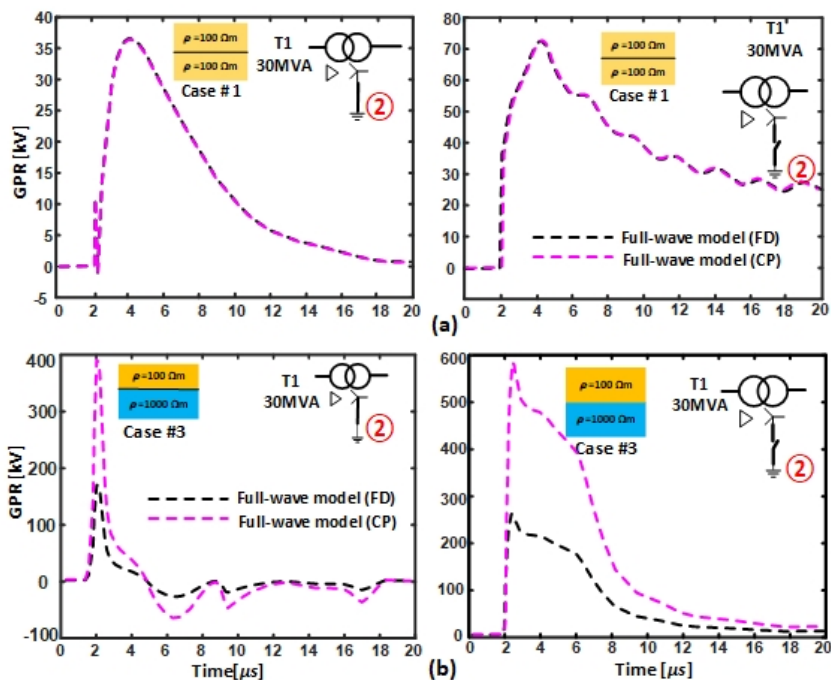
Fig. 48. Figure from **J2**, GPR value at terminal 2 subjected to the subsequent lightning current under the constant soil model (CP) and frequency-dependent soil model (FD). (a) uniform soil structure, and (b) two-layer soil structure [2].

5.2.1.7 Lightning Overvoltage Analysis Considering Full Wave Modeling of The Substation Grounding System

Direct strokes from lightning can damage substation equipment and bus work. To protect the equipment of the substation yards, lightning protection systems are required. The lightning protection system aims to intercept direct lightning strikes that can damage the substation equipment. Grid owners use effective shielding to select the station's lightning protection level. Sufficient shielding means that all lightning strikes pulses greater than the apparatus and the buses withstand maximum lightning current, which will end in the lightning protection system before getting a striking length to the buses and apparatus being protected.

In this manner, in the event of a shield failure on OHL, the buses and apparatus of the substation should withstand the resulting overvoltage. To ensure that the equipment overvoltage level is not exceeded, surge arresters are applied to protect the equipment. As the lightning strikes information is based on statistical relationships among lightning parameters, it is recognized that effective, 100% reliable shielding cannot be achieved in practice. That is why as the worst case, it is assumed that the OHLs are not equipped with guard wires.

The surge arresters are the most effective tools to protect the equipment and are installed in the incoming substation feeders and both sides of the power transformer. The suggested model of the zinc oxide surge arrester by Martinez is implemented in the time domain platform [155]. To evaluate the application of the full wave modeling of the GS on the lightning transient over voltage calculation, it is supposed that the subsequent lightning stroke hits on OHL (phase A). The location of the fault is about 50-m far from the power transformer T1. It is also assumed that the neutral terminal of power transformer T1 is opened [state 0] or solidly earthed [state 1]. The obtained voltage curves of all terminals of the power transformer's bushings (HV side (right) and LV side (left)) for three case studies (Case 1, 2, and 3) are shown in Fig. 49.
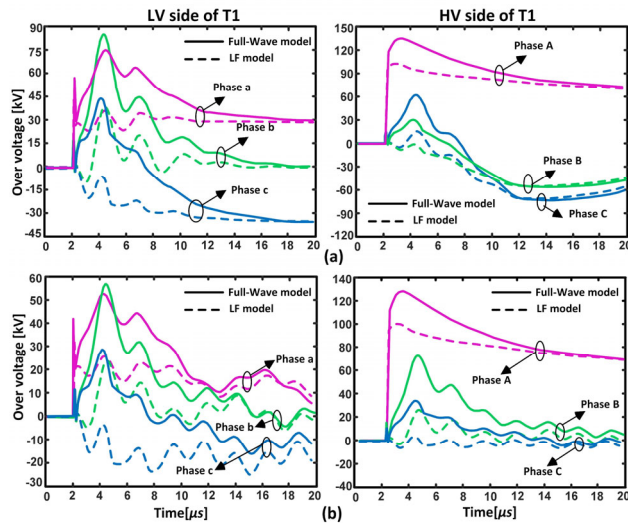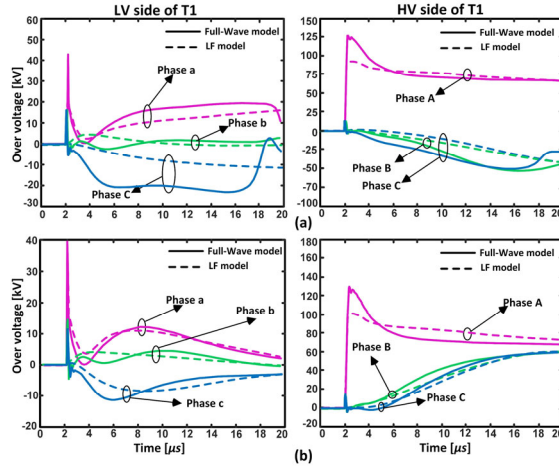
Fig. 49. Figure from **J2**, three-phase curves of the voltage between the terminal of the power transformer's bushings for both sides (HV & LV) and ground against the subsequent lighting stroke on the phase A. (a): the power transformer's neutral is closed and (b) is opened (See Table 14) [2].

These results show that the assumption of the structure of soil layers (uniform /two-layer) can change the predicted overvoltage in the substation. Generally speaking, the behavior of the GS and its harmonic impedance is a crucial parameter in the studies of high-frequency phenomena like lightning. In these results, the over-voltage values based on the full wave modeling of the GS are compared when

127

the GS's low-frequency model (LF) or resistive model is used. The resistive model is non-frequency dependent, and the effects of inductive or capacitive behavior of the GS are neglected, which causes the underestimation of overvoltage at the power transformer's terminals.

5.2.1.8   Switching Overvoltage Analysis Considering Full Wave Modeling of The Substation Grounding System

128

Case 3
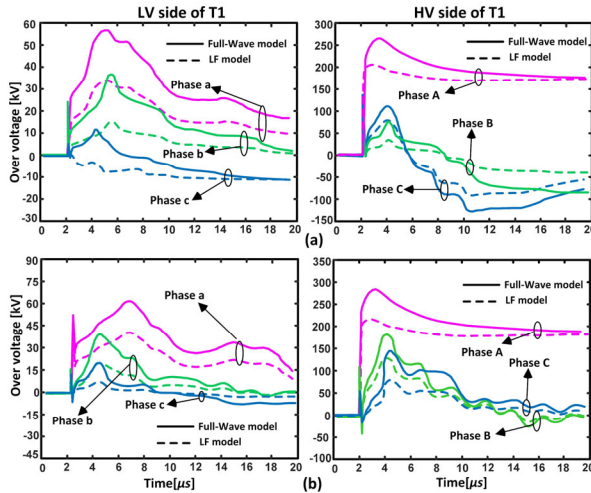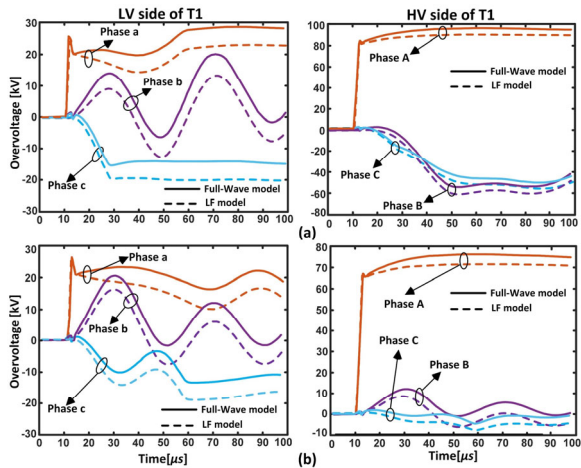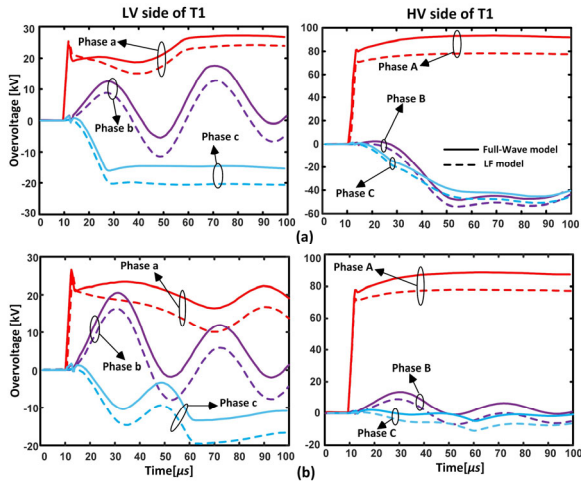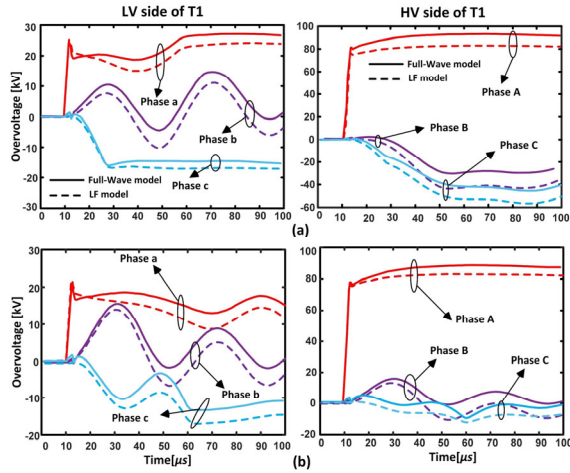
Fig. 50. Figure from **J2**, the voltage curves between the terminal of the power transformer's bushings for both sides (HV & LV) and ground against the switching event. (a): the power transformer's neutral is closed, and (b) is opened (See Table 14) [2].

Switching overvoltage is often a concern in apparatus insulation coordination studies because it can destroy insulations. This phenomenon can happen when OHLs energize/de-energize. It can also occur when the fault clears or a large load of the network sheds. This transient can create a traveling wave along with the OHLs. The timing scale of switching is about a few microseconds in the time domain and between 5 to 150kHz in the frequency domain. In the frequency domain, the switching range of frequency is much lower than the lightning frequency range.

To model a simple switching transient in the used time domain platform and to check the performance and effect of full wave modeling of the GS, it is assumed that the switching operation is performed at t=10 μs. In this condition, two different soil structures and three different soil electric parameters are tested. The voltage waveforms for all phases at the power transformer's terminals are illustrated in Fig. 50. The results are compared when the neutral terminal of the power transformer is open and solidly earthed.

Table 15 presents the peak voltage value at the power transformer T1 terminals for the transient overvoltage analysis (lightning and switching studies). These results are computed based on the two operating modes.

Mode 1: Neutral terminal of the power transformer (T1) is directly earthed.

Mode 0: Neutral terminal of the power transformer (T1) is an open circuit.

The obtained results of the mentioned cases in Table 14 show that peak values of the switching transient overvoltage do not take too many differences for the full wave (FW) and low frequency (LF) models of the GS in comparison with lightning transient over voltage peak values. It is because of having the lower frequency contents for the switching events. To have a big picture of different cases, including soil structure, and GS modeling method efficiency, and to compare the simulation results, two following indexes are determined.

Table 15. Generated overvoltage value due to happened transients (lightning and switching) [2]

Cases	GSM	State	Lightning						Switching					
			LV side			HV side			LV side			HV side		
			a	b	c	A	B	C	a	b	c	A	B	C
Case 1	LF	1	35	36	-33	104	-45	-59	22	12	-20	89	-61	-52
		0	27	25	-25	102	26	5.5	26	16	-20	72	9	-8
	FW	1	75	88	45	142	67	35	28	20	15	93	-53	-48
		0	54	58	29	129	77	36	28	22	-14	78	12	-5
Case 2	LF	1	27	6	-10	89	-42	-42	24	12	-20	78	-55	-52
		0	43	2	-8	103	60	60	21	17	-20	79	8	-13
	FW	1	45	17	-22	127	-51	-51	30	18	-15	93	-50	-49
		0	40	5	-12	142	60	60	27	23	-11	90	16	-4
Case 3	LF	1	33	16	-10	203	36	77	24	-10	-16	81	-37	-59
		0	35	19	9	210	123	74	21	15	-17	81	17	-8
	FW	1	57	37	12	265	81	112	25	-7	-15	92	-25	41
		0	62	38	17	283	179	144	22	17	-12	89	15	-6

1) Low-frequency error index (LFEI) [2]

The assumption to calculate LFEI is that the substation grounding grid for the mentioned case studies in Table 13 is the same. The LFEI is defined as a ratio between the maximum value of the calculated overvoltage based on LF and the full wave (FW) approach for GS modeling (GSM). This index shows the importance of the full wave modeling of the GS for performing transient over-voltage studies for subsequent lightning strikes or fast front waveforms. The excitation wave from frequency contents influences the maximum overvoltage at the bushings of power transformer T1. The switching impulses do not have a high-frequency content like

lightning waveforms. In the transient overvoltage study, the model of the GS will have some influences because of its inductive behavior. Table 16 shows the LFEI

values for all cases with two states (0 and 1).

Table 16. LFEI values for the obtained overvoltage are presented in Table 15 [2].

Cases	State	Lightning						Switching					
		LV side			HV side			LV side			HV side		
		a	b	c	A	B	C	a	b	c	A	B	C
Case 1	1	0.47	0.41	-0.75	0.73	-0.67	-1.67	0.81	0.61	-1.32	0.96	1.15	1.07
	0	0.50	0.44	-0.88	0.79	0.34	0.15	0.92	0.74	1.38	0.93	0.75	1.59
Case 2	1	0.62	0.33	0.47	0.71	0.81	0.82	0.81	0.71	1.38	0.84	1.11	1.10
	0	1.09	0.44	0.67	0.72	1.00	1.00	0.80	0.77	1.86	0.88	0.52	3.02
Case 3	1	0.58	0.43	-0.81	0.77	0.44	0.69	0.94	1.49	1.11	0.88	1.48	-1.42
	0	0.57	0.48	0.50	0.74	0.69	0.52	0.95	0.90	1.46	0.91	1.13	1.32

2) Soil structure impact index (SSII) [2]

In order to evaluate the impact of the earth structure of the GS and the number of earth layers on the transient overvoltage value, the homogenous soil structure is selected as a base case. The peak overvoltage values are based on the two-layer soil structure and compared with the base case (Case 1) with two different states (0 and 1). This is performed by definition of the soil structure impact index (SSII), which is the ratio between the maximum value of the calculated overvoltage based on the uniform soil and two-layer soil structure of GS modeling (GSM). The SSII is calculated to compare the simulation results of the homogenous and two-layer ground structure assumption. The electrical properties of the two-layer structure are influenced by the frequency response of GSs in the frequency domain and transient overvoltage in the time domain. Table 17 and Table 18 show the SSII for the soil structure with two layers considering uniform soil as a base value for the transient over-voltage value. The FW approach is used to model the substation's GS taking into account the soil's frequency-dependent impact.

131

Table 17. SSII (case 1 vs. case 2) [2].

State	Lightning						Switching					
	a	b	c	A	B	C	a	b	c	A	B	C
1	1.67	5.13	-2.07	1.12	-1.31	-0.69	0.93	1.14	-1.03	1.00	1.06	1.01
0	1.36	12.0	-2.39	0.91	1.29	0.61	1.06	0.97	1.32	0.87	0.77	1.21

Table 18. SSII (case 1 vs. case 3) [2].

State	Lightning						Switching					
	a	b	c	A	B	C	a	b	c	A	B	C
1	1.31	2.41	3.70	0.54	0.83	0.32	1.11	-2.94	-1.03	1.01	2.09	-1.17
0	0.87	1.50	1.65	0.46	0.43	0.25	1.30	1.31	1.20	0.87	0.83	0.81

The final ambition is to find a proper GS model of the MV substation that allows accurate modeling of the soil structure concerning complexity and computational calculation time. Further, the level of soil structure modeling details, such as the number of soil layers, can be chosen according to the approach used to balance complexity and accuracy. In this example, these indexes may highlight the importance of the soil structure and GS modeling approaches in the peak value of the transient overvoltage in case of the subsequent Lightning stroke.

Due to the direct dependence between the GS frequency response (transfer function) and the substation soil structure, having more information about the soil structure can improve the prediction of overvoltage values in lightning studies. It is shown that applying the FW method of GS modeling presents a more exact evaluation of lightning overvoltage.

The results presented in Table 17 and Table 18 demonstrated that uniform soil structure assumption might lead to over/underestimation of the predicted lightning-induced values in the different operating modes of the neutral power transformer.

5.2.2 Tower footing grounding system of the Novel composite Pylon tower (NCPT)

The CO_2 reduction agreement is seen as one lever in the countries' drive for energy independence from fossil fuels. Electricity suppliers have a sweeping plan to boost

energy production by developing renewable energy. There is a need to design new transmission lines and towers to reduce the cost of energy and CO_2 emissions. One option is novel pylon towers made of composite materials in various shapes like Y or T [11] that have a low visual impact on the environment [11].

Fig. 51 shows the concept map of the 400 kV Y-shaped composite pylon. The pylon has a steel mast with a 1.5 m radius connected with two inclined cross-arm, and it shows a 'Y' symmetric configuration. The height of this pylon tip and pylon mast is 22.5 m and 16.5 m, respectively. Each one-piece cross-arm is 12 m in length and forms a 30-degree angle to the horizontal line, which carries the three-phase wires and one shield wire. Aluminum Conductor Steel Reinforced (ACSR) conductors with radii of 0.0175-m are chosen as transmission wires. The phase conductors are mounted at the unibody cross-arms in the form of duplex bundles. Each pair of duplex bundle conductors is fixed by an aluminum clamp. According to IEC/TS 608153 [156], the minimum required phase-to-phase and phase-to-shield wire clearance on the unibody cross-arm are 3.6 m and 2.8 m, respectively [157]. Two copper conductors with the same radius of 0.0175 m as down-leads pass the unibody cross-arm and connect with the metal mast. In contrast, the cross-arm is filled with composite materials between the sheath and down-lead to enforce the cross-arm insulation strength and restrict the down-lead surface electric field [3].
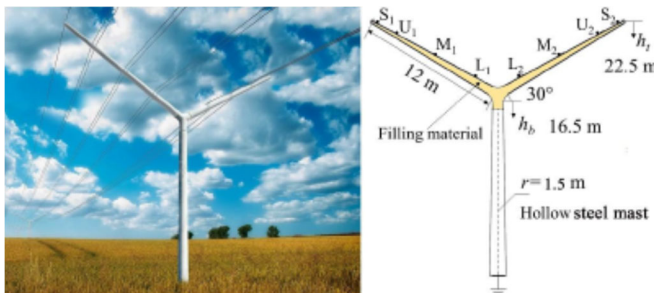

Fig. 51. Figure from C5, and J5, the concept map of the composite 'Y' pylon and the detailed parameters of the configuration. S refers to shield wires. U, M, and L refer to the upper, middle, and lower phase conductors [10], [11].
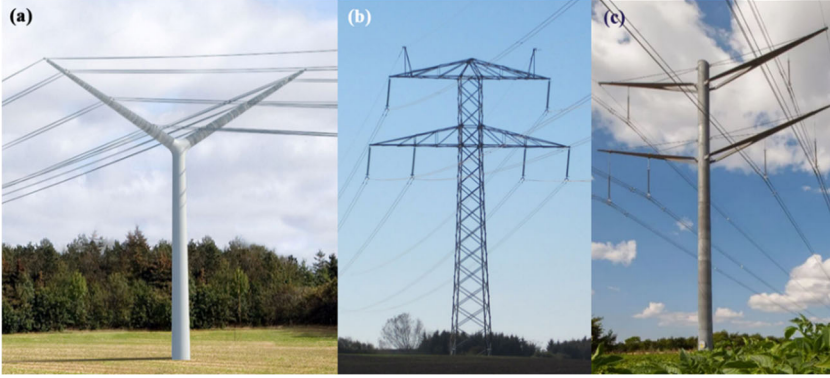
Fig. 52. Figure from **C5**, the tower of OHLs. (a) Y shape composite pylon, (b) Donau, and (c) Eagle [11].

One of the significant causes of insulation failure in OHLs is lightning. The lightning performance evaluation is necessary for newly designed towers. The lightning performance study includes the estimation of transient overvoltage across the insulator strings and predicting GPR value. With this regard, the effect of the full wave technique model on the GS should be examined [65]. The composite pylon tower has lower surge impedance because of the lower equivalent height of the tower in comparison with traditional metallic towers. Therefore, the traveling time between the shield conductor and the earth is lower than in traditional towers [11]. On the other hand, the GS impedance is a crucial parameter of lightning performance. It means that having an accurate model of the GS leads to predicting accurate overvoltage value across the insulator during the conceptual and detailed design of the tower [11], [10].

Fig. 52 shows different types of OHLs. In this example, the frequency-dependent model of the GS is used to find an exact estimation. Detailed information on the tower's geometry can be found in [11]. For the pylon tower (see Fig. 52 (a)), the downlead conductor is between the guard conductor at the cross-arm tip and the grounding terminal. The formula for the surge impedance of the pylon tower is not available, and it is calculated based on electromagnetic field theory. It is equal to the square root of the ratio inductance and capacitance [11]. To model towers (b) and (c), a multistory model represents these transmission towers.

The soil frequency-dependent model is used to calculate the harmonic impedance of the GS using MoM. A vertical ground electrode is buried in the soil with the mentioned properties in Table 15. The electrode radius is set to 12.5 mm. It is assumed the soil structure in cases 1 and 2 is uniform and, in cases 3-5, is two-layer. To analyze the impact of the electrode's length on the lightning performance of towers, different lengths of the electrodes (3,9, and 12 m) are applied.

Table 19. The ground electrode geometry and soil electrical parameters LF value [11].

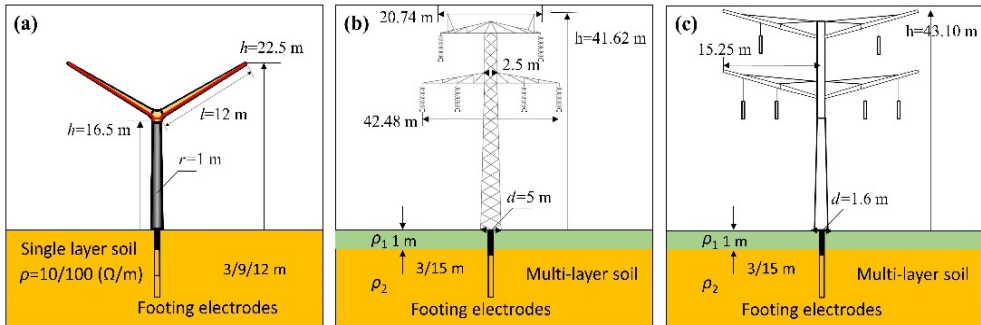| Soil Structure	Case	L[m]	$\rho_1[\Omega.m]$	$\rho_2[\Omega.m]$
Single soil	Case 1	3/9/12	10	10
	Case 2		100	100
Two-layer soil	Case 3		10	1000
	Case 4	3/15	100	1000
	Case 5		1000	10

Fig. 53. Figure from C5, three different towers to analyze the lightning performance considering uniform and two-layer soil structure [11].

Fig. 53 illustrates the tower geometry and GS configuration. The harmonic impedance of the GS for 5 cases (see Table 19) is presented in Fig. 54 and Fig. 55.
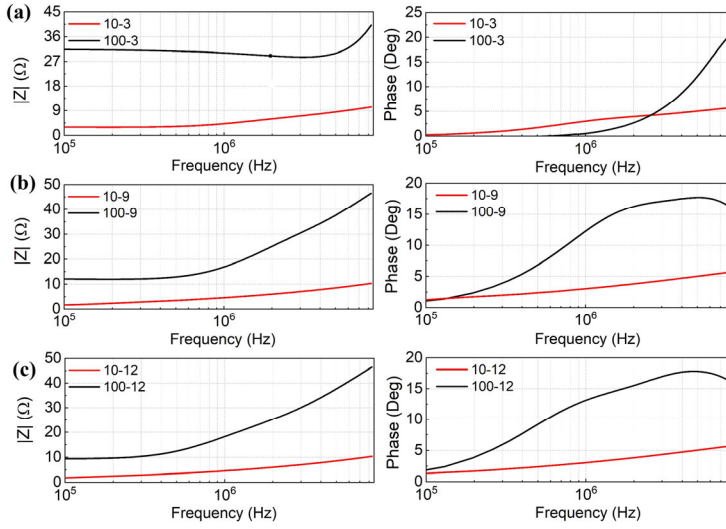
135

Fig. 54. Figure from **C5**, the harmonic impedance [(left) absolute (right) phase angle] of 3,9, and 12-m vertical ground electrode buried in single layer soil with resistivities of $\rho_{LF} = 10\Omega.m$ (red line), $100\Omega.m$ (black line), and a relate permittivity of 10 [11].
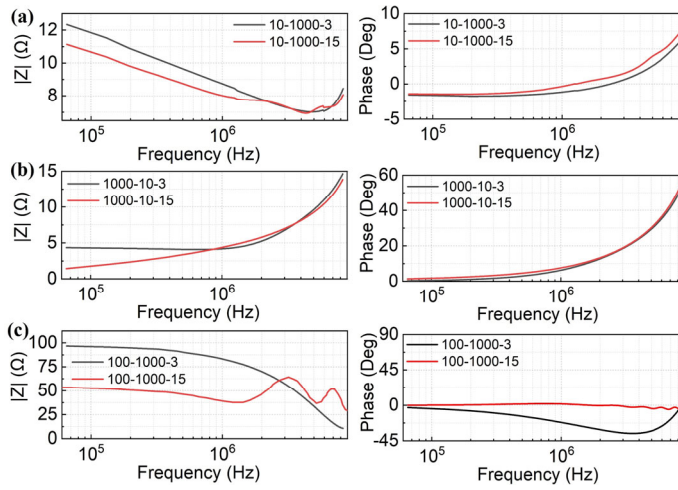
Fig. 55. Figure from **C5**, the harmonic impedance [(left) absolute (right) phase angle] of 3, and 15-m vertical ground electrode buried two-later soil structure (a) $\rho_{LF1} = 10\Omega.m$, $\rho_{LF2} = 1000\Omega.m$, (b) $\rho_{LF1} = 1000\Omega.m$, $\rho_{LF2} = 10\Omega.m$, (c) $\rho_{LF1} = 100\Omega.m$, $\rho_{LF2} = 100\Omega.m$, and relate permittivity of 10 [11].
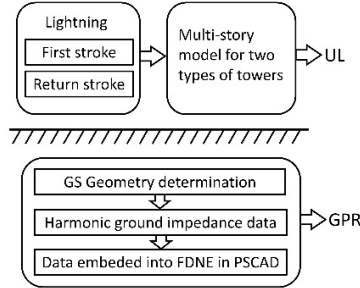

Fig. 56. Figure from **C5**, the lightning performance study procedure [11].

5.2.3 Lightning performance of the Novel composite Pylon tower (NCPT)

It is assumed that the lightning first and subsequent strokes hit the one cross-arm tip. The modeling procedure in the time domain simulator (PSCAD) is illustrated in Fig. 56.
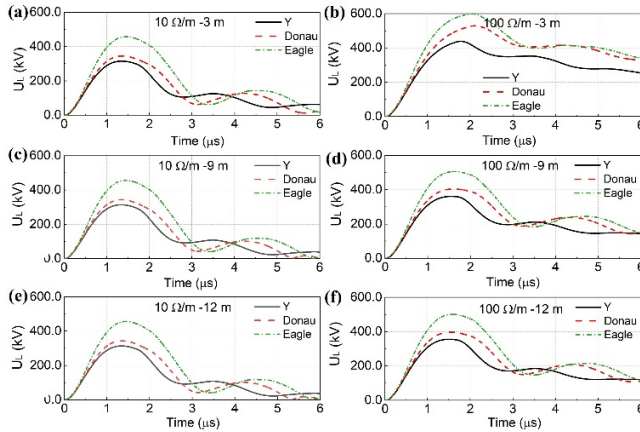

Fig. 57. Figure from **C5**, the overvoltage across insulators for three different tower shapes subjected to first lighting stroke. The towers are connected to the vertical electrode with L length placed in uniform earth. [Left] $\rho_{LF} = 10\Omega.m$, [Right] $\rho_{LF} = 100\Omega.m$. L=3, 9, and 12 m [11].

Fig. 57 and Fig. 59 present the overvoltage across the insulator of the two cases (1 and 2) subjected to the first and subsequent lightning strokes. These results are compared for the three towers connected to the different vertical ground electrodes buried in uniform soil. The soil structure is assumed to be a single layer, and the full-wave method is used.

Fig. 58. Figure from C5, the GPR curves for three different tower shapes subjected to the first lighting stroke. The towers are connected to the vertical ground electrode L buried in uniform soil. [Left] $\rho_{LF} = 10\Omega.m$, [Right] $\rho_{LF} = 100\Omega.m$. L=3, 9, and 12 m [11].

Fig. 59. Figure from **C5**, the overvoltage across insulators for three different tower shapes subjected to subsequent lightning stroke. The towers are connected to the vertical electrode with length L inserted in uniform soil. [Left] $\rho_{LF} = 10\Omega.m$, [Right] $\rho_{LF} = 100\Omega.m$. L=3, 9, and 12 m [11].

Fig. 60. Figure from **C5**, the GPR curves for three different tower shapes subjected to subsequent lightning stroke. The towers are connected to the vertical ground electrode L buried in uniform soil. [Left] $\rho_{LF} = 10\Omega.m$, [Right] $\rho_{LF} = 100\Omega.m$. L=3, 9, and 12 m [11].

Fig. 58 and Fig. 60 show the GPR curves for three different tower shapes subjected to the first and subsequent lightning strokes. It is assumed that the soil structure is a single layer.

Fig. 61. Figure from **C5**, the overvoltage across insulators for three different tower shapes subjected to the first lightning stroke. The towers are connected to the vertical ground electrode with the length of L buried in the soil with two layers. L=3 and 15 m [11].

Fig. 61 and Fig. 63 present the overvoltage across the insulator of cases 3, 4, and 5 for the first and subsequent lightning strokes, respectively. The soil structure is two-layer, and the electrode length is 3 and 15m.
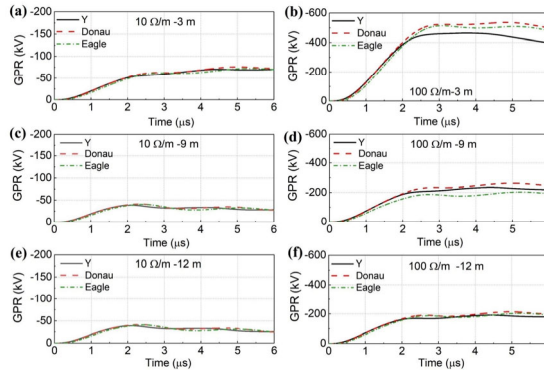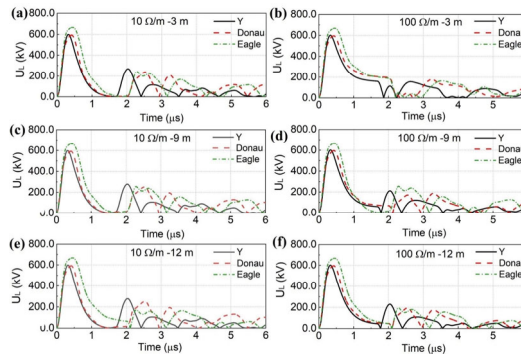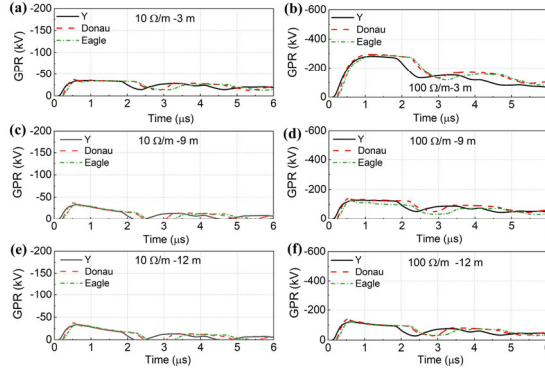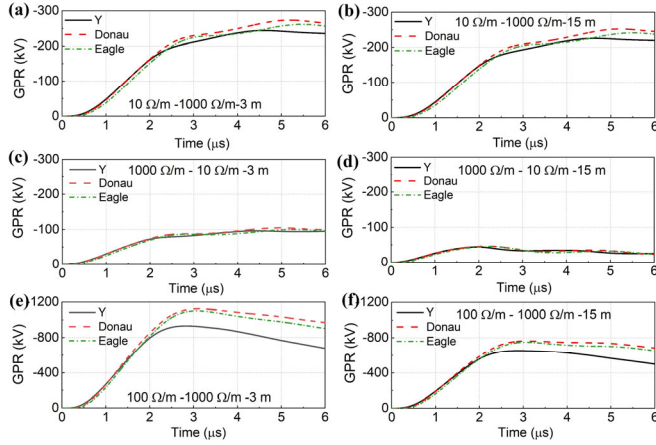
Fig. 62. Figure from **C5**, the GPR curves for three different tower shapes subjected to the first lightning stroke. The towers are connected to the vertical ground electrode with a length of L buried in the two-layer soil. L=3 and 15 m [11].
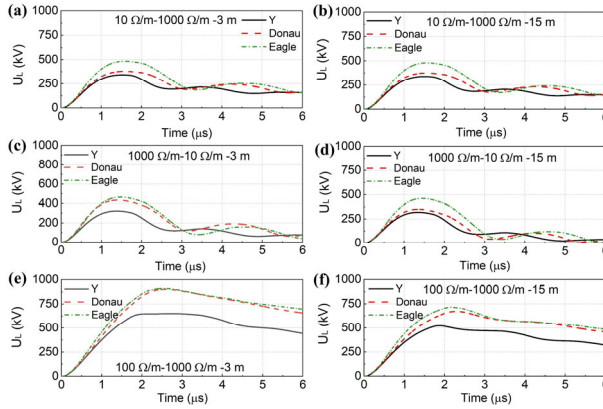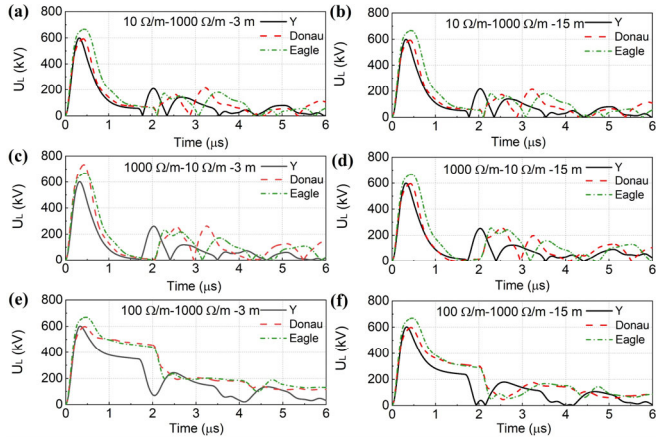

Fig. 63. Figure from **C5**, the overvoltage across insulators for three different tower shapes subjected to subsequent lightning stroke. The towers are connected to the vertical ground electrode with a length of L buried in the two-layer soil. L=3 and 15 m [11].
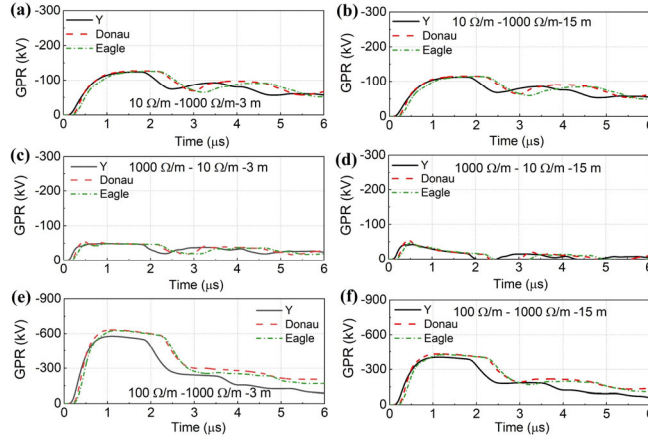
Fig. 64. Figure from **C5**, the GPR curves for three different tower shapes subjected to subsequent stroke. The towers are connected to the vertical ground electrode with a length of L buried in the two-layer soil. L=3 and 15 m [11].

Fig. 62 and Fig. 64 show the GPR curves of cases 3, 4, and 5 for the first and subsequent lightning strokes, respectively. The soil structure is two-layer, and the electrode length is 3 and 15m.

The Y shape pylon tower performs better against lightning than other traditional towers. The accurate model of the GS, including the frequency dependency of the soil electrical parameters, can predict more accurate results of the overvoltage across insulators and GPR. Briefly, the application of the GS frequency-dependent model is presented to optimize the insulation coordination and reduce construction costs due to an accurate model of the GS in the time domain platform.

5.3 Back Flashover Performance Comparison Between the Novel Composite Pylon and Metallic Tower

This section evaluates the back flashover performance of the novel pylon tower described in 5.2.2. The pylon tower specifications are different from the conventional metallic towers. The primary deviations are presented below [3]:

- Shorter span and have a smaller configuration
- Shorter tail time of overvoltage at insulation
- Lightning current path with having more inductance

In this study, the GS model can play a crucial role because of the high-frequency content of lightning impulses. In order to assess the back flashover rate and back flashover performance of pylon towers, the Monte Carlo method is applied. The simulation results are presented based on the frequency-dependent model of the GS. The OHL, tower, and lightning current model details are presented in [31]. The accurate model of the GS leads to predicting more precise resultant overvoltage values. The full-wave model of the GS based on MoM is used. The 3-m vertical ground electrode is assumed to be buried in the two-layer soil structure (see Case 4 in Table 19.
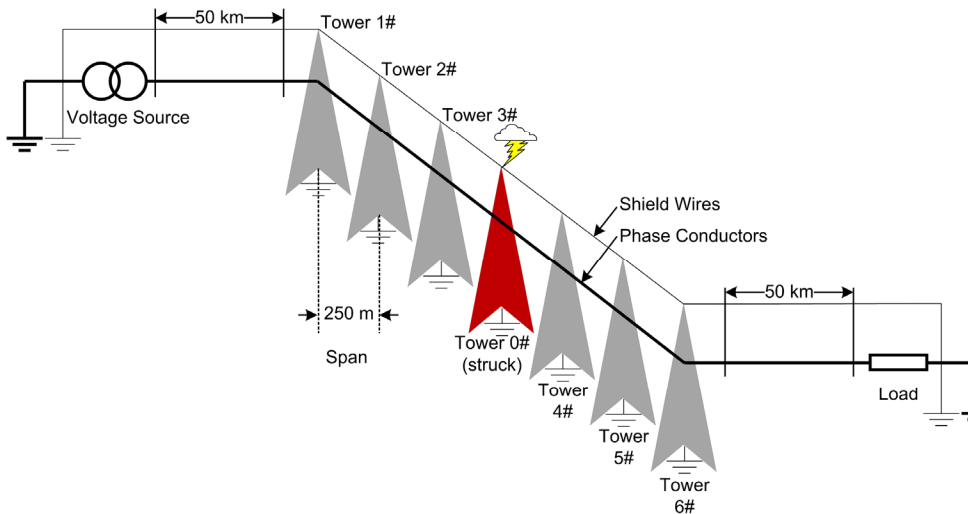
Fig. 65. Figure from J3 and C6, the OHL model demonstration [3].
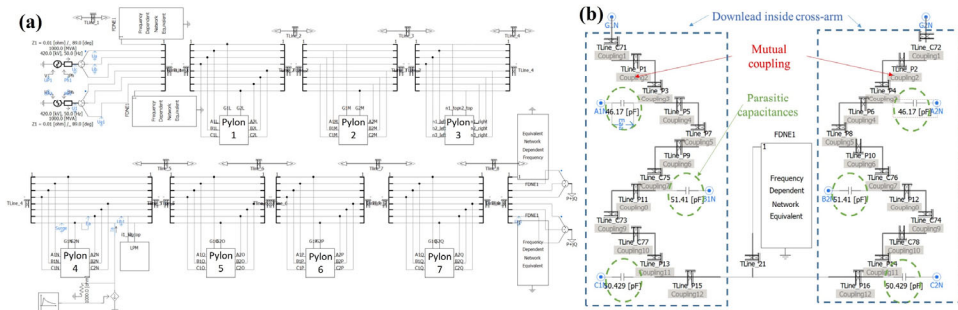
Fig. 66. Figure from **J5**, (a) overhead line and towers modeling, (b) mutual coupling effect and parasitic capacitances for the down-lead system in PSCAD.

The implemented model of the overhead line (see Fig. 65) in the time domain solver (PSCAD) is shown in Fig. 66. The Frequency dependent model of the grounding system is connected to the time domain solver via the frequency-dependent network equivalent block (FDNE) in PSCAD to perform lightning transient analysis.

| (a) Pylon | (b) Donau | (c) Eagle |

Fig. 67. Figure from **J3**, the overvoltage across cross-arm (pylon) and insulator string (metallic towers) to the upper phase conductors when the lightning current hits one of the shield wires [3].

Since a tower has a taller length, it will attract more flashes. Increasing the surge impedance leads to higher lightning overvoltage, and the shorter distance of insulator strings causes flashover to be simpler to happen at the same voltage.

In comparison with conventional metallic towers subjected to the same lightning, composite pylon towers are likely to be attracted to lower numbers of lightning

flashes, in contrast, it gives larger overvoltage, which results in more increased BFR. Composite pylon BFR is 0.4526 cases per 100 km per year, which is larger than other towers (Donau and Eagle) [3]. After computing the total probability of the lightning back flashover, the fundamental parameters affecting the back flashover rate for the three shown towers (see Fig. 53) are presented in Table 20.

Table 20. Parameters affecting back flashover rate for three towers [3].

Tower Type	Pylon	Donau	Eagle
Ground flash density [cases/km^2.year]	1.39	-	-
Height [m]	22.5	41.6	43.1
Shielding distance [m]	21.3	20.8	27.1
Line flash density [cases/100km.year]	20.3	28.3	29.6
Dc footing resistance [ohm]	50	-	-
Insulation length [m]	2.8	3.2	3.7
Critical flashover voltage [kV]	1960	2240	2604
Total back flashover probability	0.0267	0.0134	0.0121
Back flashover rate [cases/100km.year]	0.4526	0.3176	0.2992

For an illustrative example, the lightning across cross-arm (pylon) and insulator string (metallic towers) to the upper phase conductors when the lightning current hits one of the shield wires of a 400 kV transmission tower is shown in Fig. 67 [3].
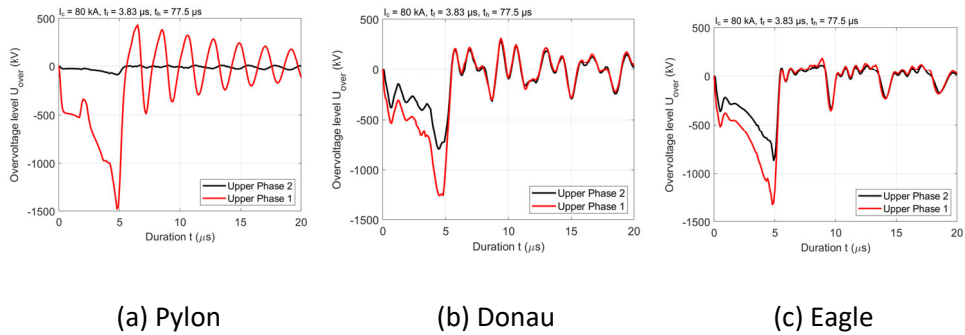

(a) Pylon   (b) Donau   (c) Eagle
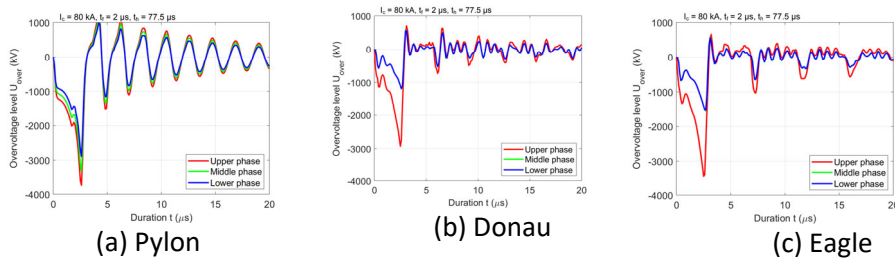
Fig. 68. Figure from **J3**, the overvoltage across cross-arm (pylon) and insulator string (metallic towers) to the conductors of three phases when the lightning current hits one of the shield wires [3].

In metallic towers, the configuration of towers influences overvoltage at different phases [31], [144]. Fig. 68 shows the 3-ph overvoltage curves at three towers. The lightning specifications for all towers are 80kA, 2/77.5 μs. In the pylon tower, the

overvoltage is computed at the position of the down-lead conductor to the phase conductors. For the other towers (Donau and Eagle), the overvoltage values are predicted at the location hanging the insulator to the phase wire.

Under the obtained results of the tower's BFR, the installation of the lightning arresters in three phases causes the finest lightning performance. With this regard, upper-phase surge arrester installation is yet more useful than upper-phase without lightning arresters.

5.4   Summary

In this chapter, the main scientific contribution of work is to propose the application of the full-wave GS modeling for the MV substation considering the two-layer soil structure. The other scientific contribution method is to employ the full wave model to evaluate the lightning performance of the composite pylon tower. In this part, the accurate model of the GS is used and the FDNE model is developed to link the frequency-response of the GS and the PSCAD platform.

In this chapter, first, the full-wave method as an extension of the proposed approach in [149] was adopted to model the MV substation GS. The effects of an accurate model of the GS, including soil structure and frequency dependence of the soil electrical parameters, on the transient overvoltage (lightning and switching) have been analyzed. According to the obtained simulation results in the transient overvoltage studies, it may be necessary to model the GS considering a more complicated soil structure like a two-layer soil structure to predict overvoltage precisely, when the fast front waveform of a lightning current (subsequent lightning stroke) with more high-frequency content is assumed to hit the tower. It has been realized that soil resistivity and structure may cause an impact on overvoltage value, while the GS model is a simple or low-frequency model.

The frequency-dependent model of the GS has been taken into account for computing overvoltage value across the insulator and GPR for the pylon tower compared with conventional metallic towers. The accurate model of the GS, including the frequency dependency of the soil electrical parameters, is predicted more precise results of the overvoltage across insulators and GPR.

Related Publications

J2. M. Ghomi, F. Faria da Silva, Amir abbas Shayegani Akmal, and C. Leth Bak, "*Transient Overvoltage Analysis in the Medium Voltage Substations Based on Full-Wave Modeling of Two-layer Grounding System*," Journal of Energy Power System Research, Elsevier 2022 [2].

> **Main contribution:**
> The procedure applied MoM to perform transient overvoltage analysis based on considering the complex grounding grid of the actual MV substation buried in the two-layer soil structure.

J3. H. Zhang, **M. Ghomi**, Q. Wang, F. Faria da Silva, C. Leth Bak, K. Yin, and H. Skouboe, "*Comparison of Backflashover Performance between a Novel Composite Pylon and Metallic Towers*," Journal of Energy Power System Research, vol.196, pp. 107263, July, 2021 [3].

> **Main contribution:**
> The tower-footing harmonic impedance is considered in the lightning surge impedance modeling of three different towers. Application of frequency-dependent impedance of GS can improve the simulation precision in tower lightning performance.

J4. K. Yin, **M. Ghomi**, Q. Wang, H. Zhang, F. Faria da Silva, C. Leth Bak, Q. Wang, H. Skouboe, "*The design and optimization of the down-lead system for a novel 400 kV composite pylon*," IEEE Transactions on Power Delivery 2022 [4].

> **Main contribution:**
> Methodical investigation to optimize and design the down-lead grounding conductor of a novel Y-shaped composite pylon.

J5. K. Yin, **M. Ghomi**, H. Zhang, C. Leth Bak, F. Faria da Silva, Q. Wang, "*Lightning transient response of bifurcation structure pylon and its empirical expression with high accuracy and general application*," International Journal of Electrical Power & Energy Systems 2022 (under review) [5].

> **Main contribution:**
> Full-wave modeling application considering the frequency-dependent model of GS for the lightning performance of the 400kV composite pylon tower.

J6. H. Zhang, **M. Ghomi**, Q. Wang, F. Faria da Silva, C. Leth Bak, and K. Yin, "*Backflashover Performance of a Novel Composite Pylon with External Grounding Down-lead Modeled in Dynamic Surge Impedance Considering Corona Effect*," IEEE Transactions on Power Delivery, 2022 Status: Under review [6].

> **Main contribution:**
> A dynamic surge impedance model with the corona effect is presented. The model is utilized on a vertical cylindrical grounded conductor, and the process of corona development associated with the lightning parameters is investigated.

C4. K. Yin, **M. Ghomi**, F. Faria da Silva, C. Leth Bak, Q. Wang, H. Zhang, H. Skouboe, "*Lightning performance and formula description of a Y-shaped composite pylon considering the effect of tower-footing impedance*," in 35th International Conference on Lightning Protection (ICLP) and XVI International Symposium on Lightning Protection (SIPDA), pp. 16, 2021 [10].

> **Main contribution:**
> The impact of an accurate model of GS on the composite pylon tower on the lightning performance is evaluated.

Chapter 6. Conclusion and Future Works

6.1 Abstract

This section discusses the future works of this study and its conclusion based on the published papers and developed concepts in the previous chapters.

6.2 Outline of The Research

This research, it is attempted to address the frequency-dependent model of GSs for power system transient analysis. Several soil structures like uniform and multilayer soil are intended to model the GS and to compute the input harmonic impedance. The full-wave approach MoM is used for this study.

The thesis begins with an introduction to the importance of the GS's impacts on the power system transient analysis in Chapter 1. Then, the methods of the full-wave modeling of the GS, tower surge impedance calculation, and dynamic behavior of the GS are reviewed.

MoM for the investigation of GSs is briefly described in Chapter 2. Vertical ground electrodes with different geometry buried in soil with different resistivities and layers are selected to investigate the effect of these parameters on the precision of the full-wave model.

In Chapter 3, the main target is to evaluate the frequency-dependent effects on the harmonic impedance of vertical ground electrodes. Different formulations for this dependence are used. The GPR value is computed when GS is subjected to lightning current. Several soil structures (uniform and multi-layer) and different lengths of vertical electrodes are taken into account. The simulation results with and without the effect of the frequency-dependent model of the soil electrical parameters are compared.

In Chapter 4, a systematic procedure based on the full-wave technique is presented. The integrated model's harmonic impedance is computed directly, which includes the tower and its GS. Various levels of detail for a full-scaled tower

are considered in the model. The harmonic impedance is calculated considering the accurate model of GS. The obtained results are compared to an estimation model of the towers in the frequency domain using TLM.

In Chapter 5, the application of full-wave modeling of the GS is evaluated. First, the GS of a real MV substation is assumed to predict the frequency response of the GS. The MoM is developed to model the large substation GS. The transient overvoltage study is performed and the lightning and switching transient voltages are calculated. Then, a detailed analysis of the influences of substation grounding soil structure on the power system transients is discussed. Then, this application is tested for a novel composite pylon to perform lightning performance analysis. The impact of an accurate model of GS on the design is discussed. The full-wave approach is used to model the vertical electrode and the fitting method is employed to connect the accurate model of the GS to the pylon tower.

Finally, in Chapter 6, the conclusion and future developments of the research are discussed.

6.3   Overall Significance and Contributions

The lightning overvoltage analysis and insulation coordination studies need to have a proper model of the GSs. The scientific design of GSs for lightning protection is a critical requirement of professional instruction. It is the responsibility of engineers to design GSs in such a way that they will improve their safety and reduce civil work costs as much as possible. To compute an exact model of the GS, there are some factors like layers of soil and soil frequency-dependent impact on the grounding model that need to be considered. Time domain simulators and platforms fail to model the GS in the lightning transient analysis. This is because of using the low-frequency or static simulation of the GSs. To address this issue, the harmonic impedance of the GS is transferred to the time domain platforms via the vector fitting method.

The concept of the electromagnetic field theory or the antenna theory in the multilayer media is developed to estimate the surge impedance of the tower considering the multilayer of the GS. In the time domain, the definition of the surge impedance of the tower depends on the injected current waveform. The proposed integrated model of the GS and towers provide the input harmonic impedance of the system in the frequency domain that is independent of the injected currents.

The most significant influence on the peak value of GPR is the GS. The contribution of this research is to estimate a more accurate value for the GPR.

The proposed method of GS modeling is applied for the lightning and back flashover performances of the pylon composite towers. The proposed full-wave method is used to compute the GPR of the pylon composite towers.

6.4 Thesis Scientific Contributions

In this thesis, the frequency-dependent model of the GS on the power system transient is the main goal. Nevertheless, the provisions of this Ph.D. thesis are planned as follows:

- Proposing a frequency-dependent model for GSs based on MoM for the multi-layer soil structure [9].
- Proposing the use of the soil frequency models in the multilayer GS, and its influences on the harmonic impedance and GPR values [7], [8].
- Proposing the integrated model of the tower and GS to compute the input harmonic impedance based on the multi-layer media concept using a full wave technique [1].
- Proposing a frequency-dependent model of GS for the MV substation to perform transient overvoltage studies [2].
- Proposing the application of the frequency-dependent model of GS to perform lightning performance of the novel composite pylon and detail electrical design and to do insulation coordination study using FDNE model in the PSCAD platform [3], [4], [5], [6], [10]–[12].

6.5 Future works

The following recommendations and suggestions can be utilized to further investigate and develop these works are listed as follows:

- The full-wave modeling of the GS is a time-consuming process and further effort is needed to optimize the computational time by frequency sampling reduction and using model-based parameter estimation (MBPE).
- The sensitivity analysis study needs to find the maximum depth of the first layer of soil for the two-layer structure on the input harmonic impedance can be studied. It can assist to reduce the GS complication from an

engineering point of view in lightning overvoltage studies and reduce the calculation time by using the uniform soil structure instead of a two-layer.

- To perform field measurement tests to calculate the harmonic impedance of the GS and to find the effective length of vertical and horizontal ground electrodes buried in the two-layer soil structure.
- Lightning performance study of wind turbines. As the blade length and wind turbine tower height are increasing, the improvement of the lightning protection system is vital to reduce the maintenance costs and the impact of GS modeling based on the multilayer soil structure is not neglectable.

References

[1]   M. Ghomi, H. Zhang, C. Leth Bak, F. Faria da Silva, and K. Yin, "Integrated model of transmission tower surge impedance and multilayer grounding system based on full-wave approach," Electr. Power Syst. Res., vol. 198, no. November 2020, p. 107355, Sep. 2021.

[2]   M. Ghomi, F. Faria da Silva, A. A. Shayegani Akmal, and C. Leth Bak, "Transient overvoltage analysis in the medium voltage substations based on full-wave modeling of two-layer grounding system," Electr. Power Syst. Res., vol. 211, no. April, p. 108139, Oct. 2022.

[3]   H. Zhang, M. Ghomi, Q. Wang, F. Faria da Silva, C. Leth Bak, K. Yin, and H. Skouboe, "Comparison of Backflashover performance between a novel composite pylon and metallic towers," Electr. Power Syst. Res., vol. 196, no. November 2020, p. 107263, Jul. 2021.

[4]   K. Yin, M. Ghomi, H. Zhang, F. Faria da Silva, and C. Leth Bak "The Design and Optimization of the Down-Lead System for a Novel 400 Kv Composite Pylon," IEEE Trans. Power Deliv., pp. 1–11, 2022.

[5]   K. Yin, M. Ghomi, H. Zhang, C. Leth Bak, F. Faria da Silva, and Q. Wang, "Lightning transient response of bifurcation structure pylon and its empirical expression with high accuracy and general application," Electr. Power Energy Syst., pp. 1–6, 2022.

[6]   H. Zhang, M. Ghomi, K. Yin, Q. Wang, F. Faria da Silva, and C. Leth Bak, "Backflashover Performance of a Novel Composite Pylon with External Grounding Down-lead Modeled in Dynamic Surge Impedance Considering Corona Effect," IEEE Trans. Power Deliv., pp. 1–8, 2023.

[7]   M. Ghomi, C. Leth Bak, and F. F. da Silva, "Frequency Dependence of Multilayer Soil Electrical Parameters: Effects on Ground Potential Rise," in 2021 35th International Conference on Lightning Protection (ICLP) and XVI International Symposium on Lightning Protection (SIPDA), 2021, no. Ml, pp. 01–08.

[8]   M. Ghomi, C. Leth Bak, and F. Faria da Silva, "Frequency dependence of multilayer soil electrical parameters: effects on the input impedance of grounding systems," in The 16th IET International Conference on AC and DC Power Transmission (ACDC 2020), 2021, vol. 2020, no. CP775, pp. 35–41.

[9]   M. Ghomi, H. R. Mohammadi, H. R. Karami, C. Leth Bak, F. F. Silva, and H. Khazraj,

"Full-Wave Modeling of Grounding System : Evaluation The Effects of Multi-Layer Soil and Length of Electrode on Ground Potential Rise1," International. Conference of Power System Transients, pp. 1–6, 2019.

[10] K. Yin, M. Ghomi, F. F. Silva, C. Leth Bak, H. Zhang, and Q. Wang, "Lightning performance and formula description of a Y-shaped composite pylon considering the effect of tower-footing impedance," in 2021 35th International Conference on Lightning Protection (ICLP) and XVI International Symposium on Lightning Protection (SIPDA), 2021, pp. 1–6.

[11] K. Yin, M. Ghomi, F. F. Silva, C. Leth Bak, H. Zhang, and Q. Wang, "The effect of frequency-dependent soil electrical parameters on the lightning response of a 'Y' shaped composite pylon for 400 kV transmission lines," in 22nd International Symposium on High Voltage Engineering (ISH 2021), 2021, pp. 2046–2051.

[12] H. Zhang, M. Ghomi, K. Yin, Q. Wang, F. Faria da Silva, and C. Leth Bak, "Evaluation of Lightning Backflashover Rate of a Fully Composite Pylon using Monte Carlo Method on Environmental Factors," in 2022 IEEE Power & Energy Society General Meeting (PESGM), 2022, pp. 1–5.

[13] H. Khazraj, B. Yousefi Khanghah, P. Ghimire, F. Martin, M. Ghomi, F. Faria da Silva, and C. Leth Bak, "Optimal operational scheduling and reconfiguration coordination in smart grids for extreme weather condition," IET Gener. Transm. Distrib., vol. 13, no. 15, pp. 3455–3463, 2019.

[14] GWEC, "Global wind report. Annual market update 2022".

[15] V. A. Rakov and M. A. Uman, "Review and evaluation of lightning return stroke models including some aspects of their application," IEEE Trans. Electromagn. Compat., vol. 40, no. 4 PART 2, pp. 403–426, 1998.

[16] Technical report, "Wind turbines: the bigger, the better," Office of Energy Efficiency & Renewable Energy, US Department of Energy, 2021.

[17] Wikipedia, "List of major power outages," https://en.wikipedia.org/wiki.org/wiki, 2019.

[18] F. Rachidi, "A review of field-to-transmission line coupling models with special emphasis to lightning-induced voltages on overhead lines," IEEE Trans. Electromagn. Compat., vol. 54, no. 4, pp. 898–911, 2012.

[19] C. A. Nucci, F. Rachidi, M. V. Michel, and C. Mazzetti, "Lightning-Induced Voltages

on Overhead Lines," IEEE Trans. Electromagn. Compat., vol. 35, no. 1, pp. 75–86, 1993.

[20]   F. Rachidi et al., "Current and electromagnetic field associated with lightning-return strokes to tall towers," IEEE Trans. Electromagn. Compat., vol. 43, no. 3, pp. 356–366, 2001.

[21]   K. Sheshyekani, S. H. Hesamedin Sadeghi, R. Moini, F. Rachidi, and M. Paolone, "Analysis of transmission lines with arrester termination, considering the frequency-dependence of grounding systems," IEEE Trans. Electromagn. Compat., vol. 51, no. 4, pp. 986–994, 2009.

[22]   L. Grcev, "Impulse efficiency of ground electrodes," IEEE Trans. Power Deliv., vol. 24, no. 1, pp. 441–451, 2009.

[23]   L. Grcev, "Modeling of grounding electrodes under lightning currents," IEEE Trans. Electromagn. Compat., vol. 51, no. 3 PART 1, pp. 559–571, 2009.

[24]   A. F. Imece et al., "Modeling guidelines for fast front transients," IEEE Trans. Power Deliv., vol. 11, no. 1, pp. 493–501, 1996.

[25]   Andrew R. Hileman, Insulation coordination for power systems. Taylor & Francis Group, 1999.

[26]   L. D. Grcev, "Computer analysis of transient voltages in large grounding systems," IEEE Trans. Power Deliv., vol. 11, no. 2, pp. 815–823, 1996.

[27]   M. R. Alemi and K. Sheshyekani, "Wide-Band Modeling of Tower-Footing Grounding Systems for the Evaluation of Lightning Performance of Transmission Lines," IEEE Trans. Electromagn. Compat., vol. 57, no. 6, pp. 1627–1636, Dec. 2015.

[28]   L. Qi, X. Cui, Z. Zhao, and H. Li, "Grounding performance analysis of the substation grounding grids by finite element method in frequency domain," IEEE Trans. Magn., vol. 43, no. 4, pp. 1181–1184, 2007.

[29]   B. Honarbakhsh, H. Karami, and K. Sheshyekani, "Direct Characterization of Grounding System Wide-Band Input Impedance," IEEE Trans. Electromagn. Compat., vol. 63, no. 1, pp. 328–331, 2021.

[30]   C. L. Longmire and K. S. Smith, "A universal impedance for soils." Mission Research Corp., Santa Barbara, CA, Rep. DNA3788T, Oct., 1975.

[31]   G. Dural and M. I. Aksun, "Closed-form Green's functions for general sources and stratified media," IEEE Trans. Microw. Theory Tech., vol. 43, no. 7, pp. 1545–1552, Jul. 1995.

[32]   V. Arnautovski-Toseva and L. Grcev, "Electromagnetic analysis of horizontal wire in two-layered soil," J. Comput. Appl. Math., vol. 168, no. 1–2, pp. 21–29, Jul. 2004.

[33]   V. Arnautovski-Toseva and L. Grcev, "Image and Exact Models of a Vertical Wire Penetrating a Two-Layered Earth," IEEE Trans. Electromagn. Compat., vol. 53, no. 4, pp. 968–976, Nov. 2011.

[34]   F. E. Modelling, "Electrode Geometry Effects .," vol. 35, no. 3, pp. 5–8, 1999.

[35]   M. Jesenik, A. Hamler, and M. Trlep, "Analyzing of a Soil Model Using the Finite Element Method for Simulation of Soil Resistivity Measurement," IEEE Trans. Magn., vol. 57, no. 7, pp. 3–6, 2021.

[36]   M. Trlep, A. Hamler, and B. Hribernik, "The analysis of complex grounding systems by FEM," IEEE Trans. Magn., vol. 34, no. 5 PART 1, pp. 2521–2524, 1998.

[37]   F. Napolitano, A. Borghetti, C. A. Nucci, F. Rachidi, and M. Paolone, "Use of the full-wave Finite Element Method for the numerical electromagnetic analysis of LEMP and its coupling to overhead lines," Electr. Power Syst. Res., vol. 94, pp. 24–29, 2013.

[38]   E. Mombello et al., "Harmonic Impedance of Grounding Electrodes Buried in a Horizontally Stratified Multilayer Ground: A Full-Wave Approach," IEEE Trans. Electromagn. Compat., vol. 59, no. 4, pp. 205-208 Vol.1, Oct. 2017.

[39]   V. Jithesh and D. C. Pande, "A review on computational EMI modelling techniques," in 8th International Conference on Electromagnetic Interference and Compatibility, 2003, vol. 2003-Janua, pp. 159–166.

[40]   T. H. Thang, Y. Baba, N. Nagaoka, A. Ametani, N. Itamoto, and V. A. Rakov, "FDTD simulation of insulator voltages at a lightning-struck tower considering ground-wire corona," IEEE Trans. Power Deliv., vol. 28, no. 3, pp. 1635–1642, 2013.

[41]   T. Noda, A. Tatematsu, and S. Yokoyama, "Improvements of an FDTD-based surge simulation code and its application to the lightning overvoltage calculation of a transmission tower," Electr. Power Syst. Res., vol. 77, no. 11, pp. 1495–1500, 2007.

[42]   V. Arnautovski-Toseva and L. Grcev, "High frequency current distribution in

horizontal grounding systems in two-layer soil," in 2003 IEEE International Symposium on Electromagnetic Compatibility, 2003. EMC '03., 2003, pp. 205-208 Vol.1.

[43]   R. Alipio and S. Visacro, "Frequency Dependence of Soil Parameters: Effect on the Lightning Response of Grounding Electrodes," IEEE Trans. Electromagn. Compat., vol. 55, no. 1, pp. 132–139, Feb. 2013.

[44]   S. Visacro, R. Alipio, M. H. Murta Vale, and C. Pereira, "The Response of Grounding Electrodes to Lightning Currents: The Effect of Frequency-Dependent Soil Resistivity and Permittivity," IEEE Trans. Electromagn. Compat., vol. 53, no. 2, pp. 401–406, May 2011.

[45]   M. Akbari, K. Sheshyekani, and M. R. Alemi, "The Effect of Frequency Dependence of Soil Electrical Parameters on the Lightning Performance of Grounding Systems," Electromagn. Compat. IEEE Trans., vol. 55, no. 4, pp. 739–746, 2013.

[46]   M. Akbari et al., "Evaluation of Lightning Electromagnetic Fields and Their Induced Voltages on Overhead Lines Considering the Frequency Dependence of Soil Electrical Parameters," IEEE Trans. Electromagn. Compat., vol. 55, no. 6, pp. 1210–1219, Dec. 2013.

[47]   F. M. Gatta, A. Geri, S. Lauria, and M. Maccioni, "Backflashover simulation of HV transmission lines with enhanced counterpoise groundings," Electr. Power Syst. Res., vol. 79, no. 7, pp. 1076–1084, 2009.

[48]   H. Chen and Y. Du, "Lightning Grounding Grid Model Considering Both the Frequency-Dependent Behavior and Ionization Phenomenon," IEEE Trans. Electromagn. Compat., vol. 61, no. 1, pp. 157–165, Feb. 2019.

[49]   B. Salarieh, J. De Silva, A. M. Gole, A. Ametani, and B. Kordi, "An Electromagnetic Model for the Calculation of Tower Surge Impedance Based on Thin Wire Approximation," IEEE Trans. Power Deliv., vol. XX, no. XX, pp. 1–1, 2020.

[50]   A. Ametani, N. Triruttanapiruk, K. Yamamoto, Y. Baba, and F. Rachidi, "Impedance and Admittance Formulas for a Multistair Model of Transmission Towers," IEEE Trans. Electromagn. Compat., vol. PP, pp. 1–12, 2020.

[51]   S. Yuda, S. Sawaki, Y. Baba, N. Nagaoka, and A. Ametani, "Application of the TLM Method to Transient Simulations of a Conductor System With a Lossy Ground: Grounding Electrodes and an Overhead Wire," IEEE Trans. Electromagn. Compat., vol. 55, no. 1, pp. 175–182, Feb. 2013.

[52]   J. R. Mosig and F. E. Gardiol, "Analytical and Numerical Techniques in the Green'S Function Treatment of Microstrip Antennas and Scatterers.," IEE Proc. H Microwaves Opt. Antennas, vol. 130, no. 2, pp. 175–182, 1983.

[53]   I. M. Dudurych, T. J. Gallagher, J. Corbett, and M. Val Escudero, "EMTP analysis of the lightning performance of a HV transmission line," IEE Proc. - Gener. Transm. Distrib., vol. 150, no. 4, p. 501, 2003.

[54]   Z. Zakaria, S. M. Bashi, N. F. Mailah, M. R. Othman, and H. Osman, "Simulation of lightning surges on tower transmission using PSCAD/EMTDC: A comparative study," 2002 Student Conf. Res. Dev. Glob. Res. Dev. Electr. Electron. Eng. SCOReD 2002 - Proc., pp. 426–429, 2002.

[55]   A. De Conti and R. Alipio, "Single-Port Equivalent Circuit Representation of Grounding Systems Based on Impedance Fitting," IEEE Trans. Electromagn. Compat., vol. 61, no. 5, pp. 1683–1685, Oct. 2019.

[56]   Bo Zhang et al., "Numerical analysis of transient performance of grounding systems considering soil ionization by coupling moment method with circuit theory," IEEE Trans. Magn., vol. 41, no. 5, pp. 1440–1443, May 2005.

[57]   A. Habjanic and M. Trlep, "The simulation of the soil ionization phenomenon around the grounding system by the finite element method," IEEE Trans. Magn., vol. 42, no. 4, pp. 867–870, 2006.

[58]   J. Cidrás, A. F. Otero, and C. Garrido, "Nodal frequency analysis of grounding systems considering the soil ionization effect," IEEE Trans. Power Deliv., vol. 15, no. 1, pp. 103–107, 2000.

[59]   R. G. Olsen and L. Grcev, "Analysis of High-Frequency Grounds: Comparison of Theory and Experiment," IEEE Trans. Ind. Appl., vol. 51, no. 6, pp. 4889–4899, Nov. 2015.

[60]   R. G. Olsen and M. C. Willis, "A comparison of exact and quasi-static methods for evaluating grounding systems at high frequencies," IEEE Trans. Power Deliv., vol. 11, no. 2, pp. 1071–1081, Apr. 1996.

[61]   J. Gholinezhad and R. Shariatinasab, "Time-Domain Modeling of Tower-Footing Grounding Systems Based on Impedance Matrix," IEEE Trans. Power Deliv., vol. 34, no. 3, pp. 910–918, Jun. 2019.

[62]   B. Gustavsen and A. Semlyen, "A Robust Approach for System Identification in the

Frequency Domain," IEEE Trans. Power Deliv., vol. 19, no. 3, pp. 1167–1173, 2004.

[63]   B. Gustavsen and A. Semlyen, "Rational approximation of frequency domain responses by vector fitting," IEEE Trans. Power Deliv., vol. 14, no. 3, pp. 1052–1061, Jul. 1999.

[64]   K. Sheshyekani, H. R. Karami, P. Dehkhoda, M. Paolone, and F. Rachidi, "Application of the matrix pencil method to rational fitting of frequency-domain responses," IEEE Trans. Power Deliv., vol. 27, no. 4, pp. 2399–2408, 2012.

[65]   R. Shariatinasab, J. Gholinezhad, K. Sheshyekani, and M. R. Alemi, "The effect of wide band modeling of tower-footing grounding system on the lightning performance of transmission lines: A probabilistic evaluation," Electr. Power Syst. Res., vol. 141, pp. 1–10, Dec. 2016.

[66]   K. Sheshyekani, M. Akbari, B. Tabei, and R. Kazemi, "Wideband Modeling of Large Grounding Systems to Interface With Electromagnetic Transient Solvers," IEEE Trans. Power Deliv., vol. 29, no. 4, pp. 1868–1876, Aug. 2014.

[67]   L. Grcev and M. Popov, "On High-Frequency Circuit Equivalents of a Vertical Ground Rod," IEEE Trans. Power Deliv., vol. 20, no. 2, pp. 1598–1603, Apr. 2005.

[68]   F. Dawalibi and D. Mukhedkar, "Influence of ground rods on grounding grids," IEEE Trans. Power Appar. Syst., vol. PAS-98, no. 6, pp. 2089–2098, 1979.

[69]   F. Dawalibi and W. Finney, "Transmission Line Tower Grounding Performance in Non-Uniform Soil," IEEE Trans. Power Appar. Syst., vol. PAS-99, no. 2, pp. 471–479, Mar. 1980.

[70]   L. Grcev and F. Dawalibi, "An electromagnetic model for transients in grounding systems," IEEE Trans. Power Deliv., vol. 5, no. 4, pp. 1773–1781, 1990.

[71]   E. D. Sunde, Earth conduction effects in transmission systems, Second ed. New York: Dover Publications Inc, 1949.

[72]   R. Andolfato, L. Bernardi, and L. Fellin, "Aerial and grounding system analysis by the shifting complex images method," IEEE Trans. Power Deliv., vol. 15, no. 3, pp. 1001–1009, 2000.

[73]   IEEE Std. 81, - Guide for Measuring Earth Resistivity , Ground Impedance , and Earth Surface Potentials of a Grounding System IEEE Power and Energy Society, vol. 2012, no. December. 2012.

[74] a P. Meliopoulos and M. G. Moharam, "Transient Analysis of Grounding Systems," Power Appar. Syst. IEEE Trans., vol. PAS-102, no. 2, pp. 389–399, 1983.

[75] R. Rudenberg, Electrical ShockWaves in Power Systems. Cambridge: Harvard Univ. Press, 1968.

[76] V. Arnautovski-Toseva and L. Grcev, "On the Image Model of a Buried Horizontal Wire," IEEE Trans. Electromagn. Compat., vol. 58, no. 1, pp. 278–286, 2016.

[77] H. Karami, K. Sheshyekani, and F. Rachidi, "Mixed-Potential Integral Equation for Full-Wave Modeling of Grounding Systems Buried in a Lossy Multilayer Stratified Ground," IEEE Trans. Electromagn. Compat., vol. 59, no. 5, pp. 1505–1513, Oct. 2017.

[78] J. Wang, A. C. Liew, and M. Darveniza, "Extension of dynamic model of impulse behavior of concentrated grounds at high currents," IEEE Trans. Power Deliv., vol. 20, no. 3, pp. 2160–2165, 2005.

[79] S. S. Devgan and E. R. Whitehead, "Analytical models for distributed grounding systems," IEEE Trans. Power Appar. Syst., vol. PAS-92, no. 5, pp. 1763–1770, 1973.

[80] R. Verma and D. Mukhedkar, "Impulse impedance of buried ground wire," IEEE Trans. Power App. Syst, no. 5, pp. 2003–2007, 2003.

[81] F. E. Mentre and L. Grcev, "EMTP-based model for grounding system analysis," IEEE Trans. Power Deliv., vol. 9, no. 4, pp. 1838–1849, 1994.

[82] S. Bourg, B. Sacepe, and T. Debu, "Deep earth electrodes in highly resistive ground: frequency behaviour," in Proceedings of International Symposium on Electromagnetic Compatibility, pp. 584–589.

[83] Y. Liu, M. Zitnik, and R. Thottappillil, "An improved transmission-line model of grounding system," IEEE Trans. Electromagn. Compat., vol. 43, no. 3, pp. 348–355, 2001.

[84] Y. Liu, N. Theethayi, and R. Thottappillil, "An engineering model for transient analysis of grounding system under lightning strikes: Nonuniform transmission-line approach," IEEE Trans. Power Deliv., vol. 20, no. 2 I, pp. 722–730, 2005.

[85] M. Heimbach and L. D. Grcev, "Grounding system analysis in transients programs applying electromagnetic field approach," IEEE Trans. Power Deliv., vol. 12, no. 1, pp. 186–193, 1997.

[86]   D. S. Gazzana, A. S. Bretas, G. A. D. Dias, and M. Telló, "Comparative analysis of EMC methodologies applied on transients studies of impulsive grounding systems," Proc. IEEE Int. Conf. Ind. Technol., pp. 710–716, 2010.

[87]   K. Sheshyekani, S. H. H. Sadeghi, R. Moini, and F. Rachidi, "Frequency-domain analysis of ground electrodes buried in an ionized soil when subjected to surge currents: A MoM-AOM approach," Electr. Power Syst. Res., vol. 81, no. 2, pp. 290–296, 2011.

[88]   L. Grcev and N. Grcevski, "Software techniques for interactive optimization of complex grounding arrangements for protection against effects of lightning," in Int. Conf. Lightning Protection, 1998, pp. 518–523.

[89]   H. D. Bruns, C. Schuster, and H. Singer, "Numerical electromagnetic field analysis for EMC problems," IEEE Trans. Electromagn. Compat., vol. 49, no. 2, pp. 253–262, 2007.

[90]   A. Mimouni, F. Rachidi, and M. Rubinstein, "Electromagnetic fields of a lightning return stroke in presence of a stratified ground," IEEE Trans. Electromagn. Compat., vol. 56, no. 2, pp. 413–418, 2014.

[91]   R. F. Harrington, "Matrix Methods for Field Problems," Proc. IEEE, vol. 55, no. 2, pp. 136–149, 1967.

[92]   V. D. K. Q. da Costa, "Software Based on Mom Model to Analyze Electromagnetic Transients in Grounding Systems," in 2nd International Conference on Lightning Physics and Effects, 2006.

[93]   H. D. Brüns, C. Schuster, and H. Singer, "Numerical electromagnetic field analysis for EMC problems," IEEE Trans. Electromagn. Compat., vol. 49, no. 2, pp. 253–262, 2007.

[94]   K. Sheshyekani and M. Akbari, "Evaluation of Lightning-Induced Voltages on Multiconductor Overhead Lines Located Above A Lossy Dispersive Soil," IEEE Trans. Power Deliv., vol. 29, no. 2, pp. 683–690, Apr. 2014.

[95]   V. Jithesh and D. C. Pande, "A review on computational EMI modelling techniques," Proc. Int. Conf. Electromagn. Interf. Compat., vol. 2003-Janua, pp. 159–166, 2003.

[96]   B. Nekhoul, C. Guerin, P. Labie, G. Meunier, R. Feuillet, and X. Brunotte, "A Finite Element Method for Calculating the Electromagnetic Fields Generated by Substation Grounding Systems," IEEE Trans. Magn., vol. 31, no. 3, pp. 2150–2153,

1995.

[97]   B. Nekhoul, "Calculating the impedance of a grounding system," IEEE Trans. Magn., vol. 32, no. 3 PART 2, pp. 1509–1512, 1996.

[98]   IEEE Power and Energy Society, IEEE Guide for Safety in AC Substation Grounding, no. February. 2013.

[99]   P. Chowdhuri, Electromagnteic transients in power systems. John Wiley and Sons, 1996.

[100]   J. He, R. Zeng, and B. Zhang, Methodology and Technology for Power System Grounding. Singapore: John Wiley & Sons Singapore Pte. Ltd., 2012.

[101]   L. Grcev, "Improved earthing system design practices for reduction of transient voltages," in CIGRÉ Session, 1998, pp. 1–6.

[102]   L. Grcev, "Improved design of transmission line grounding arrangements for better protection against effects of lightning," in Int. Symp. on Electromagnetic Compatibility, 1998, pp. 100–103.

[103]   L. Grcev, "Impulse efficiency of simple grounding electrode arrangements," in 2007 18th International Zurich Symposium on Electromagnetic Compatibility, 2007, pp. 325–328.

[104]   R. Alipio and S. Visacro, "Modeling the frequency dependence of electrical parameters of soil," IEEE Trans. Electromagn. Compat., vol. 56, no. 5, pp. 1163–1171, 2014.

[105]   R. L. Smith-Rose, "Electrical measurements on soil with alternating currents," 1934, pp. 221–237.

[106]   D. R. C. James H. Scott,Roderick D. Carroll, "Dielectric constant and electrical conductivity of moist rock from laboratory measurements," Sensor and Simulation Note 116, Kirtland AFB, NM, Aug.," 1964.

[107]   M. Messier, "Another soil conductivity model," 1985.

[108]   S. Visacro and R. Alipio, "Frequency Dependence of Soil Parameters: Experimental Results, Predicting Formula and Influence on the Lightning Response of Grounding Electrodes," IEEE Trans. Power Deliv., vol. 27, no. 2, pp. 927–935, Apr. 2012.

[109]   R. Alipio and S. Visacro, "Modeling the Frequency Dependence of Electrical

Parameters of Soil," IEEE Trans. Electromagn. Compat., vol. 56, no. 5, pp. 1163–1171, Oct. 2014.

[110]   C. Portela, "Measurement and modeling of soil electromagnetic behavior," in 1999 IEEE International Symposium on Electromagnetic Compatability. Symposium Record (Cat. No.99CH36261), 1999, vol. 2, pp. 1004–1009.

[111]   R. Alipio and S. Visacro, "Impulse efficiency of grounding electrodes: Effect of frequency-dependent soil parameters," IEEE Trans. Power Deliv., vol. 29, no. 2, pp. 716–723, 2014.

[112]   Impact of soil-parameter frequency dependence on the response of grounding electrodes and on the lightning performance of electrical systems (WG C4.3). CIGRE, Paris, 2019.

[113]   J.-H. Choi, B.-H. Lee, and S.-K. Paek, "Frequency-dependent grounding impedance of the counterpoise based on the dispersed currents," J. Electr. Eng. Technol., vol. 7, no. 4, pp. 589–595, Jul. 2012.

[114]   D. Cavka, N. Mora, and F. Rachidi, "A Comparison of Frequency-Dependent Soil Models: Application to the Analysis of Grounding Systems," IEEE Trans. Electromagn. Compat., vol. 56, no. 1, pp. 177–187, Feb. 2014.

[115]   M. Popov, L. Grcev, H. K. Hoidalen, B. Gustavsen, and V. Terzija, "Investigation of the overvoltage and fast transient phenomena on transformer terminals by taking into account the grounding effects," IEEE Trans. Ind. Appl., vol. 51, no. 6, pp. 5218–5227, 2015.

[116]   X. LEGRAND, A. XE'MARD, P. AURIOL, N. C., and C. MOUYCHARD, "Modeling of Substation Grounding for Fast Front Overvoltage Studies," in Proceedings of the 7th International Conference on Power Systems Transients (IPST), 2007, vol. 1, pp. 1–7.

[117]   C. K. Sanathanan and J. Koerner, "Transfer Function Synthesis as a Ratio of Two Complex Polynomials," IEEE Trans. Automat. Contr., vol. 8, no. 1, pp. 56–58, 1963.

[118]   W. Hendrickx and T. Dhaene, "A discussion of 'Rational approximation of frequency domain responses by vector fitting,'" IEEE Trans. Power Syst., vol. 21, no. 1, pp. 441–443, 2006.

[119]   B. Gustavsen, "Improving the pole relocating properties of vector fitting," IEEE Trans. Power Deliv., vol. 21, no. 3, pp. 1587–1592, 2006.

[120] G. Antonini, "SPICE equivalent circuits of frequency-domain responses," IEEE Trans. Electromagn. Compat., vol. 45, no. 3, pp. 502–512, 2003.

[121] M. Ishii and Y. Baba, "Numerical electromagnetic field analysis of tower surge response," IEEE Power Eng. Rev., vol. 17, no. 1, p. 69, 1997.

[122] B. Salarieh, H. M. J. De Silva, A. M. Gole, A. Ametani, and B. Kordi, "An electromagnetic model for the calculation of tower surge impedance based on thin wire approximation," IEEE Trans. Power Deliv., vol. 36, no. 2, pp. 1173–1182, 2021.

[123] L. Grcev and F. Rachidi, "On tower impedances for transient analysis," IEEE Trans. Power Deliv., vol. 19, no. 3, pp. 1238–1244, 2004.

[124] T. Hara and O. Yamamoto, "Modelling of a transmission tower for lightning-surge analysis," IEE Proc. - Gener. Transm. Distrib., vol. 143, no. 3, p. 283, 1996.

[125] "IEEE guide for Improving the Lightning Performance of Transmission Lines," 1997.

[126] C. Menemenlis and Z. Chun, "Wave Propagation on Nonuniform Lines," IEEE Trans. Power Appar. Syst., vol. PAS-101, no. 4, pp. 833–839, Apr. 1982.

[127] C. F. Wagner and A. R. Hileman, "A new approach to the calculation of the lightning performance of transmission lines III-A simplified method: Stroke to tower," Trans. Amer. Inst. Elect. Eng. Part III Power App. Syst., vol. 79, pp. 589–603, 1960.

[128] M. A. Sargent and M. Darveniza, "Tower Surge Impedance," IEEE Trans. Power Appar. Syst., vol. PAS-88, no. 5, pp. 680–687, 1969.

[129] CIGRE Technical Brochure 63, "Guide to procedures for estimating the lightning performance of transmission lines," 1991.

[130] A. Ametani; Y. Kasai ; J. Sawada ; A. Mochizuki ; T. Yamada, "Frequency-dependent impedance of vertical conductors and a multiconductor tower model," IEE Proc. - Gener. Trans. Distrib., vol. 141, no. 4, pp. 339–345, 1994.

[131] R. J. A. Gutiérrez, P. Moreno, L. Guardado, and J. L. Naredo, "Comparison of transmission tower models for evaluating lightning performance," 2003 IEEE Bol. PowerTech - Conf. Proc., vol. 4, pp. 339–344, 2003.

[132] J. A. Gutiérrez et al., "Nonuniform transmission tower model for lightning transient studies," IEEE Trans. Power Deliv., vol. 19, no. 2, pp. 490–496, 2004.

[133] Y. Baba and M. Ishii, "Numerical electromagnetic field analysis on measuring

methods of tower surge impedance," IEEE Trans. Power Deliv., vol. 14, no. 2, pp. 630–635, 1999.

[134]   Y. Baba and M. Ishii, "Numerical electromagnetic field analysis of tower surge response," IEEE Trans. Power Del, vol. 12, no. 1, pp. 483–488, 1997.

[135]   T. X. Cao, T. Pham, and S. Boggs, "Computation of tower surge impedance in transmission line," 2013 IEEE Electr. Insul. Conf. EIC 2013, no. June, pp. 77–80, 2013.

[136]   J. Takami, T. Tsuboi, K. Yamamoto, S. Okabe, Y. Baba, and A. Ametani, "Lightning surge response of a double-circuit transmission tower with incoming lines to a substation through FDTD simulation," IEEE Trans. Dielectr. Electr. Insul., vol. 21, no. 1, pp. 96–104, 2014.

[137]   Y. Baba, N. Nagaoka, and A. Ametani, "Modeling of thin wires in a lossy medium for FDTD simulations," IEEE Trans. Electromagn. Compat., vol. 47, no. 1, pp. 54–60, 2005.

[138]   A. Ametani et al., "Electromagnetic scattering and radiation by surfaces of arbitrary shape in layered media. I. Theory," IEEE Trans. Power Deliv., vol. 38, no. 3, pp. 1–1, Mar. 1990.

[139]   J. S. L. Colqui, "Transient Analysis of Grounding Electrodes in Multilayer Soils Using Method of Moments," IEEE Lat. Am. Trans., vol. 20, no. 2, pp. 269–275, 2022.

[140]   "CIGRE TB 549, Lightning Parameters for Engineering Applications, WG C4.407, V.A. Rakov, Convenor (US), A. Borghetti, Secretary (IT), C. Bouquegneau (BE), W.A. Chisholm (CA), V. Cooray (SE), K. Cummins (US), G. Diendorfer (AT), F. Heidler (DE), A. Hussein ," 2013.

[141]   F. Heidler, J. M. Cvetic, and B. V. Stanic, "Calculation of lightning current parameters," IEEE Trans. Power Deliv., vol. 14, no. 2, pp. 399–404, Apr. 1999.

[142]   "IEEE Recommended Practice for Determining the Electric Power Station Ground Potential Rise and Induced Voltage from a Power Fault," 2012.

[143]   L. Grcev and F. Rachidi, "On tower impedances for transient analysis," IEEE Trans. Power Deliv., vol. 19, no. 3, pp. 1238–1244, 2004.

[144]   G. V. Eleftheriades and J. R. Mosig, "On the network characterization of planar passive circuits using the method of moments," IEEE Trans. Microw. Theory Tech.,

vol. 44, no. 3, pp. 438–445, Mar. 1996.

[145]   G. J. Burke, "Numerical electromagnetics code (NEC- 4)- method of moment," Lawrence Livermore Nat. Lab., Livermore, CA, USA, UCRLMA-109338., 1992.

[146]   IEEE Guide for Safety, vol. 2000, no. February. 2000.

[147]   "Working Group C4.33 'CIGRE TB 781: Impact of soil-parameter frequency dependence on the response of grounding electrodes and on the lightning performance of electrical systems,'" Paris, 2019.

[148]   L. Grcev, "Lightning surge efficiency of grounding grids," IEEE Trans. Power Deliv., vol. 26, no. 3, pp. 1692–1699, 2011.

[149]   B. Markovski, L. Grcev, and V. Arnautovski-Toseva, "Fast and Accurate Transient Analysis of Large Grounding Systems in Multilayer Soil," IEEE Trans. Power Deliv., vol. 36, no. 2, pp. 598–606, Apr. 2021.

[150]   K. Sheshyekani and B. Tabei, "Multiport Frequency-Dependent Network Equivalent Using a Modified Matrix Pencil Method," IEEE Trans. Power Deliv., vol. 29, no. 5, pp. 2340–2348, Oct. 2014.

[151]   B. Gustavsen, "Fast passivity enforcement for S-parameter models by perturbation of residue matrix eigenvalues," IEEE Trans. Adv. Packag., vol. 33, no. 1, pp. 257–265, 2010.

[152]   S. Grivet-Talocia, "An adaptive sampling technique for passivity characterization and enforcement of large interconnect macromodels," IEEE Trans. Adv. Packag., vol. 30, no. 2, pp. 226–237, 2007.

[153]   B. Gustavsen, "Passivity enforcement of rational models via modal perturbation," IEEE Trans. Power Deliv., vol. 23, no. 2, pp. 768–775, 2008.

[154]   S. Grivet-Talocia, "Passivity enforcement via perturbation of Hamiltonian matrices," IEEE Trans. Circuits Syst., vol. 51, no. 9, pp. 1755–1769, 2004.

[155]   J. A. Martinez et al., "Parameter determination for modeling systems transients - Part V: Surge arresters," IEEE Trans. Power Deliv., vol. 20, no. 3, pp. 2073–2078, 2005.

[156]   IEC, TS. "60815-1. Selection and Dimensioning of High-voltage Insulators Intended for Use in Polluted Conditions-Part 1: Definitions, Information and General

Principles." International Electrotechnical Commission: Worcester, MA, USA (2008).

[157]   and B. E. T. Jahangiri, C. L. Bak, F. F. da Silva, "Determination of minimum air clearances for a 420 kV novel unibody composite crossarm," in 50th International Universities Power Engineering Conference (UPEC), 2015, pp. 1–6.

Part II. Selected Publications